



**POLITECNICO**  
MILANO 1863

SCUOLA DI INGEGNERIA INDUSTRIALE  
E DELL'INFORMAZIONE

To analyse the microstructure and mechanical properties of GTAW/TIG and laser welded joints of specific Fe-Mn-Al-C lightweight steel

TESI DI LAUREA MAGISTRALE IN  
MECHANICAL ENGINEERING-INGEGNERIA  
MECCANICA

Author: **Shaad Ahmad**  
Student ID: **969208**  
Advisor: **Prof. Carlo Mapelli**  
Co-advisor: **Giacomo Villa**  
Academic Year: 2022-2023



## Abstract:

Lightweight steels are a viable technological solution to meet the rising demand for energy-efficient, sustainable, and eco-friendly materials. The Fe-Mn-Al-C alloyed steel is a notable lightweight steel that has gained considerable interest in the past few years. The system exhibits an impressive ability to decrease density when compared to traditional steel. Despite this weight reduction, the system maintains its distinct mechanical properties. Lightweight design has emerged as a key focus area in several industries, such as automotive, transportation, aerospace, and military. The Fe-Mn-Al-C alloy possesses exceptional properties that provide it extremely suitable for the applications mentioned earlier. The reduction in automobile weight leads to enhanced fuel efficiency and decreased emissions while maintaining structural integrity and safety. The aerospace and military industries might utilise this alloy due to its lightweight properties, which allow it to improve mobility while maintaining high levels of performance and durability.

The objective of this study is to analyse the microstructure and mechanical properties of gas tungsten arc welding (GTAW) and laser welded joints of specific lightweight steel, Fe-30Mn-9Al-1C (wt%), in correlation with the thermo-mechanical treatments applied. The experimental approach aims to assess the microstructural state and mechanical properties of the material by considering two different heat treatment methods: hot rolling and solubilisation. The heat-treated materials went through GTAW and laser welding. GTAW welding was divided into AC and DC welding procedures based on welding current modes. Various analytical techniques have been utilised to achieve the intended objective. These techniques include optical microscopy, scanning electron microscopy, and Vickers micro-hardness testing. Tensile tests were conducted to investigate the mechanical properties of the alloy and of the welded joints.

This study found that the Fe-Mn-Al-C alloy with 30% Mn, 9% Al, and 1% C had specific properties. First, the hot-rolled case is higher in hardness than solubilized case. Finer grains and grain boundaries hinder dislocation movement, increasing hardness. The welded zone has long dendrites, equiaxial grains, and irregular orientation. This welded zone is harder than the heat-affected zone (HAZ), although the base zone is still harder. GTAW welding samples had better strength and elongation at the point of fracture than other welding processes. This shows that GTAW welded samples are stronger and more ductile.

### Keywords

lightweight steels; low-density steels; Fe-Mn-Al-C austenitic steels; GTAW welding; Laser welding

## Abstract in Italiano:

Gli "acciai leggeri" sono una valida soluzione tecnologica per soddisfare la crescente domanda di materiali efficienti dal punto di vista energetico, sostenibili ed ecologici. Il sistema Fe-Mn-Al-C è un notevole acciaio leggero che ha riscosso notevole interesse negli ultimi anni. Il sistema presenta un'impressionante capacità di ridurre la densità rispetto all'acciaio tradizionale. Nonostante questa riduzione di peso, il sistema mantiene le sue spiccate proprietà meccaniche. Il design leggero è emerso come un'area di interesse chiave in diversi settori, come quello automobilistico, dei trasporti, aerospaziale e militare. Le eccezionali proprietà della lega Fe-Mn-Al-C la rendono altamente adatta per le applicazioni di cui sopra. La riduzione del peso delle automobili si traduce in una migliore efficienza del carburante e in emissioni ridotte, senza compromettere l'integrità strutturale e la sicurezza. L'industria aerospaziale e militare potrebbe utilizzare questa lega per la sua leggerezza, che consente una migliore mobilità pur mantenendo alti livelli di prestazioni e durata.

L'obiettivo di questo studio è analizzare la microstruttura e le proprietà meccaniche di giunti saldati tramite saldatura ad arco di tungsteno (GTAW) e saldatura laser di uno specifico acciaio leggero, Fe-30Mn-9Al-1C (wt%), in correlazione con i trattamenti termomeccanici applicati. L'approccio sperimentale mira a valutare lo stato microstrutturale e le proprietà meccaniche del materiale sottoponendolo a due diversi metodi di trattamento termico: laminazione a caldo e solubilizzazione. I materiali trattati termicamente sono stati sottoposti a GTAW e saldatura laser. La saldatura GTAW è stata suddivisa in procedure di saldatura AC e DC basate sulle modalità della corrente di saldatura. Varie tecniche analitiche sono state utilizzate per raggiungere l'obiettivo prefissato. Queste tecniche includono la microscopia ottica, la microscopia elettronica a scansione e il test di microdurezza Vickers. Sono state condotte prove di trazione per studiare le proprietà meccaniche della lega e dei giunti saldati.

Questo studio ha rilevato che la lega Fe-Mn-Al-C con il 30% di Mn, il 9% di Al e l'1% di C aveva proprietà specifiche. In primo luogo, la condizione laminata a caldo ha una durezza maggiore rispetto alla condizione solubilizzata. Grani più fini e bordi grano ostacolano il movimento di dislocazione, aumentando la durezza. La zona saldata ha lunghi dendriti, grani equiassiali e orientamento irregolare. Questa zona saldata è più dura della zona termicamente alterata (ZTA), sebbene la zona di base sia ancora più dura. I campioni di saldatura con gas inerte e elettrodo in tungsteno (TIG) presentavano resistenza e allungamento migliori nel punto di frattura rispetto ad altri processi di saldatura. Ciò dimostra che i campioni saldati TIG sono più resistenti e più duttili.

Parole chiave

acciai leggeri; acciai a bassa densità; Acciai Fe-Mn-Al-C; Saldatura GTAW; Saldatura laser.

## Contents

Abstract:.....	I
Abstract in Italiano: .....	II
1. State of the Art .....	1
1.1. Lightweight steels .....	1
Historical Background in the Automotive Industry:.....	3
1.2. Classification : .....	5
1.3. Microstructure and Thermodynamics .....	6
Impacts of carbon content .....	6
Impact of other alloying elements .....	7
Phase Constitutions .....	9
K-carbide Precipitation: .....	11
1.4. Mechanical Behavior.....	13
Stacking fault energy:.....	13
Deformation Mechanisms:.....	14
Strengthening Mechanisms: .....	15
K-carbide hardening.....	16
1.5. Properties:.....	17
Density:.....	18
Wear resistance .....	19
Impact toughness.....	20
Fatigue strength: .....	22
Young's Modulus .....	22
Corrosion Resistance.....	23
1.6. Thermo-mechanical Treatments (TMT): .....	24
1.7. Welding Technologies .....	25
Butt Welding:.....	25
GTAW Cladding:.....	26
GTAW Welding.....	27
Laser Welding .....	28
1.8. Challenges in welding of Fe-Mn-Al-C .....	29
2. Experimental Work.....	31
2.1. Design of Experiment.....	32
2.2. Sample Preparation: .....	33
2.3. Test and Analysis .....	34
Optical Microscopy:.....	34

SEM, EDS and EBSD .....	34
Vickers micro-hardness tests .....	35
Tensile tests .....	36
3. Results:.....	38
3.1. Microstructure Evolution:.....	38
Hot-rolled Condition .....	39
Solubilized Condition : .....	39
TIG Cladded Plate.....	40
Laser Beam on Plate.....	43
TIG welded Plate.....	44
Laser welded plate .....	45
3.2. Microhardness Test:.....	46
3.3. Tensile Properties: .....	53
4. Discussion of the results: .....	57
5. Conclusions: .....	71
Future Development:.....	73
Bibliography .....	75
Appendix .....	81
List of table.....	86
List of figures:.....	87
List of Equations:.....	89



# 1. State of the Art

## 1.1. Lightweight steels

The automotive sector needs lighter components to improve fuel efficiency, reduce carbon dioxide emissions, and meet sustainability goals [1]–[3]. The weight reduction of vehicles is a key objective for manufacturers, and one approach to achieving this goal is through the use of lightweight materials [4]. Various materials have been explored for this purpose, including martensitic ultra-high-strength steels, carbon fibre composites, magnesium and aluminium-based alloys, and magnesium and aluminium-based composites [5], [6]. However, these materials have their limitations, such as difficulties in shaping them into certain forms, susceptibility to rust, and high cost [7]. Therefore, there is a need for lightweight materials that offer high strength and durability while addressing these limitations.

One promising solution is the development of lightweight steel. Steel has long been considered the backbone of industrialized societies due to its superior strength and durability [4], [8]. In recent years, researchers have focused on steels with lower density by adding optimal compositions of elements like aluminium to reduce weight without compromising strength. The Fe-Mn-Al-C low-density steel, also known as Fe-Al-X alloy, has shown promise in terms of mechanical properties, density reduction, and cost-effectiveness [8]–[11]. These steels exhibit an excellent combination of mechanical properties, including high yield strength, ultimate tensile strength, and elongation, while maintaining lower density compared to conventional steels [6], [12]–[14]. Moreover, they offer remarkable fatigue strength, toughness at low temperatures, and corrosion resistance, making them suitable for various applications, especially in the automotive and aerospace sectors [15]–[19]. Thus, researchers were intrigued. Figure 1 shows Scopus's 50-year findings on Fe-Mn-Al-C steels. The conclusions were reached by focusing on materials engineering and using the keywords "Fe-Mn-Al-C" and "Lightweight steel." This graph shows a decade of increased research into Fe-Mn-Al-C alloys [8].



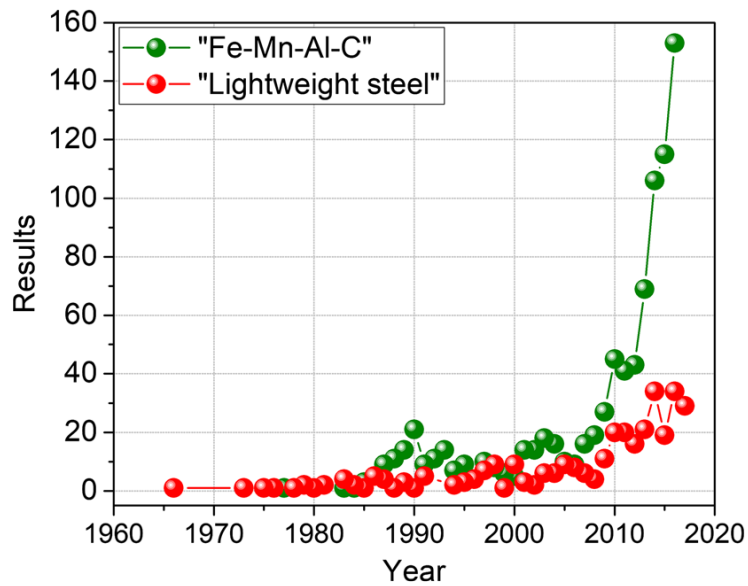


Figure 1 An increasing trend of research in Fe–Mn–Al–C in Scopus alloys during the last half-decade.

The use of Fe-Mn-Al-C steel alloys in the automotive industry can significantly contribute to weight reduction, improved fuel efficiency, and reduced emissions [2], [20], [21]. By incorporating lightweight steels into the manufacturing process, the International Council on Sustainable Transportation (ICCT) aims to achieve a substantial reduction in CO2 emissions per kilometre [2], [13], [22] As the number of electric vehicles increases, lightweight steel will play a larger role in reducing the weight of batteries, thus increasing the overall range of electric vehicles. Additionally, lightweight steel's unique composition allows for its application in making car body panels, where it hardens during the baking process after being stamped [2], [7], [22] However, it is essential to acknowledge that there are still areas that require further research and development. Figure 2 shows the strength-vs.-elongation relationship of several advanced automotive alloys [4]. Fe-Mn-Al-C steels are superior as compared to other classes of steel.

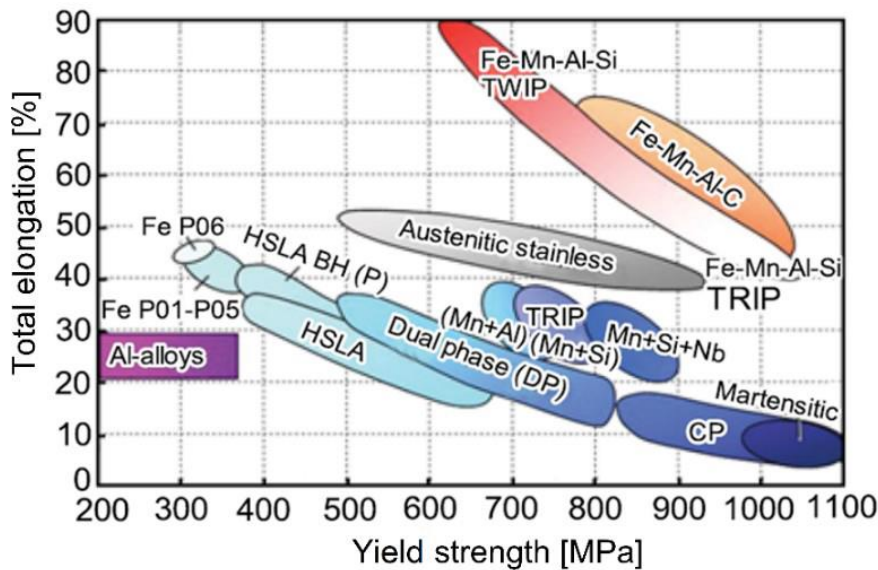


Figure 2 Yield strength-total elongation relationship of automotive steel classes.

The weldability of lightweight steels is a pressing issue that needs to be addressed, as it can affect the mechanical utility and performance of components. Furthermore, specific compositions and manufacturing processes need to be optimized to ensure the best performance and cost-effectiveness for each application [1], [4], [8].

In conclusion, the automotive sector's need for lighter components has driven the exploration of lightweight materials, including lightweight steel. These steels offer a promising solution by providing high strength, durability, and reduced weight compared to conventional steels. Their application in the automotive industry can contribute to improved fuel efficiency, reduced emissions, and increased range for electric vehicles. However, further research is required to address challenges such as weldability and optimization of compositions and manufacturing processes. Overall, lightweight steels have tremendous potential to revolutionize the automotive industry and contribute to a more sustainable future [3], [4], [21], [23].

### Historical Background in the Automotive Industry:

From a historical perspective, Fe-Mn-Al-C low-density steels have been under development ever since Robert Hadfield published his research on the exceptional toughness and wear resistance of Fe-13Mn-1.2C steel in 1882 [24]. In the subsequent decades, particularly the 1950s, 1960s, and 1970s, significant progress was achieved in the physical metallurgy of these alloys [4], [25].

During the same period, V.F. Zackay investigated the concept of "transformation-induced plasticity" (TRIP) in his research on Fe-Cr-Ni stainless steels. However, it wasn't until the 1980s that Fe-Mn-Al-C low-density steels became a viable alternative to traditional stainless steels. These steels substituted nickel with manganese and chromium with aluminium, both of which are less expensive alloy elements with similar

metallurgical effects, such as promoting the development of a protective oxide layer ( $\text{Al}_2\text{O}_3$ ) and stabilising the face-centred cubic (fcc) structure. Due to these characteristics, they were referred to as nickel-free or nickel-chromium-free steels and were even referred to as "the poor man's stainless steel"[24], [26], [27]. However, the initial results did not reveal suitable alternatives to stainless steel. In the 1980s, a great deal of research was conducted on the corrosion, welding, oxidation resistance, and mechanical properties of Fe-Mn-Al-C low-density alloys. At cryogenic temperatures, the effects of test temperature, alloy elements, and microstructure were explored by multiple authors. Particular focus was given to the mechanical properties at cryogenic temperatures. In comparison to conventional steels, promising results were obtained owing primarily to the activation of specific deformation mechanisms. This increased interest in the relationship between deformation mechanisms and mechanical properties led to the categorization of these steels according to their deformation modes. Professor Dr Frommeyer has made a significant contribution to advancing these steels at the close of the 1990s and the beginning of the 2000s by demonstrating a comprehensive knowledge of deformation mechanisms and their relationship to mechanical properties. Frommeyer's contributions cleared the way for the use of Fe-Mn-Al-C low-density steels in the automotive industry, specifically for the conformability of automobile body structures. Several alloys were also patented in this context[24], [26]. These steels exhibited distinctive deformation mechanisms that extended plastic deformation beyond conventional ductility values, enabling the formation of more intricate geometries during processing. In addition, these steels absorbed a substantial quantity of energy during automobile collisions, thereby enhancing passenger safety. Professor Wei-Chun Cheng, during the same period, has made a significant contribution regarding the physical metallurgy of these steels, including findings concerning their phase transformations. The Max Planck Institute for Iron Research in Düsseldorf, Germany, under the direction of Prof. Dr Dierk Raabe, is now at the forefront of exploring Fe-Mn-Al-C low-density steels, along with other major research organisations worldwide. Their work on the physics and physical metallurgy of these steels is comprehensive and covers several ground-breaking areas: dislocation structures during deformation,  $\epsilon$ -carbide's strain-hardening behaviour, grain size's effect on TWIP (Twinning Induced Plasticity) response, aluminium content's effect on mechanical properties, new plasticity mechanisms, nano diffusion's effect on stacking fault energy[4], [24], [27], [28]. Meanwhile, scientists worldwide are studying Fe-Mn-Al-C low-density steels and trying to make them more accessible to businesses.

## 1.2. Classification :

Lightweight steel alloys have a low density, a high ratio of strength to weight, and good mechanical properties. These alloys find extensive use in numerous industries, including the aerospace, automotive, and construction sectors [4], [24]. When determining the characteristics of steel alloys, one of the most significant factors to take into consideration is the phase composition of the alloy. Following the manner in which its phases are combined, lightweight steel can be transformed into either single- or multi-phase alloys. Single-phase alloys are characterised by a crystal structure that is consistent over the entirety of the material, whereas multi-phase alloys are distinguished by the presence of two or more unique crystal structure phases. Austenitic and ferritic stainless steels are examples of single-phase, lightweight steel alloys. Austenitic stainless steel is a nonmagnetic alloy that contains both chromium and nickel. It is not susceptible to corrosion, is highly weldable, and is extensively employed in the chemical and food processing industries [12], [22]. In contrast, ferritic stainless steel is magnetic and contains chromium but no negligible amount of nickel. Compared to austenitic steel, martensitic steel has a lower corrosion resistance; however, it has excellent thermal conductivity and is used in applications involving high temperatures [[1], [29]].

Multiphase, lightweight steel alloy examples include duplex steel and TRIP (transformation-induced plasticity) steels. Duplex steel is a variety of stainless steel that has an austenite and ferrite microstructure mixed. In comparison to conventional austenitic stainless steel, it offers better corrosion resistance, greater strength, and cost savings. Prominent applications for duplex steel include the chemical, petrochemical, and offshore oil and gas industries, as well as other disciplines that require high corrosion resistance and strength [17], [30].

Typically, a TRIP (Transformation-Induced Plasticity) steel has an austenitic structure with an austenite-matrix duplex structure. When steel is subjected to deformation, austenite transforms into martensite. This martensitic transformation enhances the strength and ductility of the steel [18], [26] Table 1 demonstrates the classification of hot-rolled lightweight steel based on its microstructure [4].

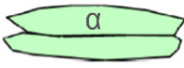
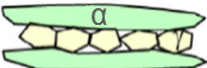


Feature	Type			
	Ferritic	Ferrite-based duplex	Austenite-based duplex	Austenitic
Hot rolled microstructure				
Typical composition	Al ~ 5-9% Mn < 5% C < 0,05%	Al ~ 3-7% Mn ~ 2-12% C ~ 0,05-0,5%	Al ~ 5-10% Mn ~ 5-30% C ~ 0,4-0,7%	Al ~ 5-12% Mn ~ 12-30% C ~ 0,6-2,0%
Tensile properties	UTS ~ 200-600 MPa TE ~ 10-40%	UTS ~ 400-900 MPa TE ~ 10-40%	UTS ~ 800-1300 MPa TE ~ 10-40%	UTS ~ 800-1500 MPa TE ~ 30-80%

Table 1 Classification of lightweight steels based on their microstructures prior to hot rolling.

In conclusion, lightweight steel alloys can be classified based on their phase composition. Single-phase alloys, like austenitic and ferritic stainless steel, have only one form of crystal structure, whereas multi-phase alloys, like dual-phase and TRIP steels, have two or more distinct crystal structures. Duplex steel is a type of multiphase lightweight steel with multiple phases. This form of steel contains a balanced proportion of austenite and ferrite phases, which endows it with exceptional properties such as excellent strength, tensile strength, and corrosion resistance. When selecting the proper alloy for a variety of applications, a thorough comprehension of the phase composition of lightweight steel is essential[4], [24].

### 1.3. Microstructure and Thermodynamics

The careful consideration of the relative balance of each alloying element is crucial in the design process of lightweight steels. This is necessary to attain the desired microstructure, which may include ferrite-based, austenite-based, duplex, or triplex structures[4], [8]. The austenite-based microstructure is commonly favoured in Fe-Mn-Al-C systems because of its superior physical and mechanical properties. The characteristics of lightweight steels are primarily determined by their alloy chemistry and composition. Therefore, it is essential to have a thorough comprehension of the current phases and their transformations. However, acquiring comprehensive knowledge in this area continues to be a difficult undertaking. Numerous investigations have been carried out to examine the microstructure and thermodynamics of Fe-Mn-Al-C steels[6], [7], [17]. These studies have concentrated on the impact of alloying elements, phase constitution, and precipitation phenomena are reported below:

#### Impacts of carbon content

Carbon content can have a substantial effect on the weight and strength of steel. Steel's hardness and strength increase as its carbon content rises while its ductility and resilience decrease. The yield strength increases at greater rates than the ultimate tensile strength, indicating that the strain hardening potential gradually decreases with

increasing C content. Total elongation increases until the matrix transforms into single-phase austenite and then considerably decreases with increasing C content after reaching a maximum of 0.8% C. A higher carbon content makes the steel more brittle and susceptible to fracture [5], [31] Figure 3 shows Carbon's effect on mechanical properties. Al 9%, Mn 30%. Quenching from 1050 ° Celsius in water (dashed curves) and quenching from 1050 degrees Celsius in water, followed by 16 hours of ageing at 550 degrees Celsius (solid curves) [32].

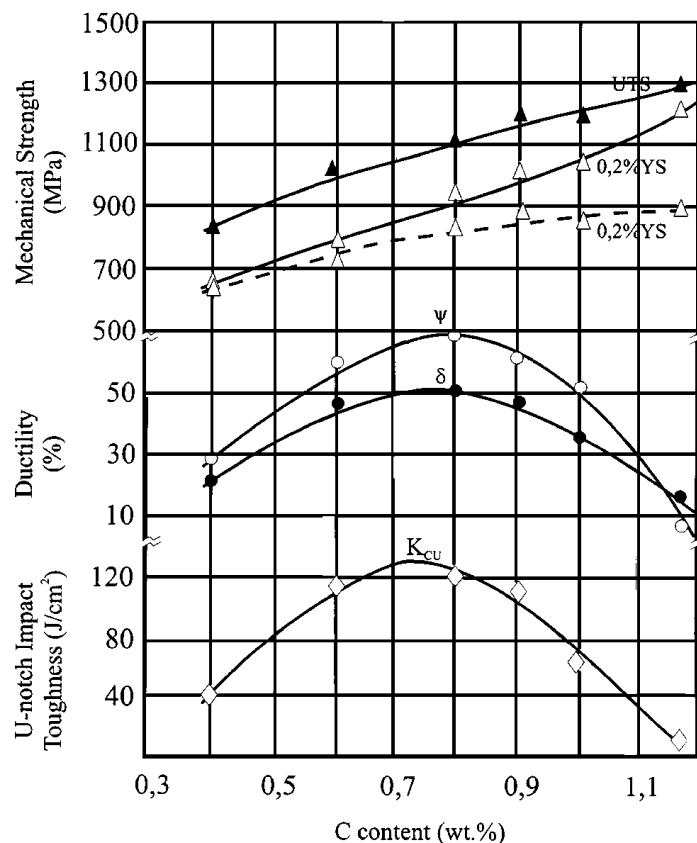


Figure 3 Carbon's effect on mechanical properties. Al 9%, Mn 30%.

Carbon enhances the face-centred cubic (fcc) lattice parameter in Fe-Mn-Al-C low-density alloy. Carbon atoms cause lattice expansion by occupying interstitial spaces in the iron-based matrix. As the fcc lattice expands, it can change the mechanical characteristics of the alloy, such as its yield strength and ductility. The fatigue strength of Fe-Mn-Al-C low-density alloys is reduced with the addition of carbon, at least in the low cycle fatigue (LCF) and extremely low cycle fatigue (ELCF) regimes. Microstructural defects that are caused by the presence of carbon, such as carbides, may function as stress concentration sites and contribute to the development and propagation of cracks when the material is subjected to cyclic loading [4], [8], [31].

### Impact of other alloying elements

In the Fe-Mn-Al-C low-density alloy, aluminium has a significant stabilising effect on the phase (ferrite). At high temperatures, the presence of aluminium contributes to the

stability of the ferrite phase. Aluminium in the alloy reacts readily with atmospheric oxygen to form a protective layer of alumina ( $\text{Al}_2\text{O}_3$ ) on the alloy's surface. This layer acts as a barrier, preventing corrosion and oxidation of the alloy beneath it. Carbon diffusivity in a Fe-Mn-Al-C low-density alloy can be reduced by the addition of aluminium. This reduced carbon diffusivity benefits in retaining carbon within the alloy, thereby preventing its loss and sustaining properties such as hardness and strength. The addition of aluminium to steel increases its stacking fault energy (SFE). The SFE represents the energy necessary to generate stacking defects within the crystal lattice structure. The addition of aluminium to the alloy decreases the steel's overall density. The addition of aluminium increases the lattice parameter of the alloy's face-centred cubic (FCC) crystal structure [33]–[36]. In Fe-Mn-Al-C low-density alloys, manganese is an austenite promoter, so it promotes the austenitic phase. The austenitic phase is characterised by a face-centred cubic (fcc) crystal structure that provides desirable mechanical properties, such as ductility and durability. Additionally, manganese may promote the formation of the beta-Mn phase in Fe-Mn-Al-C low-density alloys. Compared to the austenitic phase, the beta-Mn phase is typically brittle. Figure 4 shows The influence of manganese on the mechanical characteristics of the material [4].

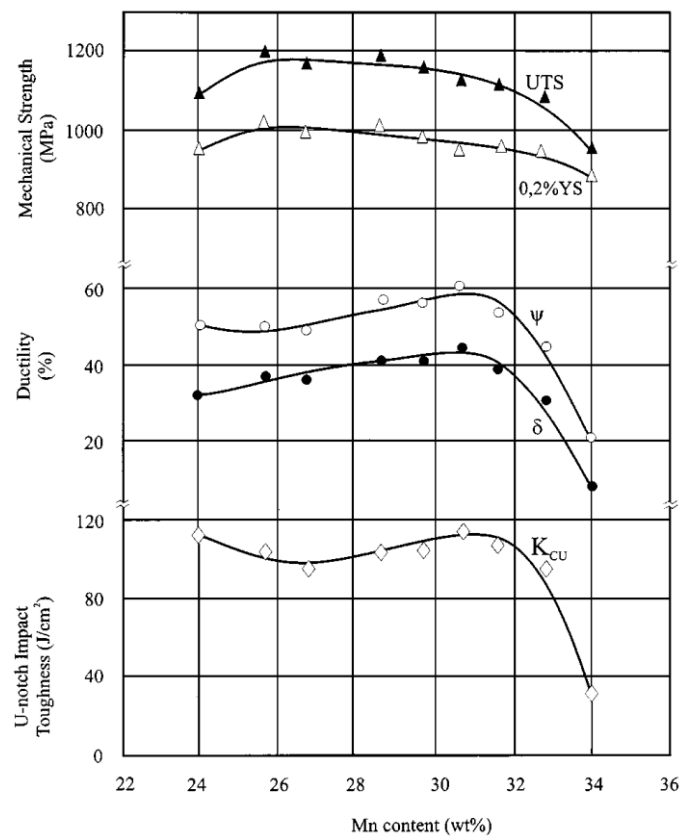


Figure 4 Effect of manganese on mechanical properties

Manganese enhances the oxidation resistance of Fe-Mn-Al-C low-density alloys by producing a protecting oxide scale primarily composed of (Fe, Mn)O, which acts as a barrier between the alloy and the external environment, preventing oxidation. The lattice parameter of the fcc crystal structure increases with the addition of Manganese content [12], [30], [37]. In addition to Mn, Al and C, other secondary alloying elements might be employed [8]. The addition of titanium to Fe-Mn-Al-C alloy can result in various improvements such as grain refinement, strengthening, precipitation strengthening, and enhanced corrosion resistance. These effects enhance mechanical properties, increase high-temperature stability, and improve resistance to grain coarsening and corrosion [8]. It is necessary to ensure that the titanium content of the Fe-Mn-Al-C alloy is correctly managed to prevent the formation of brittle phases. This can have a negative effect on the alloy's mechanical properties as well as its ductility. Because of this, optimisation of the titanium composition is required to ensure the desired properties. When molybdenum is added to lightweight steel, it makes the steel stronger and more resistant to wear. In addition, it increases the material's resistance to creep and corrosion at high temperatures [38]. Utilising molybdenum in conjunction with other alloying elements, particularly chromium and nickel, is common practice. Chromium is an element that is often added to steel to make it stronger and more resistant to corrosion. In addition, it increases the material's hardness and corrosion resistance. It is common to practice combining the use of chromium with other alloying elements, especially molybdenum and nickel. Nickel is sometimes added to lightweight steel to increase its strength and tensile strength. In addition, it increases the material's resistance to creep and corrosion at high temperatures. In a given application, it is usually to combine nickel with other alloying elements such as chromium and molybdenum [37-38]. Vanadium is added to lightweight steel to increase its strength and tensile strength. In addition, it increases the material's high-temperature tensile strength and abrasion resistance. Vanadium is frequently combined with other alloying elements, such as chromium and molybdenum, in a variety of applications [38,39].

In conclusion, the performance of lightweight steel is significantly influenced by the presence of alloying elements such as aluminium, manganese, titanium, molybdenum, chromium, nickel, and vanadium. These components have the potential to significantly improve the material's mechanical properties. However, to keep the material's ductility, weldability, and cost-effectiveness, it is necessary to make a careful selection of these alloying components and maintain control over them.

## **Phase Constitutions**

The equilibrium phases of Fe-Mn-Al-C low-density steels have been the subject of an extensive amount of investigation. Researchers have looked into the phase composition of the Fe-Mn-Al-C low-density system, as well as its mechanical properties and phase equilibrium diagrams. When attempting to anticipate the structure of an alloy and gain a better knowledge of how various compositions and



treatments affect its behaviour, the phase equilibrium diagrams can be a useful way. The significance of Fe-Mn-Al-C low-density steels and their potential industrial applications have been emphasised by researchers. Comparable to stainless steel, Fe-Mn-Al-C low-density steels have exceptional mechanical properties, including yield strength (1 GPa), ultimate tensile strength (1.8-2.0 GPa), and true elongation (40-50%) at 77K [9], [32], [34]. Due to these characteristics, they are acceptable choices for structural applications requiring high strength and ductility. It has been reported that chemical composition and temperature impact the equilibrium phases of the Fe-Mn-Al-C low-density system. These phases consist of  $\beta$ -Mn,  $\Gamma$ -austenite,  $\alpha$ -ferrite,  $\kappa$ -carbide, and M<sub>3</sub>C carbide ( $\Theta$ )[28], [32], [34].

In addition, researchers have developed phase equilibrium diagrams for the quaternary Fe-Mn-Al-C low-density system. These diagrams illustrate the phase stability regions at different temperatures and compositions. They facilitate the understanding of phase transformations and the prediction of equilibrium phases under various conditions[8]. In addition, the matrix phase structure of Fe-Mn-Al-C low-density steels can be classified as ferritic, austenitic, or duplex based on composition and processing parameters. Each category possesses unique microstructural and compositional characteristics[5], [24] Using phase equilibrium diagrams, the equilibrium and actual phase compositions of Fe-Mn-Al-C low-density alloys have been examined. Figure 5 shows four equilibrium Fe-Mn-Al-C phase diagrams [9]. These systems have 20–35 wt. % Mn and 10% Al. Phase diagrams range from 60–1100 °C. Discuss each Mn concentration's observations: Fig 5(a) shows 20% Mn where Ferrite doesn't exist at above 1 wt.% of carbon content at 1000 °C. At lower temperatures, austenite and  $\kappa$ -carbides coexist. C content increases stability in  $\kappa$ -carbides below 950 °C. Fig 5(b) shows 25% Mn where Mn stabilises the austenite monophasic region. For low C levels (< 0.5 wt.%), the  $\beta$ -Mn phase emerges in a limited temperature range (~700–750 °C). Due to the low solubility of dissociated Mn in the ferrite bcc lattice,  $\beta$ -Mn precipitates in the  $\alpha$ -phase. Below 627 °C, austenite, ferrite, and  $\kappa$ -carbides are found with  $\beta$ -Mn. In fig 5(c), with 30% Mn, at Lower temperatures and C concentration increase, monophasic austenite stability. Higher temperatures enhance  $\beta$ -Mn stability, while in fig 5(d) at 35 wt.—% Mn: Lower temperatures and C content increase austenite's stability. Ferrite only occurs with C content below 0.7 wt.%, while  $\kappa$ -carbides remain stable. These findings showed that Mn and C stabilise, while Al stabilises  $\alpha$ . Solution treatment above 900 °C and cooling to room temperature can produce a completely austenitic (metastable) microstructure in alloys with 25-30 wt.% Mn, 10 wt.% Al, and 0.8-1.4 wt.% C [4]. These results could help design lightweight, crash-resistant automobile body structures and cryogenic industry components by revealing the phase transitions and microstructural behaviour of Fe-Mn-Al-C systems with varying Mn concentrations[10]

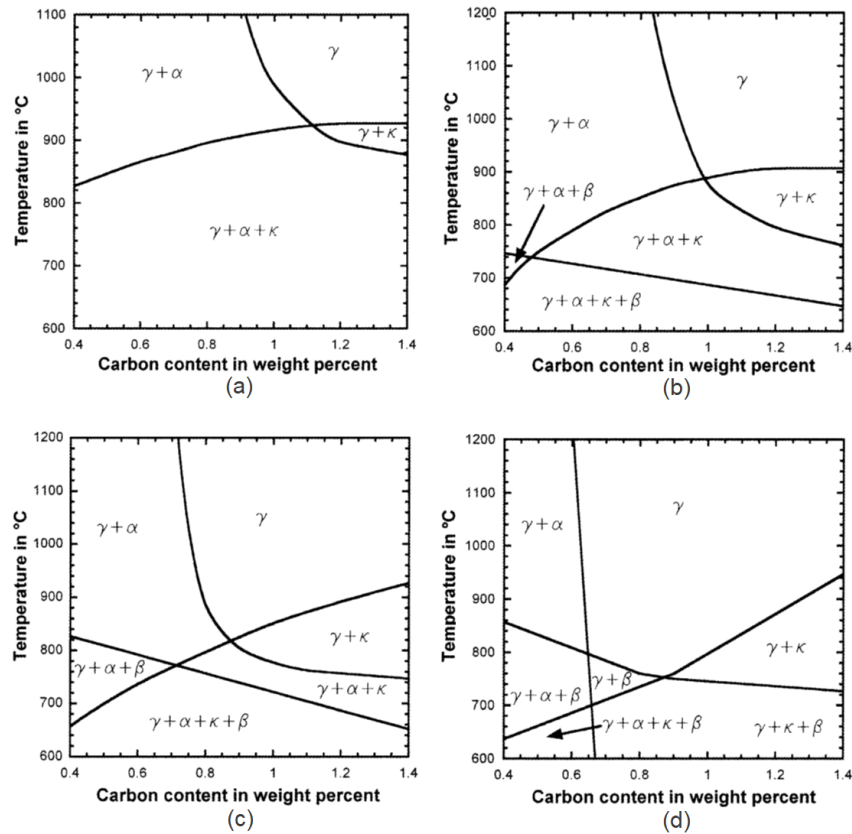


Figure 5 Phase diagrams at the equilibrium of four Fe-Mn-Al-C systems with respectively 20 wt.% (a), 25 wt.% (b), 30 wt.% (c) and 35 wt.% (d) Mn content, as a function of the C content.

In conclusion, research on the equilibrium phases of Fe-Mn-Al-C low-density steels has produced substantial insights into their phase composition, mechanical properties, and phase equilibrium diagrams. These investigations contribute to our understanding of Fe-Mn-Al-C low-density steels' behaviour and potential industrial applications.

### K-carbide Precipitation:

These steels see a decrease in density as a result of the inclusion of aluminium (Al), which also serves to improve the steels' mechanical qualities [4], [38], [39]. K-carbides contribute significantly to the process of strengthening steels composed of iron, manganese, aluminium, and carbon while preserving the materials' ductility. The total strength of the steel grades can be improved through the precipitation of  $\kappa$ -carbide [40]. The precipitation kinetics and mechanisms of  $\kappa$ -carbide have been investigated through isothermal and thermomechanical treatments. The kinetics and mechanisms of  $\kappa$ -carbide precipitation in Fe-Mn-Al-C steels have been studied through isothermal experiments conducted at different temperatures and durations. The studies have improved the understanding of precipitation behaviour by investigating the nucleation and growth processes of  $\kappa$ -carbides under varying conditions.  $\kappa$ -carbides can precipitate rapidly during thermomechanical treatments. Thermo-mechanical treatments (TMTs) entail applying both thermal and mechanical processes, such as hot deformation and rapid cooling, to steel. [41]. It was previously assumed that

spinodal decomposition followed by an ordering reaction was the mechanism that led to the development of intragranular  $\kappa$ -carbide in the  $\Gamma$ - austenite phase of Fe-Mn-Al-C steel. However, recent research employing better characterisation techniques has shown that ordered nuclei of  $\kappa$ -carbide can directly form in the disordered gamma-austenite, thus avoiding the spinodal breakdown mechanism [[31]. Figure 6 demonstrates the unit cell, from left: (a) as initially conceived; (b) with ideal stoichiometry; (c) and Mn<sub>2</sub>FeAlC transitions observed experimentally; (d) and (e) with the partial carbon vacancy [4]

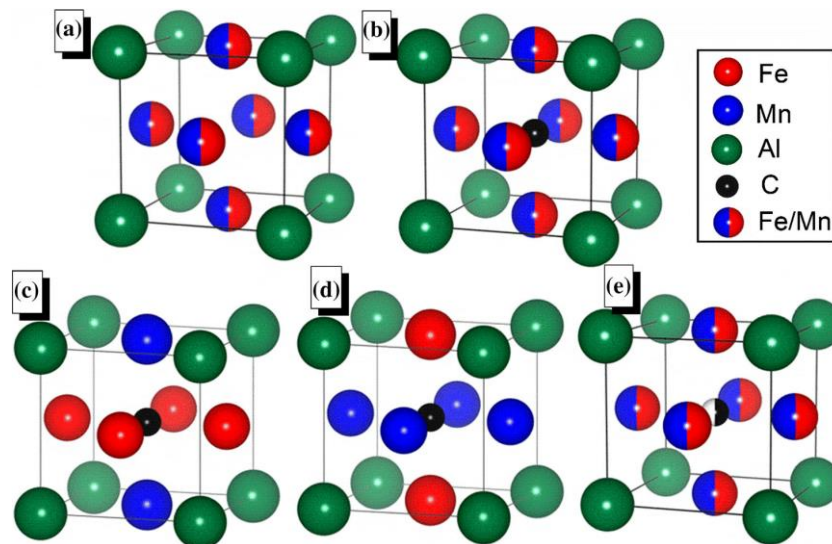


Figure 6 The  $\kappa$ -carbide unit cell, from left: (a) as initially conceived; (b) with ideal stoichiometry; (c) and Mn<sub>2</sub>FeAlC transitions observed experimentally; (d) and (e) with the partial carbon vacancy.

In conclusion, the occurrence of  $\kappa$ -carbide precipitation in Fe-Mn-Al-C steel is an essential process that plays a significant role in the strength and ductility of these lightweight steels. To further develop Fe-Mn-Al-C steels and apply them in a variety of different industries, it is vital to have a solid understanding of the kinetics, processes, and impacts of  $\kappa$ -carbide precipitation.

## 1.4. Mechanical Behaviour

The mechanical properties of lightweight steels can be improved through various methods such as work hardening, solid solution strengthening, precipitation hardening, and deformation mechanism tailoring. The activation of various deformation mechanisms, namely TRIP, TWIP, SIP, MBIP, and DSBR, is closely linked to the stacking fault energy (SFE) of austenite[4], [8], [15].

### Stacking fault energy:

The stacking fault energy (SFE) is a crucial microstructure feature in austenitic steels, particularly Fe-Mn-Al-C low-density steels. It plays a vital role in regulating the deformation mechanism and optimizing the mechanical properties of these steels. The SFE determines the mobility of dislocations within the crystal lattice, which directly affects the material's strength, ductility, and work hardening capacity. Numerous studies have focused on investigating the stacking fault energy of Fe-Mn-Al-C low-density steels and the influence of various alloying elements on this property [2][5]. Alloying elements, including carbon (C), manganese (Mn), aluminium (Al), and silicon (Si), have significant effects on the stacking fault energy in Fe-Mn-Al-C low-density steels. For instance, the carbon content has a negligible effect on the stacking fault energy gradients compared to aluminium and silicon [5]. Aluminium, as a primary alloying element, plays a crucial role in determining the primary plastic deformation mechanism, and the stacking fault energy of Fe-Mn-Al-C low-density alloys can vary based on their concentration [2][28]. Figure 7 shows a Schematic representation of the stacking sequence of perfect structure [8]

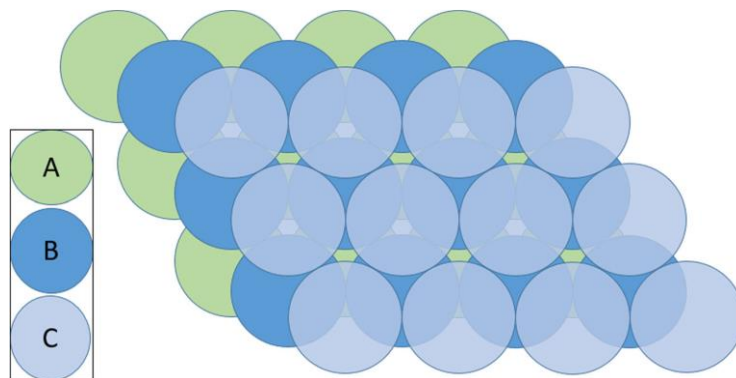


Figure 7 Schematic representation of the stacking sequence of perfect structure

Several factors influence the stacking fault energy of Fe-Mn-Al-C low-density steels, including temperature, particle size, and compositional variations. Studies have examined the impact of these factors on the stacking fault energy and have highlighted their significance [19][21]. Additionally, the SFE can be affected by the concentrations of carbon, manganese, aluminium, and silicon [5]. While the stacking fault energy is a crucial parameter in understanding the deformation mechanism and mechanical properties of Fe-Mn-Al-C low-density steels, there are limited, accurate computational

tools available for modelling the SFE in these steels. Therefore, further research and development are necessary to better comprehend the intricate relationship between alloying elements, microstructure, and stacking fault energy in Fe-Mn-Al-C low-density steels [2][28].

## Deformation Mechanisms:

Along with the effect of alloying elements, extensive research has been conducted on the deformation mechanisms of Fe-Mn-Al-C low-density steels. These mechanisms and their effect on the mechanical properties of steels are crucial for understanding their behaviour under different loading conditions. There is a complicated relationship that exists between the alloy components, phase composition, mechanical properties, and external factors that are present in Fe-Mn-Al-C low-density steels. Table 2 describes the deformation mechanisms in austenitic Fe–Mn–Al–C steels as a function of SFE [4]

SFE [mJ/m <sup>2</sup> ]	< 20	20-40	40-60	> 60
Main deformation mechanism	ε-martensite + dislocation glide	Twinning + dislocation glide	Cross-slip and activation of slip systems	Microbands or dynamic slip band refinement

Table 2 Deformation mechanisms in austenitic Fe–Mn–Al–C steels as a function of SFE

The incorporation of aluminium (Al) into high-manganese (Mn) austenitic steels not only helps cut down on the overall weight of automotive bodies but also alters the deformation mechanisms of the material. It can switch between transformation-induced plasticity (TRIP) and twinning-induced plasticity (TWIP) as deformation mechanisms[5], [22], [26]. Due to the complexity of their alloy composition and the relationship between alloy composition and mechanical properties, it has been challenging to comprehend the deformation mechanisms of Fe-Mn-Al-C low-density steels. A number of variables influence the deformation mechanisms, including the stacking fault energy (SFE) and the carbon, manganese, copper, aluminium, and silicon contents. For instance, to establish a relationship between SFE and tensile properties in Fe-Mn-C TWIP steels, the tensile behaviours of high-manganese steels with varying alloy contents have been studied [6]. Fe-Mn-Al-C low-density steels may undergo deformation via twinning, Taylor lattices, or deformation bands. These mechanisms contribute to producing some steels, such as high-entropy steel with 10% aluminium, which is exceptionally strong and durable[4]. Using thermomechanical treatments and ageing treatments, the effects of deformation mechanisms and hardness in Fe-Mn-Al-C low-density steels [39] are studied. A significant role is played by alloying elements in the deformation mechanisms of Fe-Mn-Al-C low-density steels. Aluminium, in addition to carbon and manganese, can modify the deformation behaviour and mechanical properties of steels. These alloying elements modify deformation mechanisms by interacting with the microstructure [42]. The deformation

mechanisms of Fe-Mn-Al-C low-density steels are complex and influenced by alloying elements such as aluminium. The aforementioned mechanisms include transformation-induced plasticity (TRIP), twinning-induced plasticity (TWIP), twinned structures, Taylor lattices, deformation bands, and dislocation motion. Understanding these concepts is crucial for optimising the mechanical characteristics of Fe-Mn-Al-C low-density steels for specific uses. Figure 8 represent a schematic representation of the deformation mechanisms of Fe-Mn-Al-C steel [8]

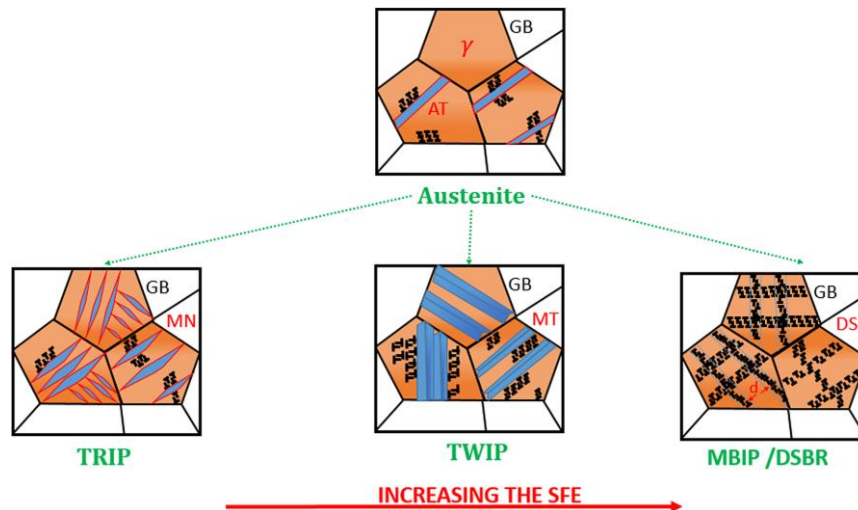


Figure 8 A schematic representation of the deformation mechanisms of Fe-Mn-Al-C steel

## Strengthening Mechanisms:

To enhance the mechanical properties of Fe-Mn-Al steel for a variety of applications, intensive research has been conducted on this material's strengthening mechanisms. Among these mechanisms are the halting of dislocation motion, the introduction of intermetallic phases, work hardening, and alloying effects. The slowed-down motion of dislocations is one process by which crystal lattices are strengthened. Alloying elements, such as aluminium (Al), are added to metals to increase their strength by impeding the migration of dislocations [4]. The strength of Fe-Al alloys can be improved by adding more Al content. Work hardening is another essential strengthening mechanism for Fe-Mn-Al steel. This mechanism occurs when a material is plastically deformed, resulting in an increase in dislocation density and the formation of internal stress fields, thereby enhancing its strength. It has been discovered that the combination of ageing and deformation improves both the ductility and strength of high-Mn steel [13], [22], [38]. The composition of Fe-Mn-Al steel, particularly the aluminium content, serves a crucial role in determining the strengthening mechanisms. Diverse aluminium contents have been studied to comprehend the underlying mechanisms responsible for the increased strength of Fe-Mn-Al steel. To decrease energy consumption, interest has been drawn to Fe-Mn-Al steel with a reduced specific strength (strength-to-weight ratio). The work-hardening behaviour of fcc

materials with varying stacking fault energies (SFE) during tensile testing is depicted in Figure 9. The dashed line curve is indicative of a material that possesses medium to high surface free energy (SFE) and has a coarse grain size. The dotted line curve represents the material with medium to high surface free energy (SFE) and small grain size, as shown by the curve. The low SFE TWIP steel with the fine grain is depicted by a solid line curve. Dislocation glide (DG), grain boundaries (GB), stacking faults (SF), and dynamic strain ageing (DSA) are terms used in materials science to describe specific phenomena [43].

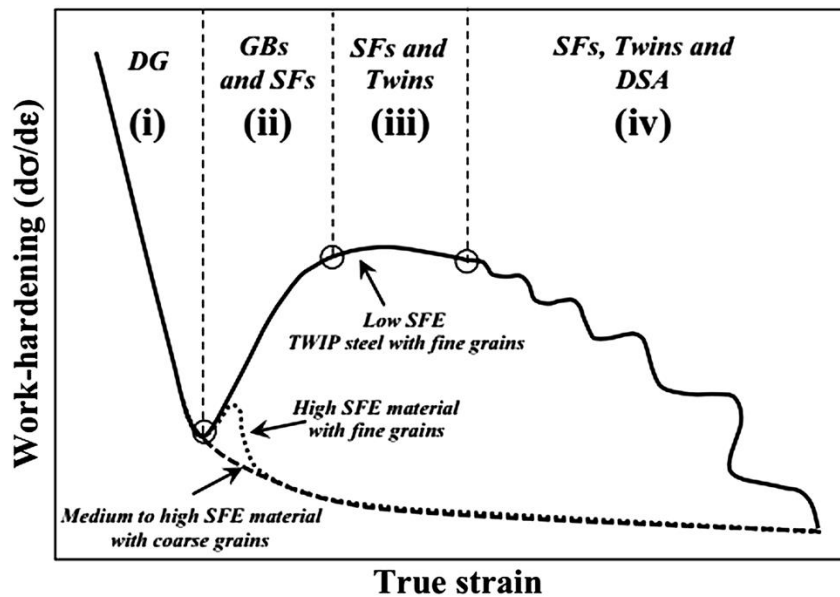


Figure 9 fcc materials with different stacking fault energies

## K-carbide hardening

K-carbide hardening is a method of enhancing the strength of Fe-Mn-Al-C steel by inducing the formation of  $\kappa$ -carbides. The strain-hardening properties of Fe-Mn-Al-C steels are enhanced by coherent precipitates, including  $\kappa$ -carbides. These precipitates are responsible for the favourable balance between strength and ductility that is characteristic of these steels.  $\kappa$ -carbides precipitate during thermomechanical or ageing treatments of Fe-Mn-Al-C steel. In the past, ageing treatments required increased holding times and high temperatures, resulting in energy-intensive procedures [2][6]. Recent studies indicate that  $\kappa$ -carbide precipitation may occur within seconds of TMTs, offering a more effective alternative [2][6]. The mechanical properties of Fe-Mn-Al-C steels are significantly improved by the formation of  $\kappa$ -carbides. The hardness of a material increases rapidly due to the presence of  $\kappa$ -carbides but softens when annealed at higher temperatures [7]. The change in hardness can be determined by the development of  $\kappa$ -carbides, which includes their transformation within ferrite and austenite phases [7]. Extensive research has been conducted on the  $\kappa$ -carbides found in Fe-Mn-Al-C steels to comprehend their structure, precipitation mechanism, and deformation behaviour due to their significant impact on

the mechanical properties of these steels. Studies have examined the microstructure of Fe-Mn-Al-C steels, specifically the development of austenite lamellar  $\kappa$ -carbides and ferrite-dispersed nano-scale particulate  $\kappa$ -carbides [7].  $\kappa$ -carbides have been investigated for their elastic and magnetic properties [8]. Figure 10 report presented an analysis of the mechanical properties acquired through the RAP experiments, considering the alloy composition and applied ageing treatment as variables. The focus is on providing an overview of the results obtained. The following are important mechanical properties that are commonly used to describe the behaviour of materials under stress: yield stress (YS), ultimate tensile stress (UTS), total elongation (TE), and hardness. RAP stands for Rapid Alloy Prototyping [44].

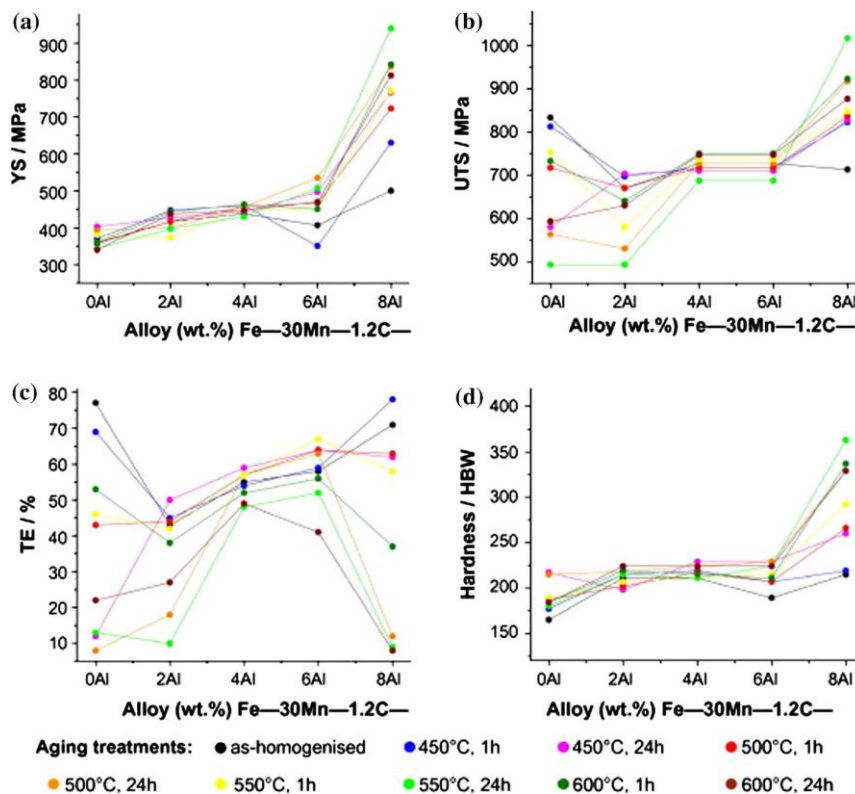


Figure 10 Overview of the mechanical properties with respect to alloy composition

## 1.5. Properties:

Due to the fact that Fe-Mn-Al-C low-density alloys, commonly known as low-density steels, have the potential to be used in a wide number of industries, particularly the automotive industry, there has been a significant amount of interest in these materials. Because of the better mechanical qualities they possess, in addition to their reduced weight, these alloys are ideal for use in the construction of lightweight structural components. The following is a list of some of the most significant application qualities of the alloy Fe-Mn-Al-C low density:



## Density:

The presence of various alloying elements can affect the density of Fe-Mn-Al-C low-density steel. Studies have provided formulas for estimating the densities of various steel compositions. It is possible to compute the density of Fe-Al ferritic steels and Fe-Mn-Al-C low-density austenitic alloys by making use of linear combinations of the influences of each constituent. The density of the Fe-Al-Mn-C austenitic alloy can be thus formulated as the linear combination of these contributions,

$$\rho_{\gamma} = 8,15 - 0,101 \cdot (\% Al) - 0,41 \cdot (\% C) - 0,0085 \cdot (\% Mn) \text{ (g/cm}^3\text{)} = 7.874 - 0.098 \text{ (wt\% Al)}.$$

*Equation 1 demonstrates the austenitic alloy with a linear combination of alloy elements*

Similarly, ferritic alloy density can be expressed as:

$$\rho_{\alpha} = 7,874 - 0,098 \cdot (\% Al) [4], [8]$$

*Equation 2 demonstrates the ferritic alloy with a linear combination of alloy elements.*

These formulas estimate the steel's density based on the alloying elements' weight percentages. By altering the composition of Fe-Mn-Al-C low-density steel, its density can be regulated within a certain range. The function of alloying elements in determining the properties and characteristics of Fe-Mn-Al-C low-density steel is crucial. In addition to aluminium (Al), manganese (Mn), and carbon (C), other alloying elements can affect the steel's density. In Fe-Mn-Al-C low-density steel compositions, chromium (Cr), nickel (Ni), and silicon (Si) are frequent alloying elements. These elements can affect the steel's density by modifying its crystal structure and precipitation behaviour [7], [34], [45]. Depending on their concentrations and interactions with other elements, the specific impacts of alloying elements on the density of Fe-Mn-Al-C low-density steel may vary. Apart from alloying elements, several factors can influence the density of Fe-Mn-Al-C low-density steel. The steel's microstructure is a significant factor. The composition, thermal treatment, and processing conditions influence the microstructure [4], [45]. The presence of hydrogen in steel is an additional factor that can influence density. Aluminium addition to Fe-Mn-Al-C low-density steel mitigates hydrogen embrittlement, resulting in increased hydrogen solubility and decreased hydrogen permeability and diffusivity [8]. This effect can contribute to a decrease in the overall density of Fe-Mn-Al-C low-density steel. Figure 11 demonstrates the Effect of alloy elements on the density of austenite [8].

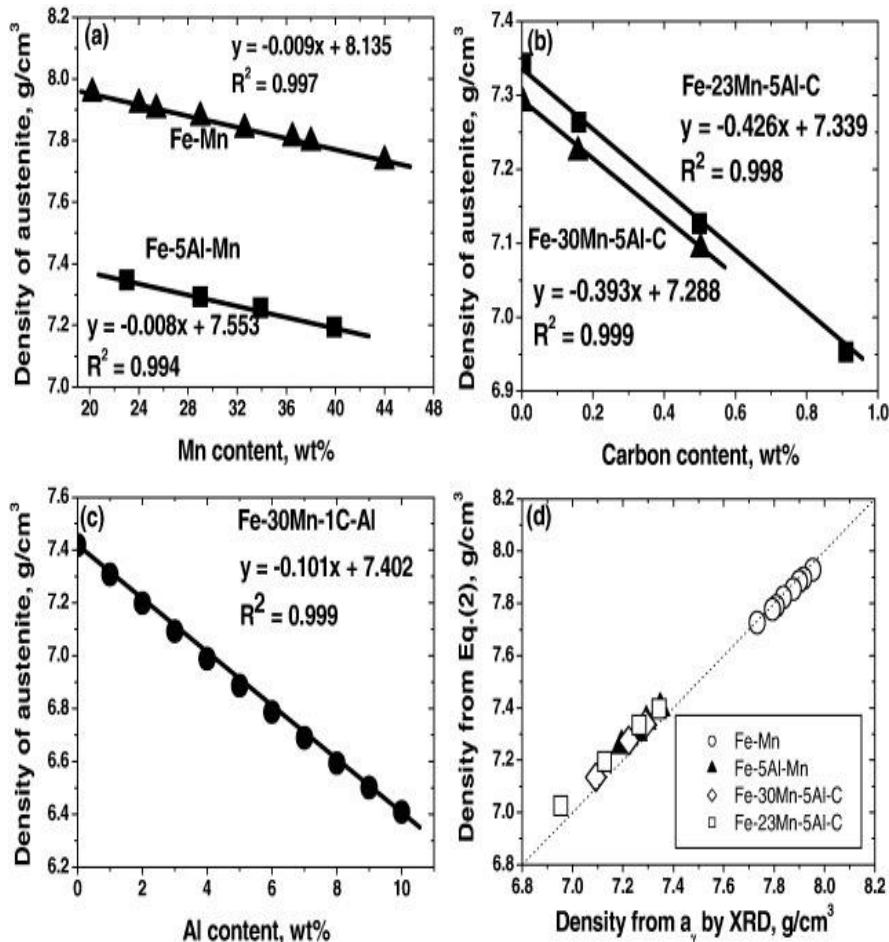


Figure 11 Effect of alloy elements on the density of austenite

To summarise, it is feasible to generate an approximation of the density of steel composed of Fe, Mn, Al, and C by employing linear combinations of alloying components. Alloying components, including aluminium, manganese, and carbon, as well as several others, have a key role in determining the density of steel. In addition, the microstructure of the Fe-Mn-Al-C low-density steel, the presence of hydrogen, and the processing procedures used all have an impact on the material's density.

## Wear resistance

Fe-Mn-Al-C low-density steel exhibits favourable wear characteristics and has drawn desire as a potential structural material for numerous industries. However, the specific wear properties of Fe-Mn-Al-C low-density steel and the factors that influence its wear resistance might vary based on the specific composition of the alloy as well as the processing procedures that are utilised. The wear resistance of Fe-Mn-Al-C low-density steel can be attributed, in part, to the material's underlying microstructure. This higher ductility can contribute to improved wear resistance by minimising catastrophic failure and fracture propagation during wear. This is accomplished by preventing fractures. Fe-Mn-Al-C low-density steel wears differently due to alloying constituents

including Al, Mn, and C. These elements affect steel's microstructure, mechanical characteristics, and corrosion resistance. High-aluminium Fe-Mn-Al-C low-density steels exhibit better wear resistance. Alloying elements promote wear resistance in Fe-Mn-Al-C low-density steel through surface coatings, hardness, and tribological properties [6], [8], [22], [40].

In addition, the processing techniques utilised on Fe-Mn-Al-C low-density steel can affect its wear characteristics. Microstructure and surface characteristics can be altered by heat treatment, rolling, forging, and surface finishing, thereby impacting wear resistance. To achieve the desirable wear performance in Fe-Mn-Al-C low-density steel, it is necessary to select and optimise these processing parameters with care. In addition, external factors, such as strain, sliding speed, and environmental conditions, can affect the wear characteristics of Fe-Mn-Al-C low-density steel. Different conditions of wear testing may bring information on the tribological properties of Fe-Mn-Al-C low-density steel and help determine its suitability for particular applications.

In conclusion, Fe-Mn-Al-C low-density steel demonstrates promising wear resistance and is being studied for a variety of structural applications. This steel's wear behaviour is influenced by microstructure, alloying elements, processing techniques, and environmental conditions. The presence of nanosized precipitates and the effects of alloying elements, such as aluminium, manganese, and carbon, contribute to the wear resistance of Fe-Mn-Al-C low-density steel. Further research and development are required to optimise the composition and processing parameters of Fe-Mn-Al-C low-density steel to achieve the desired performance in specific applications.

## **Impact toughness**

Impact toughness refers to the ability of lightweight steel to withstand impulsive shocks or impacts without cracking. Typically, lightweight steel is distinguished by its high strength-to-weight ratio and its ability to absorb impact energy. For structural uses, a material that combines mechanical strength and fracture durability is desirable [6], [46][7]. The formation of  $\kappa$ -carbides and the presence of  $\delta$ -ferrite are two factors that affect the impact toughness of Fe-Mn-Al-C low-density steels. The plasticity and ductility of such alloys are reduced, while the anisotropy of their mechanical characteristics is increased when the Al content rises above 10% and the banded phase  $\delta$ -ferrite is introduced into the microstructure. Duplex steels typically crack at the interfaces because the two phases cannot deform together. Due to the increase in the volume fraction of the austenitic phase, solution hardening, and  $\kappa$  precipitation hardening in austenite, increasing the carbon content of a material can improve its strength, ductility, and impact toughness up to 0.7% C in an aged condition. It's possible to do so. Above 0.7% C, strength improves at the expense of ductility. Studies have shown that the impact resistance of lightweight steel can be greatly improved by adding microalloying elements, including niobium, vanadium, and titanium. Lightweight steel often offers good impact resistance due to its high strength and

ductility. However, correct processing and treatment of the steel are needed if its impact resistance is to be maximised. This could require heat treatment, forging, or other manufacturing processes to get the desired microstructure and characteristics of the steel [4], [7], [12], [13]. The figure 12 shows the variation of impact energy with respect to the test temperature. The impact energy of CVN can be expressed as a function of the test temperature for the austenitic steels specified in the following manner:

Curve 1 represents a sample of Fe-28Mn-5Al-1C that was subjected to solutionizing at a temperature of 1050 °C for 75 minutes. The resulting grain size of the sample was measured to be 41 µm. Curve 2 represents a Fe-28Mn-5Al-1C alloy that has been solutionized at a temperature of 1050 °C for 8 hours. The resulting grain size of the alloy is 135 µm. Curve 3 represents a sample of Fe-30Mn-10Al-1C-1Si alloy that was subjected to solutionizing at a temperature of 1050 °C for 1 hour. The resulting grain size of the sample was measured to be 120 µm. Curve 4 represents the mechanical behaviour of a Fe-28Mn-5Al-1C alloy that underwent a solutionizing treatment at 1050 °C for 8 hours, followed by an ageing process at 550 °C for 16 hours. Curve 5 represents the Fe-30Mn-10Al-1C-1Si alloy that underwent solutionizing at a temperature of 1050 °C for 1 hour, followed by ageing at 550 °C for 16 hours [47].

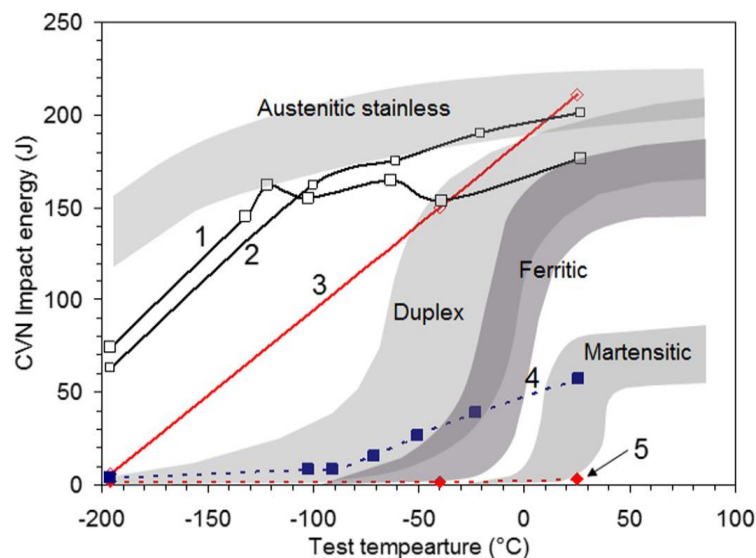


Figure 12 CVN impact energy as a function of test temperature for two austenitic steels

Lightweight steel's resistance to impact can be evaluated using several different tests, including the Charpy impact test and the Izod impact test. The amount of force a notch in a steel sample can withstand before cracking is measured by striking the sample with a hammer or pendulum. The results of these tests can be utilised to evaluate the impact resistance and utility of various steel kinds.

## **Fatigue strength:**

Under cyclic loading conditions, the fatigue strength of Fe-Mn-Al-C low-density steel is a crucial factor in determining its fatigue resistance failure. The specific fatigue strength of Fe-Mn-Al-C low-density steel can vary based on several variables, including alloy composition, thermal treatment, microstructure, and loading conditions. Improving fatigue resistance necessitates a thorough comprehension of the material's behaviour and the factors influencing its fatigue performance. Microstructural characteristics, mechanical properties, and phase structures have been the primary focus of research on Fe-Mn-Al-C low-density steels. The influence of microalloying elements, such as niobium and vanadium, on the low-cycle fatigue properties of Fe-Mn-Al-C low-density steels has also been investigated [23], [48]. In conclusion, the fatigue strength property of Fe-Mn-Al-C low-density steel is a determining factor in its resistance to fatigue failure. In terms of their specific strength, the trade-off between ultimate tensile strength and ductility, and potential for lightweight applications, Fe-Mn-Al-C low-density steels have shown promise.

## **Young's Modulus**

It is advantageous to increase Young's modulus (E modulus) in order to increase the rigidity of automotive components. However, Young's modulus of low-density steels containing aluminium decreases. Polycrystalline Fe-Al alloys exhibit a decrease in Young's modulus with increasing aluminium content as a result of a decrease in lattice energy in the Fe-Al solid solution and an increase in the distance between coexisting Fe and Al atoms [8]. Young's modulus has been measured for these alloys, and dynamic measurements such as the resonance method or ultrasonic technique are accurate for determining Young's modulus. Si and Cr are reported to increase the E modulus of high-Al steels by a small amount, while Mn decreases it by a small amount [12], [14].

The processing condition also affects Young's modulus of Fe-Mn-Al-C low-density steels. The material in its as-cast state has a relatively low E value, but this value increases once it has been heated and rolled. After cold rolling and annealing, the E modulus is somewhat lower than the as-hot-rolled value. This is because the existence of micro-cavities lowers Young's modulus, which in turn lowers Young's modulus. During the process of solidification, the incorporation of Al broadens the compositional and temperature ranges of the primary delta phase. This, in turn, makes it easier for cavities to be formed. In addition, casting flaws such as shrinkage voids and segregations among dendritic arms lower Young's modulus of the material after it has been cast. Production of steel is made more difficult because of the significant amount of aluminium present in Fe-Mn-Al-C low-density steels. Defects in cast structures are also reliant on the environment that is used during melting as well as the size of the

ingots that are produced [4], [13], [16]. Young's modulus of hot-rolled steel is higher than that of cold-rolled steel because the former has fewer microcracks as a result of reheating and hot rolling. However, cold deformation has a lowering influence on Young's modulus, and annealing may alter the material's microstructure, which also affects the modulus as shown in figure 13. Both of these processes have an effect on the modulus of the material. Cast steel is manufactured through a process of melting the steel and subsequently pouring it into a mould to allow for solidification. The described process allows a slowed cooling rate, resulting in the formation of a microstructure that is more irregular in nature, characterised by grain structures that are randomly oriented. Young's modulus of cast steel is generally lower than that of hot-rolled steel due to its less structured grain arrangement.

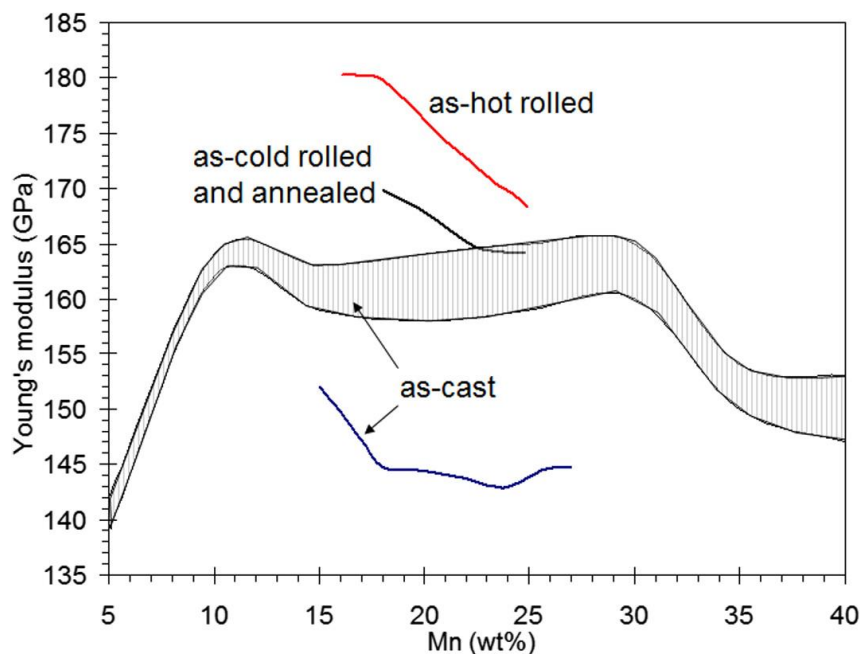


Figure 13 Effect of Mn content on Young's modulus

## Corrosion Resistance

Fe-Mn-Al-C low-density alloys are corrosion-resistant due to their protective oxide layer. The oxide layer consists of aluminium oxide ( $Al_2O_3$ ) and manganese oxide ( $MnO_2$ ), acting as a barrier to prevent corrosion of the underlying metal. Due to the alloy's high aluminium content, the formation of an oxide layer is formed. In addition to the formation of a protective oxide layer, the unique microstructure of Fe-Mn-Al-C low-density alloys is one of the contributing factors to the corrosion resistance of these

materials. A ferritic matrix forms the basis of the microstructure, with austenite and intermetallic phases also present in the material. The austenite and intermetallic phases inhibit the formation of corrosion sites on the metal surface by acting as micro-galvanic cells [8], [40], [49], [50]

Fe-Mn-Al-C low-density alloys resist corrosion due to their microstructure and protective oxide layer. Fe-Mn-Al-C alloys have corrosion resistance in an aqueous environment comparable to ordinary high-strength steels but lower than AISI304 stainless steel [12]. The microstructure is composed of a ferritic matrix with austenite and intermetallic phases disseminated throughout. The austenite and intermetallic phases inhibit the formation of corrosion sites on the metal surface by acting as micro-galvanic cells. Fe-Mn-Al-C low-density alloys are appropriate for a variety of applications because their microstructure provides both high strength and excellent ductility. Because pitting is the major kind of corrosion in duplex Fe-Mn-Al-C low-density alloys and occurs preferentially within a grain and on grain boundaries, the corrosion resistance of duplex Fe-Mn-Al-C low-density alloys is lower than that of austenitic Fe-Mn-Al-C low-density alloys. To obtain a completely austenitic structure, the Cr and C contents must be properly balanced. While Fe-Mn-Al-C low-density alloys are known to be susceptible to stress corrosion cracking, this vulnerability is not mitigated by the inclusion of Al, which is thought to perform an active protective function[17], [30].

Fe-Mn-Al-C low-density alloys can be utilised in severe environments, such as the marine and chemical processing industries. In marine environments, the alloys are resistant to the known highly corrosive nature of salinity. In the chemical processing industry, the alloys are resistant to the acids and bases that can cause corrosion in other materials.

## **1.6. Thermo-mechanical Treatments (TMT):**

Thermal treatment of steel involves subjecting the material to specific heating and cooling treatments to modify its microstructure and enhance its mechanical properties. This was further subdivided into Hot rolling and solubilisation processes. Heating steel above its recrystallization temperature and passing it through a series of rolling mills to reduce its thickness and form it into plates constitutes hot rolling. During heated rolling, the steel undergoes considerable plastic deformation, which refines its grain structure, improves its mechanical properties, and eliminates internal stresses. The surface treatment of steel begins in the hot rolling process when the kind and thickness of the scale that forms are controlled by the reheating, rolling temperature, and cooling pace[8], [39].

Solubilisation is a heat treatment used to dissolve specific alloying elements into the steel matrix in order to achieve the desired properties. This method is frequently used in the thermal treatment of a variety of steel alloys, including lightweight steels. Temperatures above the steel's critical temperature, known as the austenitizing

temperature ( $A_{c3}$ ), are commonly used for solubilisation. This temperature is found in the iron-carbon equilibrium diagram, and it changes depending on the amount of carbon in the steel. By maintaining the steel at the austenitizing temperature for a specified period, the alloying elements are dissolved into the austenite phase, resulting in a homogeneous solid solution. [8], [12], [42]. Figure 14 illustrates the effect of the isothermal holding temperature utilised during solution treatment on the size of the austenite grains [51].

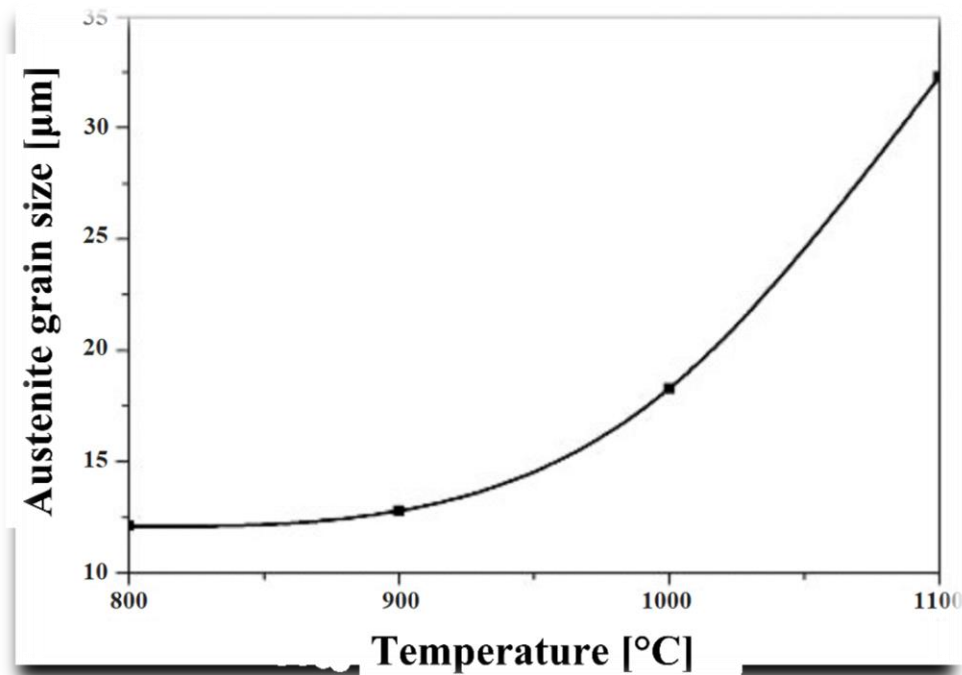


Figure 14 Effect of Austenitic grain size with respect to temperature

## 1.7. Welding Technologies

In recent decades, there has not been a substantial amount of research done on the weldability of Fe–Mn–Al–C alloys. The recent acceptance of these alloys in the automotive industry, on the other hand, led to a study into the weldability of these materials. The context in which the welding technologies of Fe–Mn–Al–C alloys are utilised is covered in this section.

### Butt Welding:

Butt welding is a welding process that involves joining two metal pieces together by aligning their ends without overlapping and then welding along the joint. The workpieces being joined are flush, and the weld metal is contained within the planes



of the surfaces. The joint that features workpieces with nearly parallel edges is known as a butt joint. It can be applied to a range of metals, such as steel and copper. The process can be accomplished through manual means or by utilising automated welding machinery [52], [53]. The procedure involves surface preparation of the metal, edge alignment, and the application of a continuous weld along the centerline to achieve the fusion of the metal pieces.

### **GTAW Cladding:**

Gas tungsten arc welding (GTAW) cladding, commonly referred to as tungsten inert gas (TIG) cladding, is a precise welding technique utilised to deposit a shielding layer of material onto the outer surface of a base metal. In the GTAW cladding process, the cladding material is melted and then allowed to solidify, resulting in the formation of a protective layer on the base metal's surface. The coating layer exhibits exceptional resistance against corrosion, abrasion, and various types of wear, resulting in an elongated lifespan of the structure or component. Gas Tungsten Arc Welding (GTAW) cladding provides several advantages, such as improved resistance to corrosion, enhanced wear resistance, and increased durability[54], [55] The GTAW cladding process commences with meticulous cleaning and preparation of the workpiece to eliminate all impurities and surface contaminants. The aforementioned step is of utmost importance to attain a robust metallurgical connection between the underlying metal and the cladding substance. Subsequently, the welder precisely regulates the heat input through the manipulation of welding current and travel speed. The implementation of this control is crucial in order to avoid overheating, as it may result in deformation or other metallurgical complications. In order to mitigate the risk of base metal deformation, it is imperative to minimise the heat-affected zone (HAZ)[53], [54], [56] Figure 15 describes the schematic diagram of TIG cladding[55].

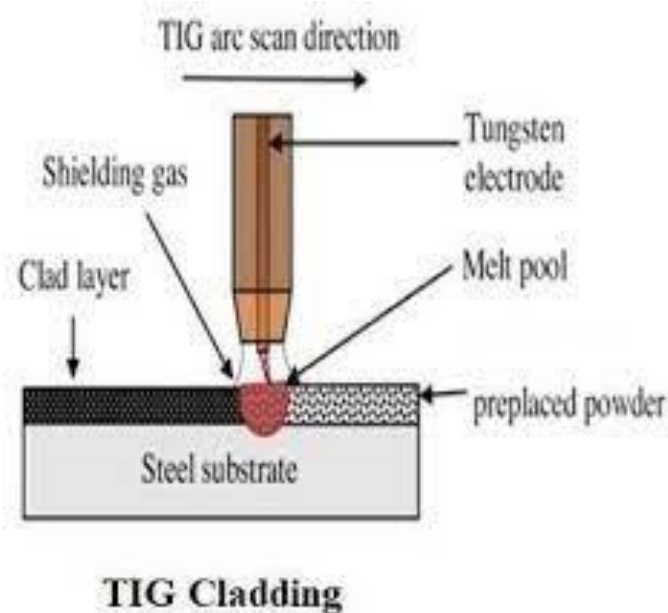


*Figure 15 Schematic diagram of TIG welding*

During the process, the welder introduces cladding material, which can be in the form of a wire or rod, into the molten weld pool as they move the torch along the workpiece. The selection of cladding material is dependent upon the desired characteristics and specifications of the end product. Stainless steel, nickel-based alloys, and cobalt-based alloys are among the frequently used cladding materials[57] Gas tungsten arc welding (GTAW) cladding is a commonly employed technique across multiple industries such as oil and gas, chemical processing, power generation, and aerospace. This feature is advantageous in scenarios where the underlying metal is required to withstand severe surroundings or challenging operational circumstances.

## **GTAW Welding**

Gas tungsten arc welding (GTAW), commonly referred to as TIG welding, is a welding process that employs a non-consumable tungsten electrode to generate an arc between the electrode and the workpiece. The welding process involves the generation of heat through an arc, which is utilised to melt the base metal and subsequently create a weld joint. This technology is utilised in diverse sectors such as construction, aerospace, and automotive manufacturing. During this process, the fusion region is prevented from contamination by the utilisation of a shielding gas, which is commonly either argon or helium. TIG welding results in a weld that is of high quality is exact, can be used to weld materials of a thin thickness, and offers superior control over the weld bead. The power source, tungsten electrode, shielding gas, filler material, and workpiece are the essential components of the TIG welding procedure. The current required to create an arc between the tungsten electrode and the workpiece is supplied by the power source. The tungsten electrode is non-consumable and remains constant for the duration of the welding procedure. The shielding gas prevents atmospheric gases from penetrating the fusion zone, protecting it from contamination. The filler material is used to add material to the weld, and the material being welded is the workpiece. TIG welding's capability to produce precise, high-quality welds is one of its most important advantages. This is a result of the welder's control over the heat input and the extent of the weld basin. In addition, the use of a non-consumable tungsten electrode reduces the quantity of heat introduced into the workpiece, minimizing distortion and producing a clear, precise weld[4], [8], [58], [59]. Figure 16 demonstrates the schematic representation of TIG welding [60]

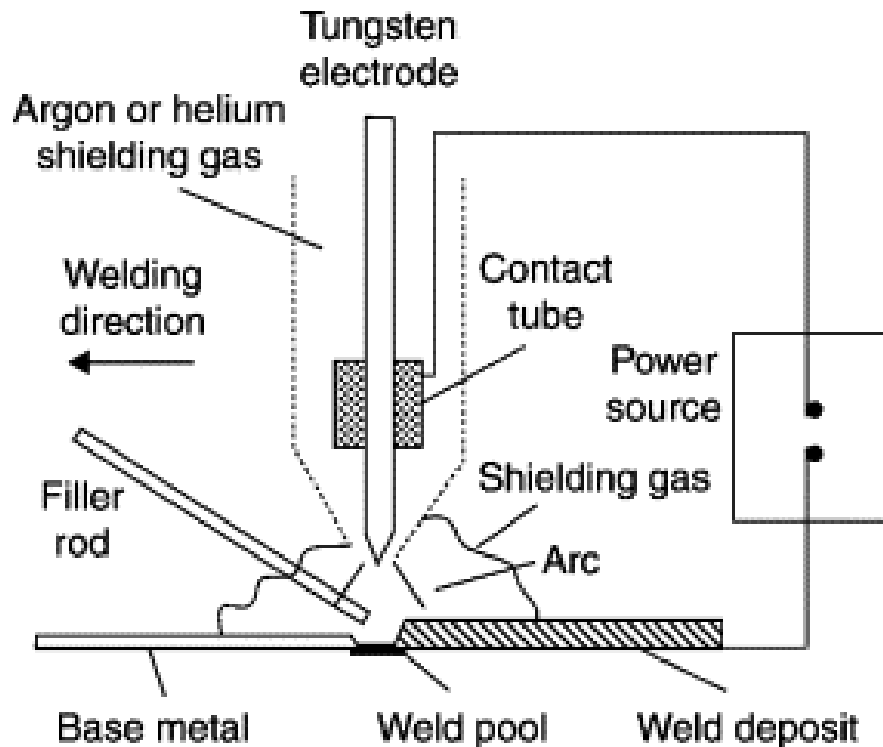


Figure 16 Schematic representation of TIG welding

The versatility of TIG welding is another advantage. This method can be used to weld a variety of materials, such as stainless steel, aluminium, copper, and titanium. Because it generates a small heat-affected zone and reduces the possibility of warping or burning through the material, TIG welding is ideally suited for welding thin materials. However, TIG welding does have some limitations. This method is slower than other types of welding, such as MIG welding, which can be a disadvantage in environments with high production rates. In addition, TIG welding requires a higher level of expertise and experience than other welding techniques, making it more difficult for novice welders to master. Welding input process parameters serve a crucial role in determining the quality or mechanical properties of the welded joint, such as hardness, tensile strength, fatigue strength, etc. [3], [58], [61]. Consequently, the correct selection of welding process parameters and their levels is crucial for achieving optimal mechanical properties. TIG welding is an excellent method for generating high-quality, precise welds on a variety of materials. Its adaptability and control make it a popular choice in numerous industries, especially for applications requiring the highest quality[62], [63].

## Laser Welding

Laser welding is a high-precision welding technique that employs a laser beam to melt and weld two or more metal components. A high-energy laser beam is focused on the joint area, causing the metal to melt and then solidify as it cools, producing a strong

bond. The laser welding procedure consists of several distinct stages. Preparing the materials to be welded involves scrubbing and positioning the components to ensure a precise fit. The laser beam is then focused on the joint, and the beam's energy causes the metal to dissolve. As the molten metal cools, it solidifies and forms a strong bond. Laser welding techniques include conduction welding, deep penetration welding, and keyhole welding. Thin materials or components requiring a small weld depth are welded using the most common method, conduction welding. For thicker materials, deep penetration welding is utilised, whereas keyhole welding is utilised for extremely thick materials. It has several advantages, including high precision, low heat input, and minimal distortion. In addition to metals, plastics, and ceramics, laser welding can be performed on a wide variety of materials. Among others, the process is widely utilised in the automotive, aerospace, and electronics industries [8], [64], [65]. Laser welding is a high-precision welding technique that offers several advantages over conventional welding techniques. It is widely used in the automotive, aerospace, and electronics industries, among others, and has been shown to produce minimally flawed, high-quality welds.

## 1.8. Challenges in welding of Fe-Mn-Al-C

When welding steels such as Fe-Mn-Al-C alloys, several challenges need to be considered and addressed. One of the challenges is the potential evaporation of manganese (Mn) in the fusion zone, which can have an impact on local deformation mechanisms. As the temperature increases, the vapour pressure of Mn also rises. To control the evaporation of Mn, it is possible to modify the instantaneous power input during welding. Another factor to consider is the precipitation of  $\kappa$ -carbide at grain boundaries. This precipitation can affect the mechanical properties of the welded joint. Additionally, deformation incompatibility can arise in duplex Fe-Mn-Al-C steels, leading to the formation of voids. Phase transformation-induced hardening or softening is another challenge associated with welding these steels. The phase transformations that occur during welding can result in changes in the hardness and strength of the material. Welding medium manganese Fe-Mn-Al-C alloys and other high-advanced steels like TRIP-TRIP, TRIP-HSLA, and TRIP-DP980 steels can produce efficient joint performance. It has been observed that laser welding has an impact on the mechanical properties of high-manganese Fe-Mn-Al-C steel welds, whereas beam welding does not show the same effect. In laser-welded high-manganese duplex Fe-Mn-Al-C steels, an incompletely melted zone can be observed in the welds. This zone is characterized by partial melting of the ferrite and complete melting of the austenite matrix, leading to the formation of precipitates. Despite ongoing research, there is still much to learn about the complete potential of laser welding for these steels [47], [48]. Further studies are needed to explore and understand the intricacies of laser welding in relation to Fe-Mn-Al-C alloys. In summary, welding Fe-Mn-Al-C steels poses challenges related to local deformation mechanisms, Mn evaporation,  $\kappa$ -carbide precipitation, deformation

incompatibility, and phase transformation-induced hardening or softening. However, advancements in welding techniques can lead to efficient joint performance, and ongoing research is focused on uncovering the full potential of laser welding for these steels.

## 2. Experimental Work

The primary purpose of this work is to examine the microstructure, and mechanical characteristics of laser and GTAW welded joints of a particular Fe-Mn-Al-C lightweight steel. The material received was a 5-mm-thick, hot-rolled, water-quenched plate as part of the European RFCS initiative "DELIGHTED." Using analytical instruments, namely optical emission spectroscopy (OES), the steel's elemental composition was determined. Changes in austenitic particle size, the precipitation of coherent and noncoherent k-carbides, and the resulting changes in mechanical properties were anticipated to be distinguishable aspects of the alloy's chemistry. Table 3 shows the actual composition of Fe-Mn-Al-C lightweight steel.

Elements	C	Si	Mn	P	S	Al	Cr
HR-J	0.613	0.086	30.60	<0.0005	0.016	8.256	0.045
HR-K	0.611	0.082	29.16	0.0088	0.018	8.084	0.095
SOL-J	0.522	0.083	30.48	<0.0005	0.017	7.936	0.047
SOL-K	0.528	0.079	29.06	0.0089	0.018	8.373	0.094

Table 3 Chemical composition of Fe-Mn-Al-C lightweight steel

The experimental strategy intended to evaluate the microstructural condition and mechanical performance of the material using two distinct heat treatment conditions, namely hot rolling and solubilisation. GTAW and laser welding were performed on each of the heat-treated materials, with GTAW welding further subdivided by welding current modes, i.e., AC and DC welding procedures. The cladding was performed before the actual welding process as a preparatory stage. Therefore, each sample was expected to have distinct microstructures as well as distinct mechanical properties. The sample was mounted, grinded, and polished in order to conduct microstructural and mechanical tests. The microstructural properties were exhaustively defined using analytical techniques such as optical microscopy (OM), scanning electron microscopy (SEM), electron diffraction spectroscopy (EDS), and electron backscatter diffraction (EBSD).

Vickers microhardness testing was selected as one of the best methods for measuring the hardness of various types of steel based on microstructure observations. Lastly, stress vs strain graphs derived from tensile testing of chosen samples was shown.

## 2.1. Design of Experiment

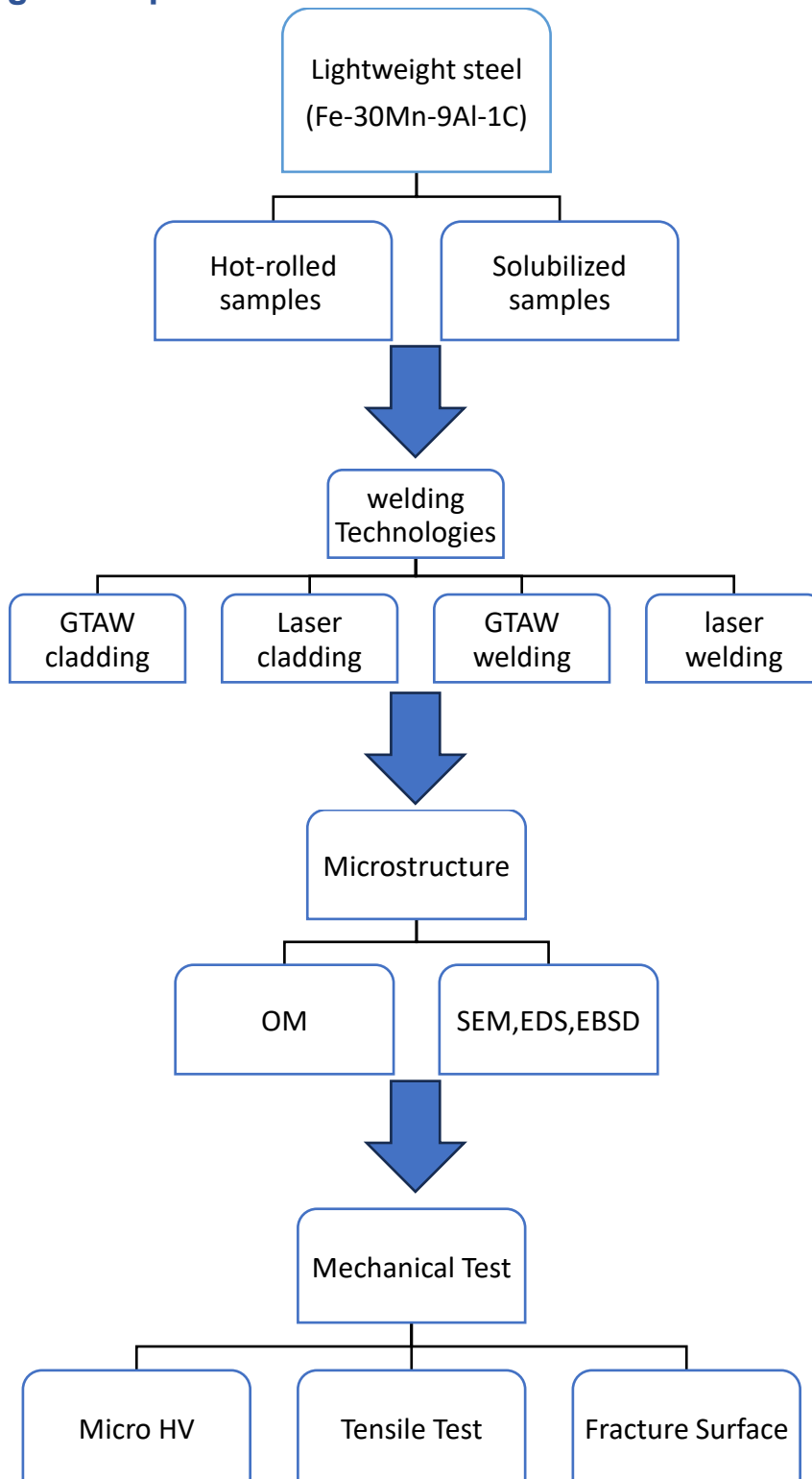


Figure 17 Design of Experiments

## 2.2. Sample Preparation:

The first stage in the preparation procedure is mounting, which involves the specimen to a mount for easy handling and subsequent processing. This process ensures that the specimen's structural elements remain intact and that the surface is free from scratches and distortion. Thermoset polymeric resin and a hot mounting tool manufactured by Hitech Europe EP 15 were utilised to complete this task. It was possible to create pastilles with a diameter of about 30 mm. (Figure 18) demonstrates a hot-rolled sample after embedding.



*Figure 18 Hot rolled samples after embedding.*

The saw marks are removed, the surface is levelled, and it is cleaned after the mounting process, which is followed by grinding of the specimens. Grinding is necessary in order to obtain a surface with a minimum of damage and to get it prepared for further examination. This procedure assists in generating a smooth and level surface, which is necessary for subsequent testing. After starting with a roughness of 200  $\mu\text{m}$ , the surface of the sample is ground down to a roughness of 10  $\mu\text{m}$  using rotating plates made of silicon carbide and using water as a lubricant. During the grinding procedures, Metkon Forcipol V and Hitech Europe MP311T metallographic grinder were both utilised. Following the completion of the grinding step, the next step is surface polishing. The objective of polishing is to refine the specimen's surface, eliminate any marks left by grinding, and create a mirror-like finish that enables precise microstructural observation. It is done in three stages using rotating cloth plates and a diamond suspension lubricant. Each stage corresponds to a different level of surface roughness, such as 6  $\mu\text{m}$ , 3  $\mu\text{m}$ , and 1  $\mu\text{m}$ , and it was done using a Hitech Europe MP22V metallographic polishing machine.

After the grinding process, the surfaces were given a thorough cleaning with the assistance of flowing water. In between each of the many stages of completion, the same procedure was carried out. In order to facilitate a microscopic examination of the surface, a chemical etching with a solution called Nital 10% (10% nitric acid, 90% ethanol) was performed. The composition of the solution was proposed by the



research group at Politecnico di Milano that was researching these types of steels, and it was ultimately chosen to be used. The optimal amount of time spent submerged in Nital 10% solution was found to be between 30 and 50 seconds.

## **2.3. Test and Analysis**

In the study aimed at determining the microstructure and mechanical properties of laser and GTAW-welded joints of a particular lightweight steel alloy, a variety of techniques were used to determine the sample properties. These techniques consisted of optical microscopy, scanning electron microscopy, micro-hardness tests, and tensile testing.

Using optical emission spectroscopy (OES), the composition of the alloy was determined to initiate the investigation. This method of analysis involves determining the emission spectrum emitted by the substance. By analysing the emitted spectrum, the elemental composition of the substance can be determined. This preliminary step allows to determine the alloy's composition prior to conducting a thorough examination of the samples. The primary objective of the study was to obtain a better understanding of the microstructure and mechanical properties of laser and GTAW-welded joints formed with lightweight steel alloys. Understanding the microstructure is essential because it provides information about the arrangement, distribution, and size of the material's numerous components. On the other hand, evaluating the mechanical properties, such as hardness and tensile strength, helps in determining the performance of the material under various loading conditions.

### **Optical Microscopy:**

The utilization of an optical microscope, enabled the examination of various material samples to analyze their microstructure. The images of the samples were captured with a Nikon Eclipse LV150NL optical microscope, a Nikon Digital Sight DS-U3 camera, and Nikon NIS Elements v4.60 software. The microstructure of the samples was analyzed with the help of the photographs, which were captured at several magnifications ranging from 25 to 500 times their original size. The pictures obtained from the optical microscope were processed with the ImageJ application to determine the typical grain size. In general, the procedure offers a method that is both comprehensive and consistent for analysing the microstructure of different materials employing optical microscopy.

### **SEM, EDS and EBSD**

Scanning electron microscopy (SEM) is a common technique for investigating the morphology and microstructure of materials. SEM analysis was conducted using a Zeiss Sigma500 field emission microscope. This advanced microscope has imaging capabilities with a high resolution, making it suitable for the study of secondary phases

and carbide precipitation. SEM provides substantially greater magnification than optical microscopy, allowing for a more thorough examination of the microstructure of materials. 1000x, 5000x, and 10000x magnifications were chosen for the SEM analysis because they are commonly used for such studies and permit a comprehensive evaluation of the investigated materials. The SEM analysis was especially helpful for examining the structure and distribution of secondary phases and carbides in the material. By investigating these characteristics, it could gain insight into the effect of processing techniques and heat treatment on the microstructure and properties of the material. In addition, Energy-Dispersive X-ray Spectroscopy (EDS) analysis was utilised to qualitatively differentiate the subsequent phases of the samples under study. EDS determines the elemental composition of a material by analysing the characteristic X-rays emitted when an electron beam hits the sample. In addition, Electron Backscatter Diffraction (EBSD) analysis was used to investigate the average misorientation of grains and the crystallographic properties of the secondary phases identified by SEM examination. The ability to map crystallographic orientation and grain boundaries within the sample makes EBSD an effective tool for determining the crystal structure and orientation of materials. In addition to microstructure analysis, a Zeiss Evo50 thermionic microscope was used to investigate the fracture surfaces of tensile test specimens. At various magnifications, including 500x, 1000x, 3000x, and 7000x, the fracture surfaces were observed. This examination revealed the fracture characteristics and behaviour of the material under tensile loading conditions.

### **Vickers micro-hardness tests**

The Vickers microhardness test is a widely employed method for measuring the microscale hardness of a material. During a Vickers microhardness test, a diamond indenter with a square base is pressed into the surface of the material under a predetermined load. The experiments were conducted using a Future-Tech FM-810 micro-hardness tester in accordance with the ASTM E92-17 standard for Vickers and Knoop hardness testing of metallic materials. The load and measurement regions were chosen based on the standard, and a load of 1000 g and 300 g were employed. The hardness of the material is determined by measuring the size of the indentation produced by the indenter. There was a 15-second interval of idleness, and each sample was measured three times for statistical significance. The Vickers microhardness test offers several advantages over other hardness testing methods. Firstly, it can be performed on a small scale, allowing for localized hardness measurements and examination of different regions within a material. By conducting Vickers microhardness tests on the samples, data were gathered on the material's hardness distribution and variations at a microscopic level. This information has a significant effect on understanding the mechanical behaviour and performance of the laser, and GTAW welded joints in the lightweight steel alloy under investigation.

The experiment follows ASTM standards, specifically regarding the distance between indentations and the distance from the centre of the indentation to the edge of the specimen. These distances are required to be greater than 2.5 times the diameter of the indent. The experiment adheres to ASTM standards, which dictate that the distance between indentations and the distance from the centre of the indentation to the edge of the specimen must be greater than 2.5 times the diameter of the indent. The experiment adheres to ASTM standards, which dictate that the distance between indentations and the distance from the centre of the indentation to the edge of the specimen must be greater than 2.5 times the diameter of the indent as shown in table 4.

Standard	Distance between indentations	Distance from the centre of the indentation to the edge of the specimen
SO 6507-1	$> 3 \cdot d$ for steel and copper alloys and $> 6 \cdot d$ for light metals	$2.5 \cdot d$ for steel and copper alloys and $> 3 \cdot d$ for light metals
ASTM E384	$2.5 \cdot d$	$2.5 \cdot d$

Table 4 ASTM standard, which is utilized for microhardness test

## Tensile tests

Tensile testing is a fundamental mechanical test used to evaluate the properties of steel and other materials. This test consists of subjecting a standard test specimen of steel to a controlled tension until failure, yielding valuable information regarding its mechanical behaviour. The test measures parameters indicative of the material's mechanical properties, such as ultimate tensile strength, yield strength, maximal elongation, and area reduction [8], [15]. During a steel tensile test, the test specimen is typically shaped like a dog bone, with a narrower "necked" region in the middle and wider extremities for gripping [66]. This shape encourages failure in the monitored region, making it simpler to analyse the fracture surface in that particular area. Various standards, such as EN 10 002, which provides guidelines for tensile testing of steel, define the dimensions and geometry of the specimen to be tested. Fracture surface analysis is an essential component of tensile testing, as it permits the examination of the material's fracture surface. By analysing the fracture surface, one can obtain valuable information regarding the type of fracture, the location of fracture initiation, and the failure characteristics. In the case of steel, the fracture surface can display distinct characteristics, such as ductile dimples or brittle characteristics, which provide insight into the material's behaviour under tension. The fracture surface can be examined using various methods, such as scanning electron microscopy (SEM) and optical microscopy. These techniques provide high-resolution imaging capabilities, enabling the observation and analysis of the fracture morphology in great detail.

Commonly, SEM is utilised to determine the size and nature of inclusions or defects that may have contributed to the fracture [4], [39], [67] Regarding tensile testing standards, numerous organisations and standards bodies provide guidelines to ensure consistent and reliable testing procedures. For conducting tensile tests on steel, standards such as ASTM E8/E8M define the procedures and requirements. To assure accurate and comparable results, these standards cover specimen preparation, test equipment specifications, test methods, and result reporting. Figure 19 shows the draft of the specimen used for tensile testing.

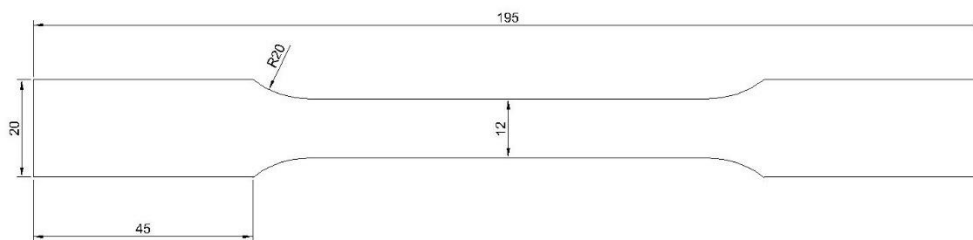


Figure 19 Draft of the specimen adopted for tensile tests.

In conclusion, the tensile test is widely used to evaluate the material's mechanical qualities. The specimen is subjected to regulated tension until it breaks. Fracture surface analysis is essential for comprehending the failure mechanisms and fracture characteristics. By analysing the fracture surface with techniques such as SEM, valuable information about the fracture type, initiation points, and the presence of defects or inclusions can be obtained. Steel tensile testing is governed by standards such as ASTM E8/E8M which ensure consistent and reliable testing procedures.

## **3. Results:**

In this chapter, the key findings of the study are summarised, and the results of the conducted analyses are presented and briefly discussed. This includes the examination of all generated samples, optical micrographs, and hardness values. In addition, stress versus strain curve results derived from tensile testing of selected specimens are presented.

### **3.1. Microstructure Evolution:**

This section provides a presentation of the microstructural evolution in relation to the specific thermo-mechanical processing applied. An experimental strategy intended to evaluate the microstructural condition and mechanical performance of the material using two distinct heat treatment conditions, namely hot rolling and solubilisation. GTAW and laser welding were performed on each of the heat-treated materials, with GTAW welding further subdivided by welding current modes, i.e., AC and DC welding procedures. Each subsection contains relevant information, such as optical micrographs and hardness data. For a comprehensive collection of optical micrograph images, please refer to Appendix. To illustrate the relationship between the microstructural evolution and micro-HV (micro-hardness) results, graphical maps were generated. However, in Chapter 4, the SEM (scanning electron microscopy), EDS (energy-dispersive X-ray spectroscopy), and EBSD (electron backscatter diffraction) outputs are utilized to support the discussion of the observed features. Please be aware that these SEM, EDS, and EBSD outputs are not specifically presented in this particular section.

Initially, heat-treated samples are divided into solubilized and hot-rolled samples. This division allows for a comprehensive understanding of the microstructure of the samples before any welding is performed. By studying the microstructural evolution of both cases, valuable insights are gained regarding the initial state of the samples and how they may behave during the welding process. Figure 20 and Figure 21 demonstrates the optical micrographs of hot-rolled and solubilized condition with a magnification of 500x.

## Hot-rolled Condition

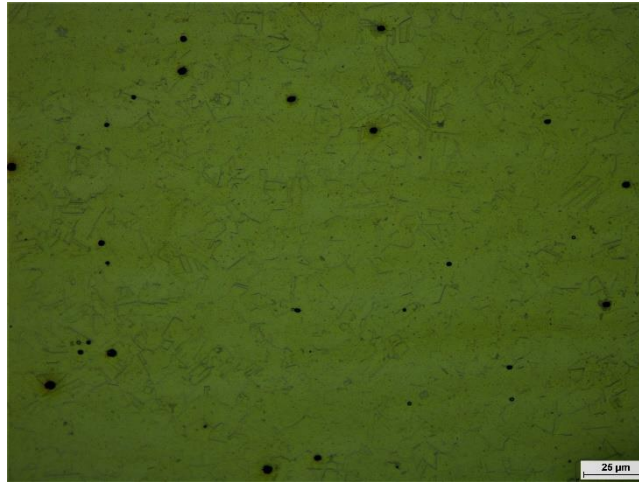


*Figure 20 Optical micrograph of Hot-rolled case (500x)*

The Fe-30Mn-9Al-1C alloy exhibits equiaxial and randomly oriented austenitic grains. In terms of plastic deformation mechanisms, the presence of twin boundaries and deformation micro-bands suggests the dominant influence of two specific mechanisms: Twinning Induced Plasticity (TWIP) and Microband Induced Plasticity (MBIP). Furthermore, it is observed that the hot-rolled condition of the alloy typically exhibits finer grains compared to the solubilized condition. The hot rolling process, involving deformation at elevated temperatures, promotes dynamic recrystallization, leading to the formation of smaller, more equiaxed grains.

## Solubilized Condition :

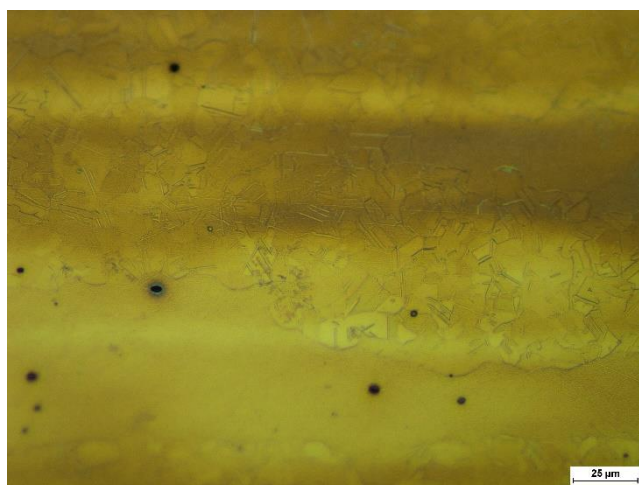


*Figure 21 Optical micrograph of Solubilized sample (500x)*

From the optical micrographs, it is evident that the sample exhibits equiaxial and randomly oriented austenitic grains. There is an extensive presence of twin boundaries. It can be formed during plastic deformation or due to specific crystallographic orientations in the material. It is found that grain size is coarse.

## **TIG Cladded Plate**

In a cladded joint, similar to a welded joint, the joint can be divided into three zones: the fusion zone, the heat-affected zone, and the base zone, as shown in Figure 22 and Figure 23. Understanding the microstructural changes and characteristics of these zones is crucial for assessing the mechanical properties and integrity of the cladded joint. In the welded zone, long dendritic structures are observed under an optical microscope. These dendrites form as the molten material solidifies, and their presence indicates the solidification front. The microstructure of the HAZ may exhibit some alterations compared to both the welded zone and the base metal, depending on the specific heat input and cooling rate. These changes can include grain growth, precipitation of secondary phases, and changes in hardness. Understanding the microstructural characteristics of each zone in a cladded joint helps in predicting the mechanical properties, such as strength, toughness, and corrosion resistance, of the joint. It also assists in evaluating the integrity and performance of the cladded joint in various applications. In AC cladding, the weld pool tends to be shallower compared to DC cladding. The cladded and HAZ regions were measured with the use of imageJ software. Table 5 demonstrates the Dimensions of fusion and HAZ regions of GTAW cladded samples.

This is primarily due to the alternating current polarity, which causes a less concentrated heat input and a more balanced distribution of heat between the electrode and the workpiece. As a result, the depth of penetration into the base material is generally reduced in AC welding compared to DC welding. In DC welding, the weld pool is typically deeper. With direct current, the heat is concentrated at the point of contact between the electrode and the workpiece, leading to more localized and intense heat input. This results in a deeper weld penetration into the base material. In DC welding, the HAZ area is generally larger compared to AC welding. The concentrated heat input in DC welding causes a more significant thermal influence on the base material, resulting in a broader HAZ. In AC welding, the heat input is more evenly distributed due to the alternating current polarity. As a result, the thermal effects on the base material are less concentrated, leading to a comparatively smaller HAZ area. Additionally, twinning can be observed in both the HAZ and base material zone. Twinning is a crystallographic phenomenon where certain regions of the material exhibit a mirror image-like arrangement of atoms. This twinning is a result of the stress and strain experienced during the cladding process. The presence of equiaxed grains

indicates that they have a similar size in all directions, while the random orientation suggests that the grains are not aligned in any specific direction. The base material region exhibits a variety of microstructural characteristics, such as elongated dendrites and small equiaxial grains. Additionally, the grain size in this region is finer than that of the Heat Affected Zone (HAZ).

Dimension	DC Cladded Plate ( $\mu\text{m}$ )	AC Cladded Plate ( $\mu\text{m}$ )
Cladding pool Width	7204.05	6830.45
Cladding pool height above the plate (From centre to top)	1562.34	1338.54
the plate from centre to bottom	1169.54	707.24
Heat Affected Zone thickness Radial	817.64	548.98

Table 5 Dimensions of fusion and HAZ regions of GTAW cladded samples

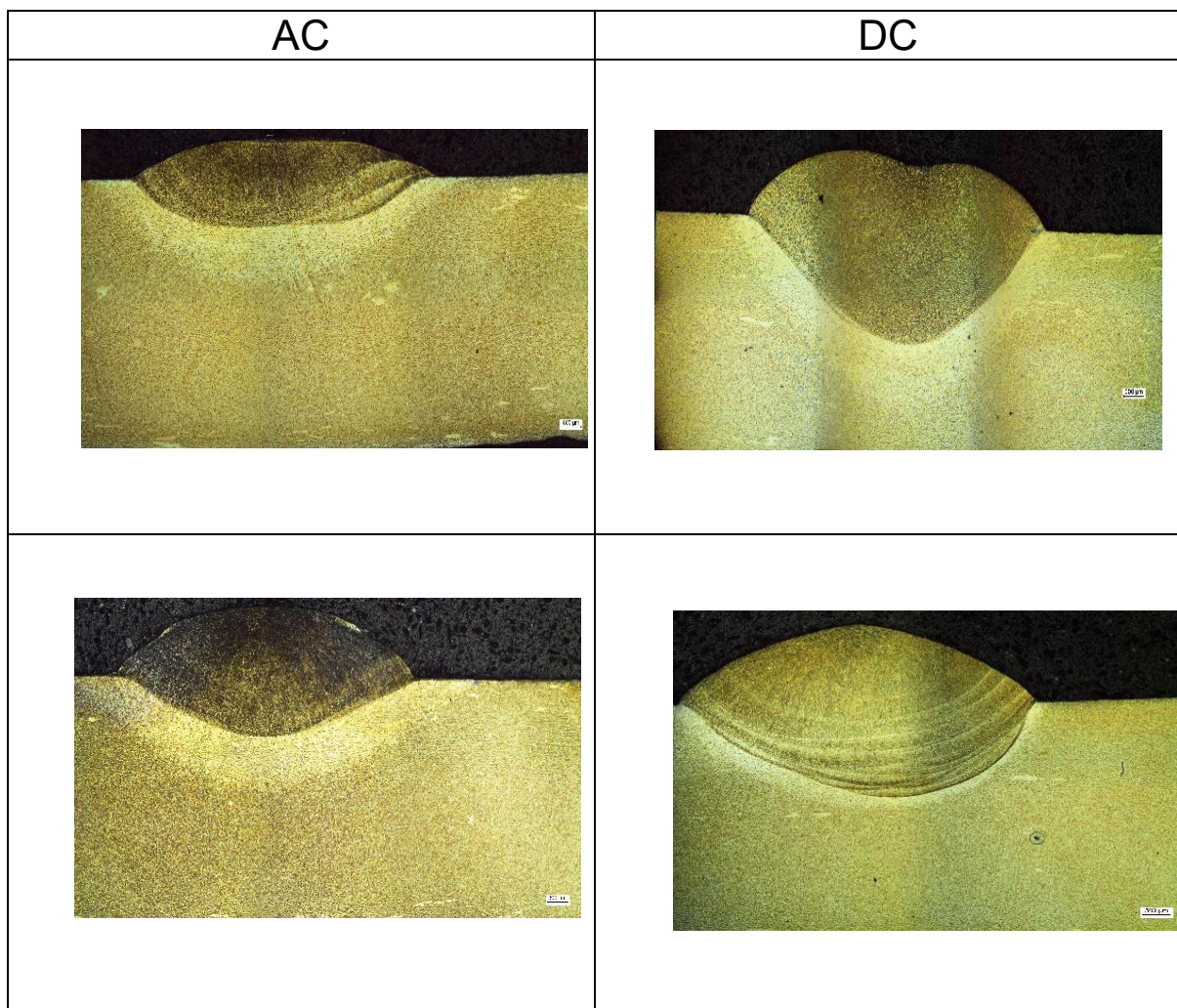


Figure 22 Optical micrograph of TIG cladded plate



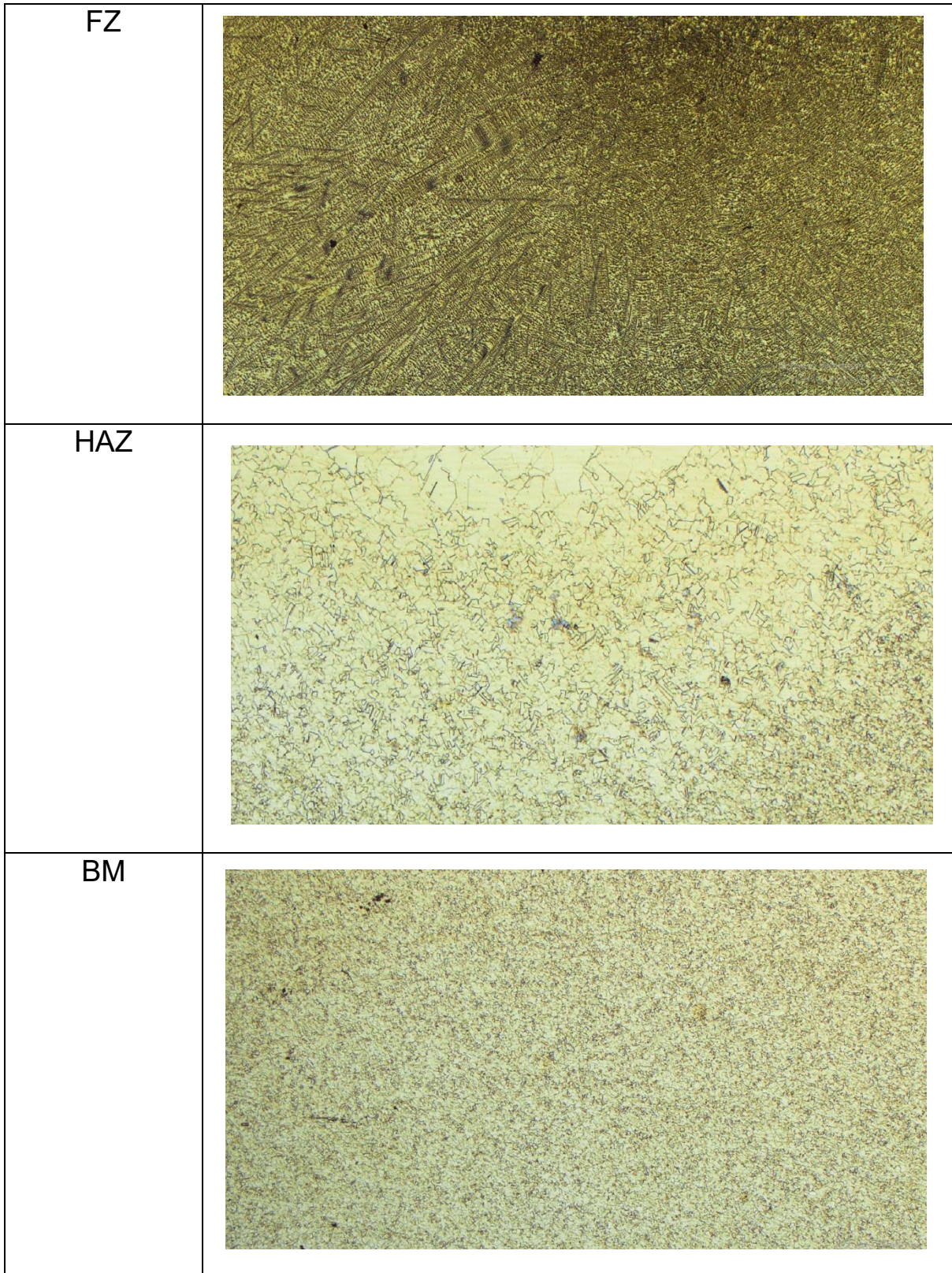


Figure 23 Magnified optical micrograph of DC cladded sample.

## Laser Beam on Plate

During the laser beam on the plate, similar to the TIG cladding process, the region is subdivided into distinct zones, each with unique and distinct properties. In the fusion zone, a number of noteworthy features can be observed. The laser beam interacts with the base material in the fusion zone, causing localised melting and subsequent solidification. This zone's rapid heating and cooling rates produce distinctive microstructural characteristics. As the molten substance solidifies, grains grow epitaxially. In the HAZ zone, the microstructural characteristics differ from those observed in the fusion zone. The HAZ experiences elevated temperatures during the laser cladding process but does not undergo complete melting. The HAZ can exhibit larger and coarser grain sizes compared to the base material and the fusion zone as shown in figure 24 and figure 25. This is primarily due to the heat input from the laser beam, which causes grain growth and coarsening in the HAZ. The elevated temperatures in the HAZ allow the existing grains to grow and recrystallize, resulting in a larger grain size compared to the base material. The base material part has a finer grain size than the fusion zone and heat-affected zone. This fine-grain structure strengthens and toughens the material. Base material also undergoes fine-grain twinning. Twinning is a crystallographic phenomenon when atoms are arranged in a mirror image. Twinned regions can impact the material's mechanical characteristics and deformation. The base material's microstructure determines its mechanical properties and laser cladding compatibility. Grain size and twinning can indicate laser-cladded component performance and integrity. This understanding is crucial for laser cladding applications and material attributes.

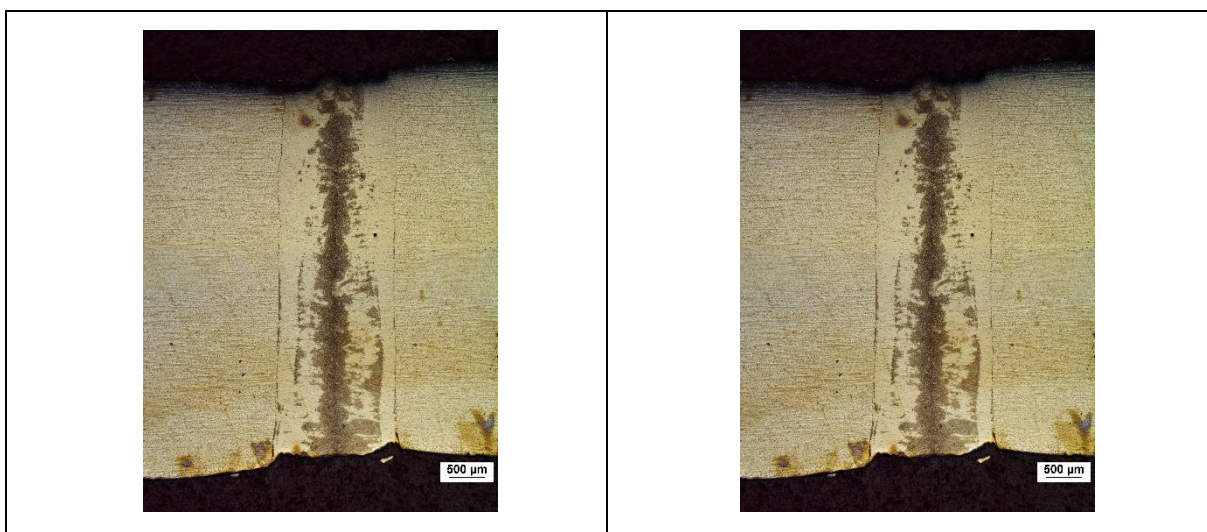


Figure 24 Optical micrograph of the laser beam on plate

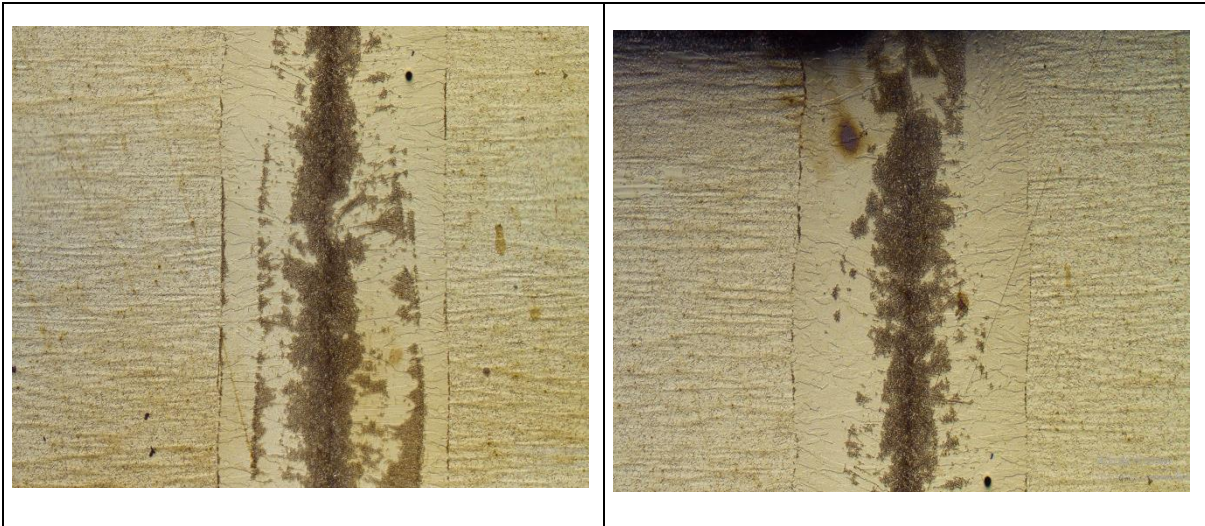


Figure 25 Magnified micrograph of the laser beam on the plate.

## TIG welded Plate

For better understanding, welded joint is divided into three sections, namely fusion zone (FZ), Heat affected zone (HAZ), and Base material (BM), as shown in Figure 26. In the fusion zone, the microstructure exhibits fine grain, which is due to the fact of rapid solidification during the welding process. It can be understood that finer grain depends on the rate of cooling rate. It is also noted that there is an increase in the grain boundary density, and it is due to the solidification process, which results in the formation of new grain boundaries. In the fusion zone, the formation of a dendritic structure grows from the solidification front, and it is easily visible from an optical microscope. As visible, the material inside the “FZ” has reacted differently to chemical etching. That could be due to a chemical inhomogeneity or a different microstructure (probably with very thin constituents). To verify such assumptions, a further investigation using SEM has been carried out. In HAZ, melting did not occur during the welding process can contribute to the formation of coarse grains in the heat-affected zone (HAZ), resulting in larger grain size. The slower cooling rate allows atoms to diffuse and rearrange, promoting the growth of existing grains in the base part and exhibiting microsegregation, where certain elements are unevenly distributed within the solidified structure( due to hot-rolled or solubilized conditions).

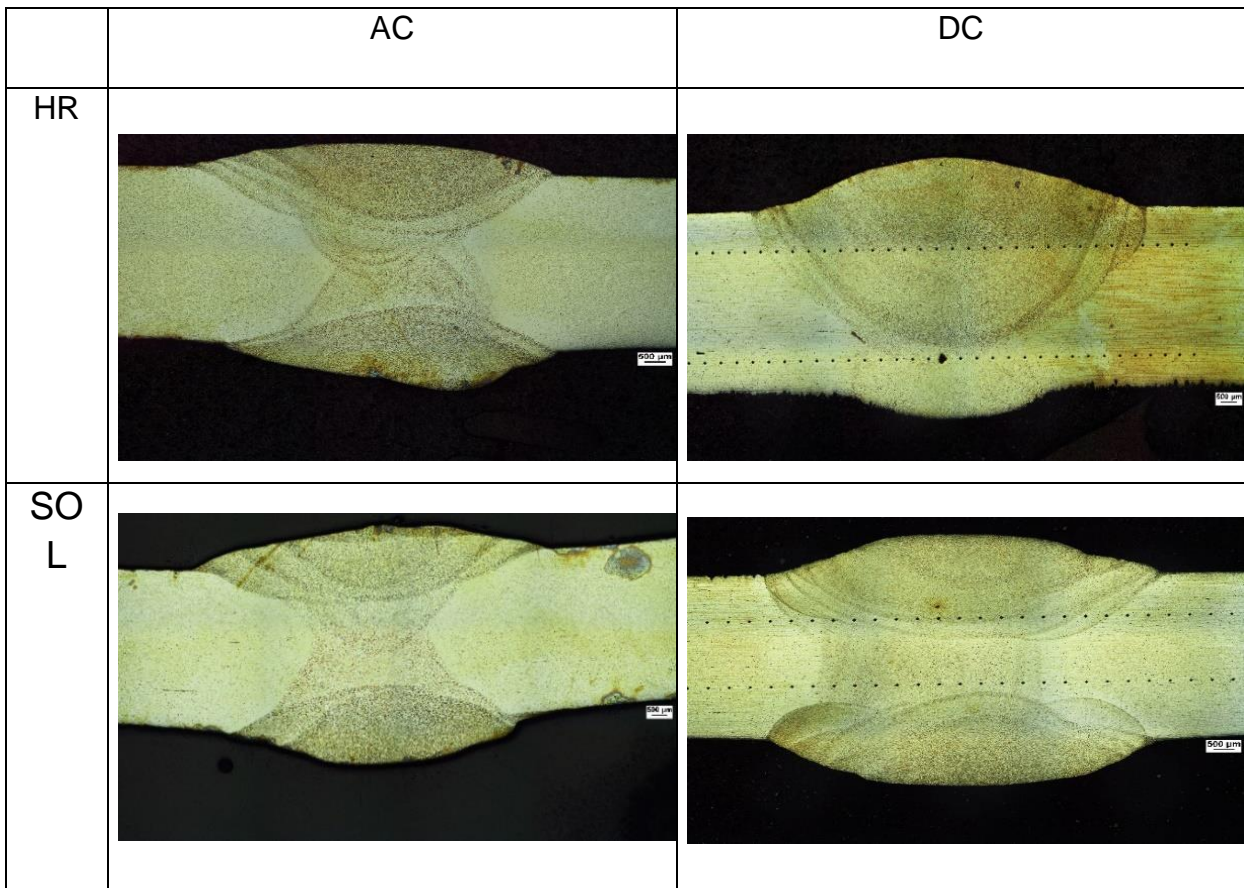


Figure 26 Optical micrograph of TIG welded plate

## Laser welded plate

In laser welding, three separate zones can potentially be identified by the different microstructures, i.e., the fusion region, the heat-affected zone (HAZ), and the base section shown in Figure 27. Long dendrites are seen as solidified structures created in the fusion zone during the cooling process of molten metal, and they can be detected in the fusion region. The quick cooling and solidification that takes place during the process of laser welding give rise to these dendrites. A fine-grained structure can be seen in the fusion region's microstructure as a result of the rapid cooling caused during the welding process. This fine-grained structure exhibits a columnar grain morphology that is aligned with the direction in which heat is moving through the material. The fusion region is the region where the two materials that are being welded together are united.

The heat-affected zone (HAZ) is located nearby the fusion region. When compared to the fusion region, the heat-affected zone (HAZ) region is not able to reach its melting point, which results in a coarser grain structure. The thermal cycling that occurs during welding can cause changes in the characteristics of the material, which can be caused by variations in the temperature of the heat-affected zone (HAZ). The base material part has a finer grain size than the fusion zone and heat-affected zone. This fine-grain structure strengthens and toughens the material. Base material also undergoes

fine grain and twinning. In this region, the microstructure and material properties remain the same (not affected by welding) due to being far from the welding zone.

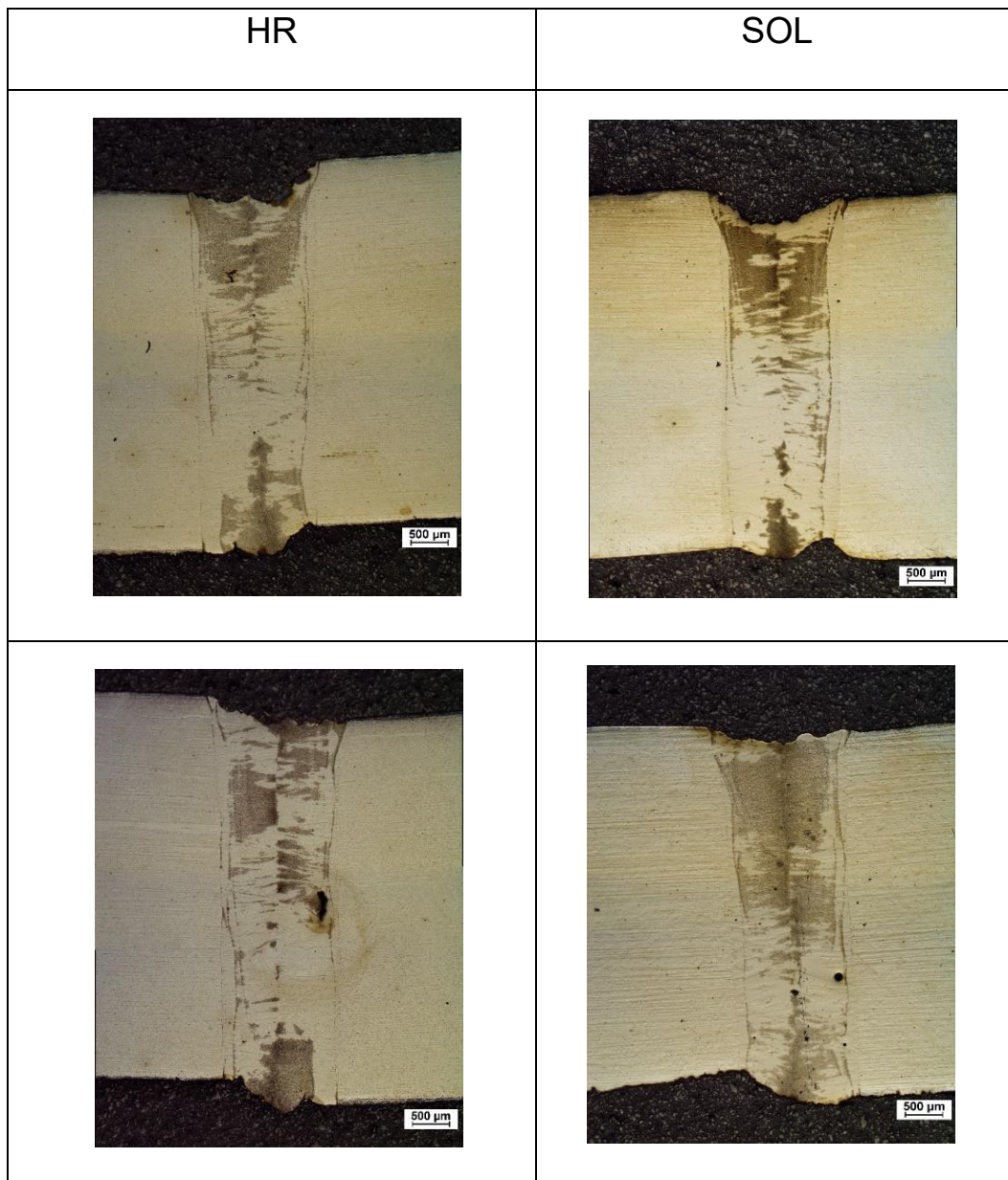


Figure 27 Optical micrograph of laser welded plate

### 3.2. Microhardness Test:

The investigation comprised the execution of microhardness tests on various samples before welding or cladding. The analysis was conducted on thermally treated samples, which revealed that the hardness of hot-rolled samples was greater than that of solubilized cases refer to (figure 28). Comparable results were achieved through

a microhardness examination of the samples carried out for the welding or cladding procedure. The specimens were categorised into three distinct areas, namely the welded region, the heat-affected zone (HAZ), and the base region. In different welding and cladding scenarios, the base region consistently displayed the highest levels of hardness. The superior hardness of the material can be attributed to various factors, including its inherent composition, previous heat treatments, and specific microstructural characteristics. Upon comparison between the fusion region and the Heat Affected Zone (HAZ), it was observed that the former consistently exhibited higher hardness. The aforementioned trend was detected in every instance of welding and cladding. The elevated hardness observed in the cladded region can be attributed to multiple factors. The process of cladding induces rapid solidification, which facilitates the development of finer microstructures and grain refinement. This, in turn, leads to an increase in hardness. The hardness of the cladded region is increased due to the introduction of a distinct material during cladding, as well as the dilution of the substrate material. The HAZ (Heat Affected Zone) region consistently demonstrated reduced hardness in comparison to the cladded region. The reason behind this phenomenon is the reduced cooling rates and the impact of thermal cycling that the heat-affected zone (HAZ) undergoes during the process of welding or cladding. The aforementioned factors contribute to the development of larger grains and alterations in microstructure, ultimately leading to a decrease in hardness. When comparing the Tungsten Inert Gas (TIG) cladding hardness results with the reference graphs (Figure 28), it is evident that the hardness values obtained for both Alternating Current (AC) and Direct Current (DC) cladding demonstrate analogous trends throughout all sections of the material. It can be inferred from the data that the current cladding modes exhibit minimal impact on the material's hardness. Figure 28 presents reference graphs that can be utilised to establish a baseline or anticipated range of hardness values for the material being evaluated. The conformity of results and any deviations or discrepancies can be identified by comparing the actual hardness values obtained through TIG cladding (as shown in Figure 29) with the reference graphs.

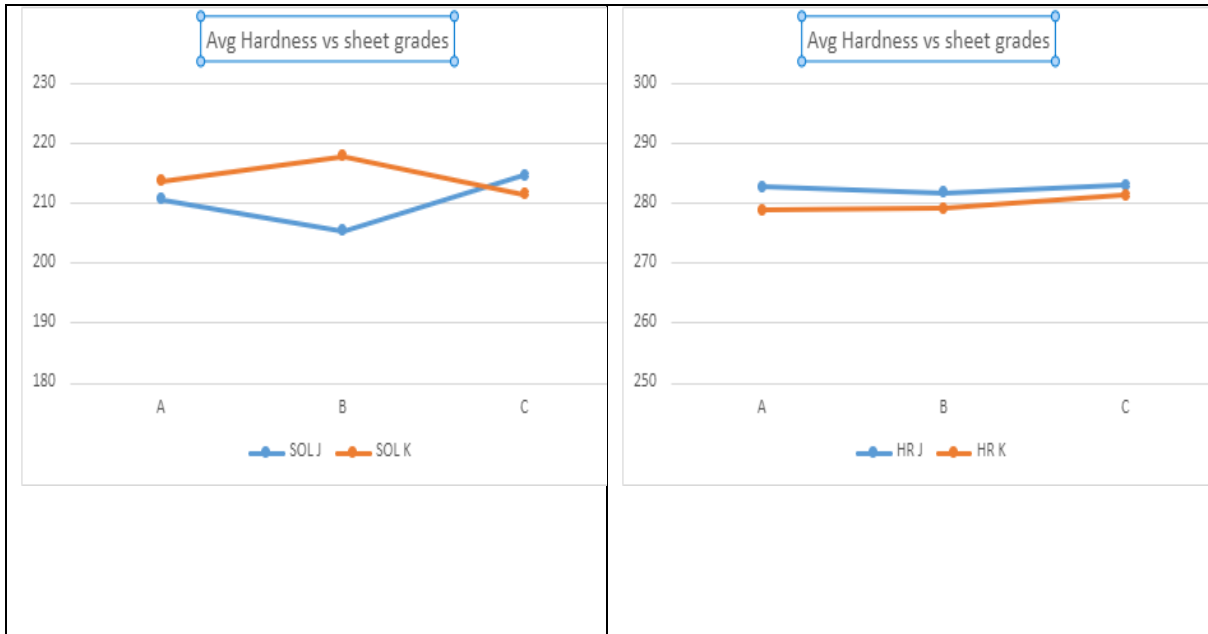
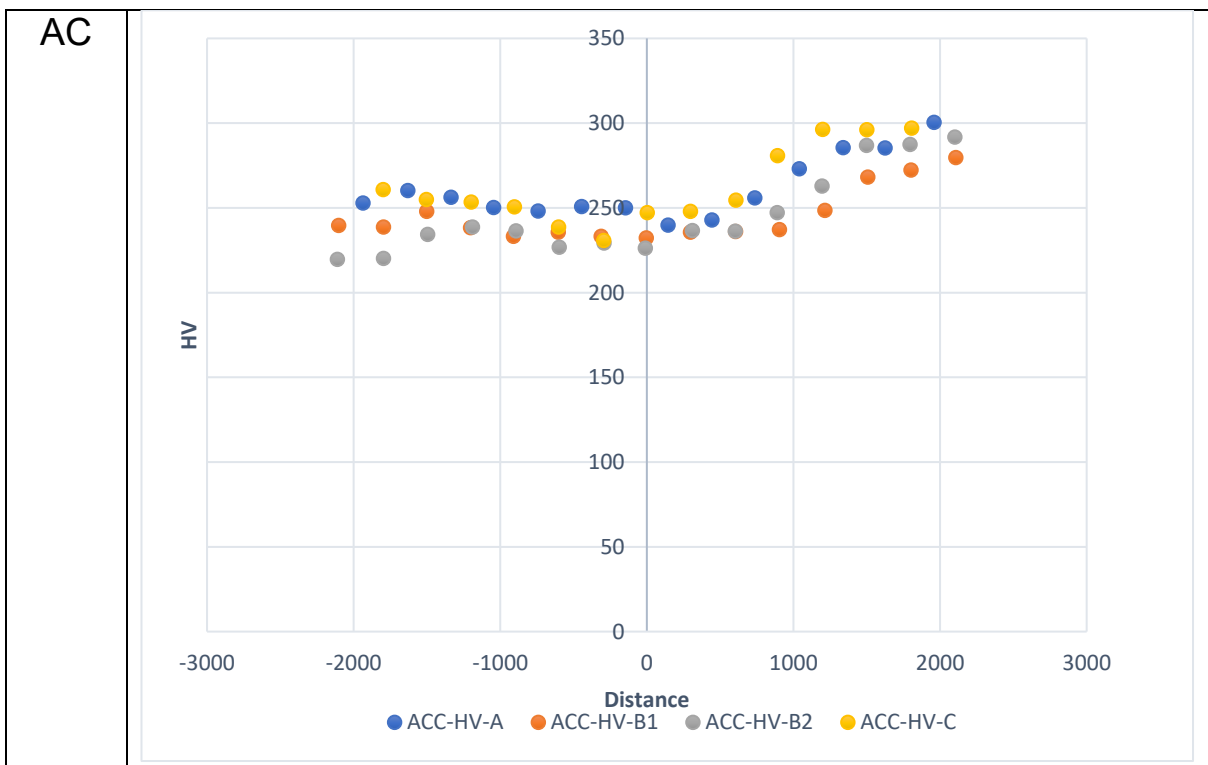


Figure 28 HV profile for HR and SOL condition for different sheet grades



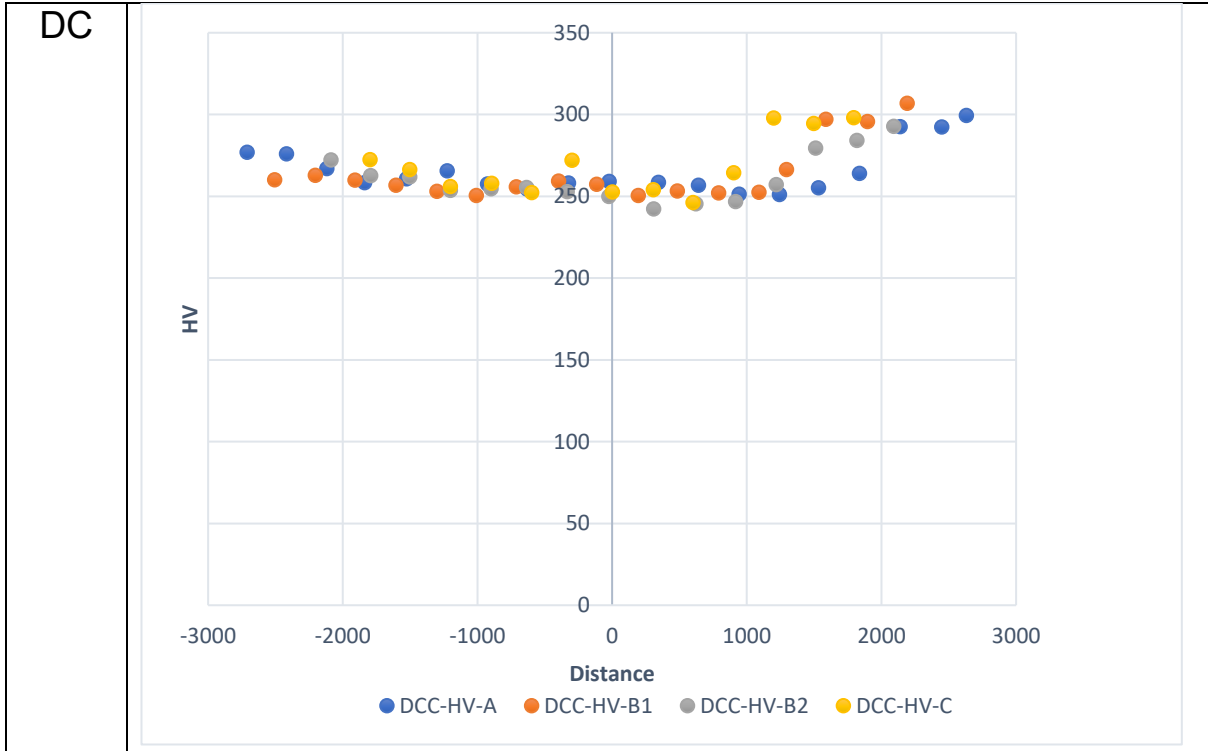


Figure 29 shows the variation of hardness value with the distance in TIG cladding.

Upon comparison of the HV profile of the laser beam on plate samples (as shown in Figure 30) with the reference graphs (as depicted in Figure 28), it can be observed that the overall results remain comparable. The base material's HV values exhibit certain deviations that may be attributed to defects. Base material defects can occur due to multiple factors, including impurities, inclusions, uneven heat distribution, or process parameters. Additional investigations should be carried out to determine the specific factors responsible for these variations.



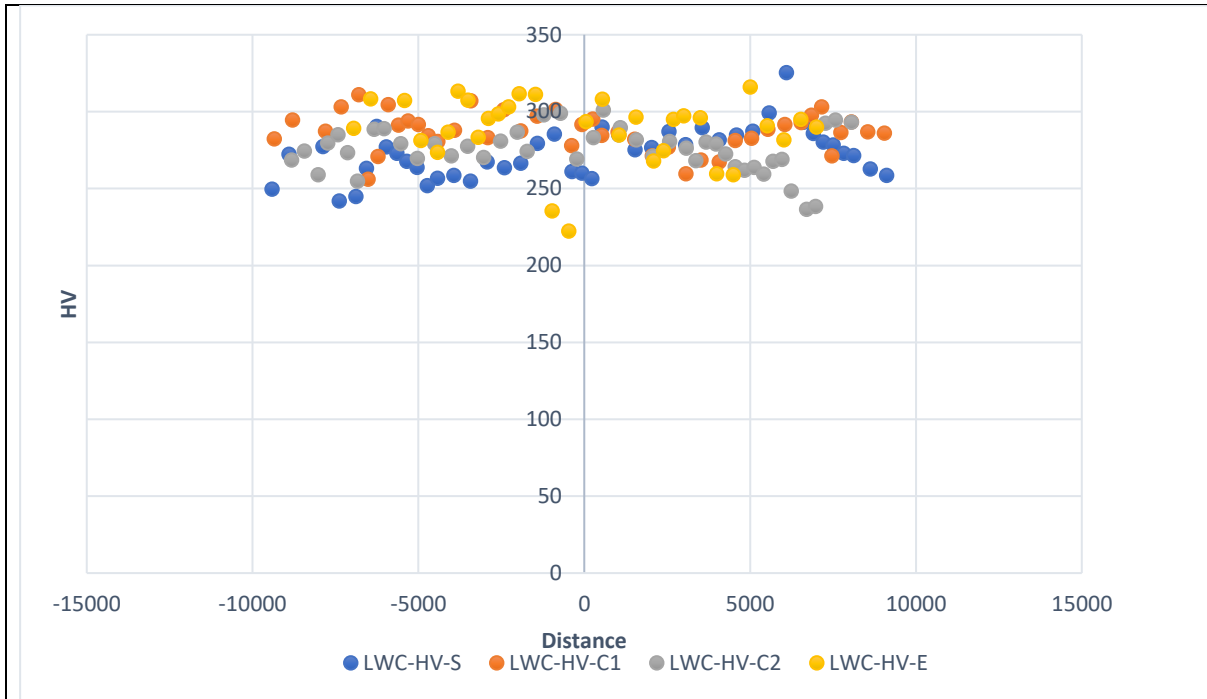


Figure 30 shows the variation of hardness value with the distance on the laser beam.

It is noteworthy to contrast the TIG welding results (Figures 31 and 32), which were obtained for both AC and DC modes, with the results for cladding (Figure 29) and the reference results (Figure 28). The results indicate that the hardness values obtained from Tungsten Inert Gas (TIG) welding exhibit an increase in comparison to the cladding results. However, they still demonstrate similar trends to the reference results. The rise in hardness values observed during Tungsten Inert Gas (TIG) welding can be attributed to the welding process. In Tungsten Inert Gas (TIG) welding, the material undergoes elevated temperatures and increased heat input in comparison to the cladding procedure. Elevated heat input may cause alterations in the microstructure of the material, which can result in variations in its hardness. It is noteworthy that the hardness trends from Tungsten Inert Gas (TIG) welding remain consistent with the reference graphs (Figure 28), despite the observed increase in hardness values. This indicates that the welding procedure has attained the desired level of hardness properties within an acceptable range.



Figure 31 shows hardness variation with distance in TIG AC welding.

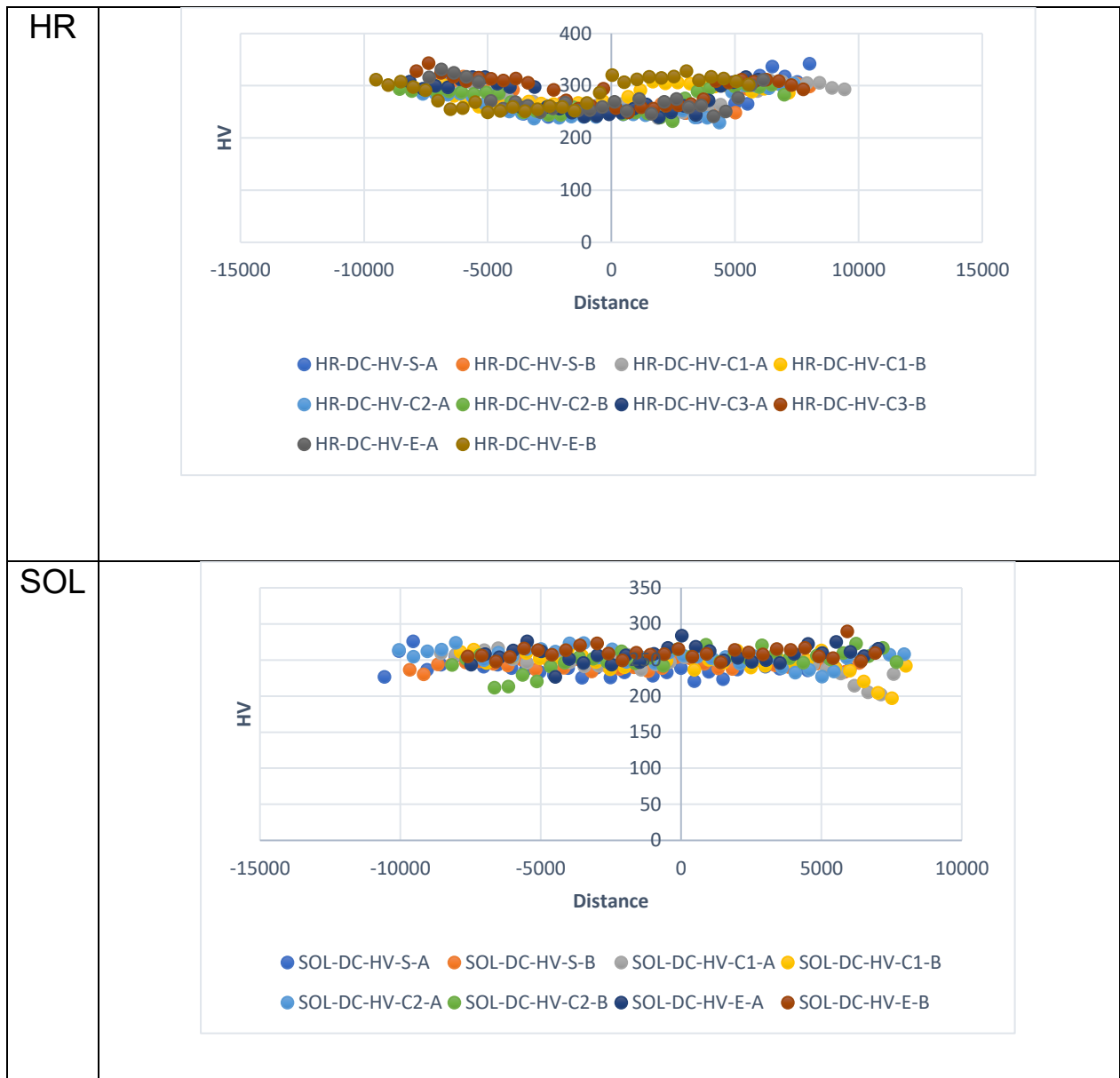


Figure 32 shows hardness variation with distance in TIG DC welding.

Upon comparison of the laser welding HV outcome (as depicted in Figure 33) with the reference results (as illustrated in Figure 28) and laser beam results (as shown in Figure 30), it has been observed that the welding exhibits superior hardness outcomes in comparison to both laser beam and reference results. The increase in hardness attained via laser welding can be attributed to multiple factors. The utilisation of laser welding technology enables the application of a concentrated heat source, which facilitates accurate control of the heat input and focuses on the melting of the material. As a result, the microstructure becomes more refined, perhaps leading to better hardness levels.

Upon comparison of the laser welding HV result with the reference results, it can be inferred that the welding process has effectively attained the desired hardness properties, as evidenced by the superior hardness values. In addition, upon

the comparison of the HV results obtained from laser welding and laser beam processes, it can be inferred that the former has resulted in an increase in hardness as compared to the latter. In laser welding, the energy densities are usually higher, and the heating is more localised in comparison to laser beam processes. This can result in notable alterations in the material microstructure and consequent hardness.

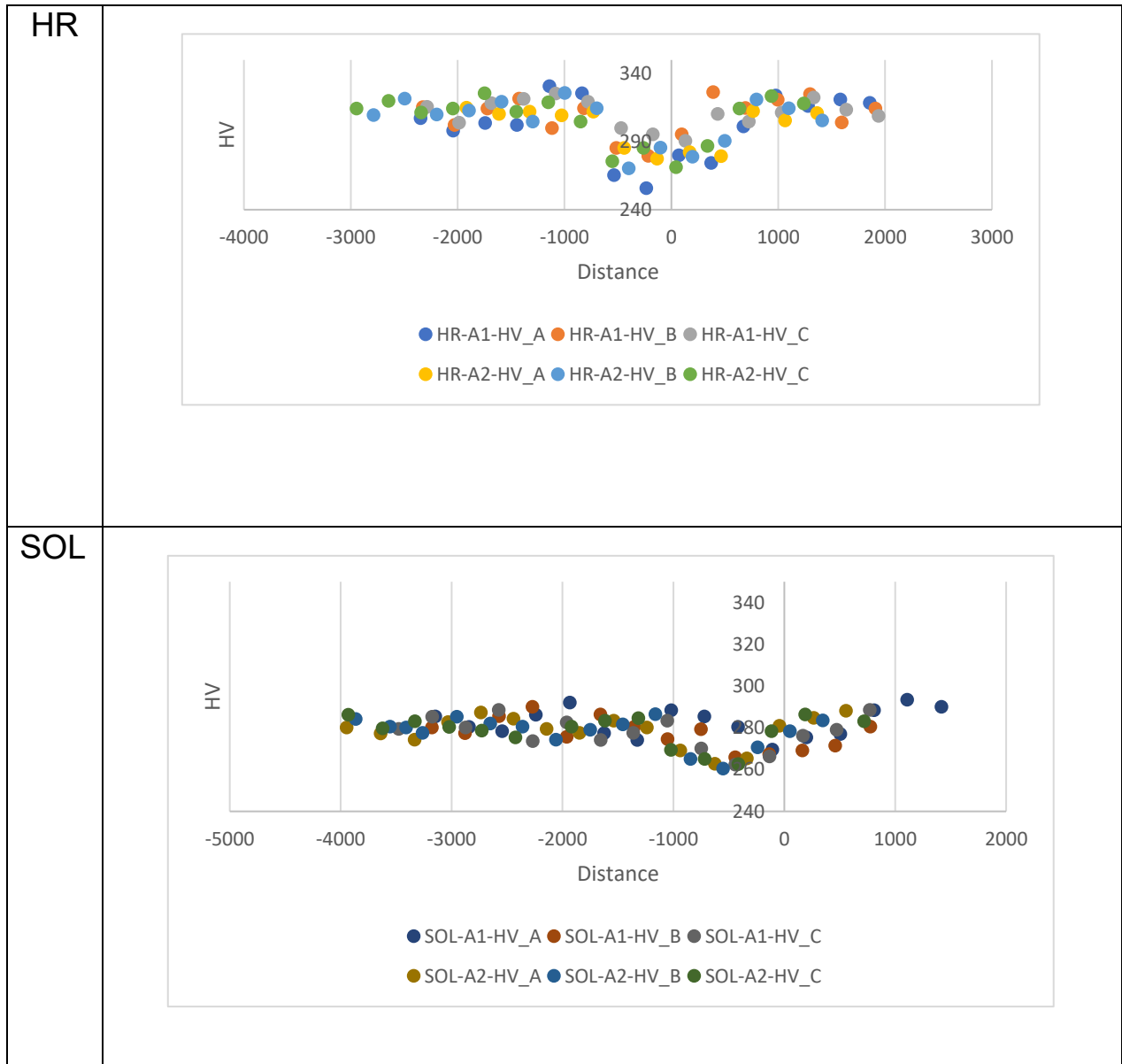


Figure 33 Hardness variation with distance in laser welding

### 3.3. Tensile Properties:

The objective of dividing the samples into hot rolled and solubilized sections and employing Tungsten Inert Gas (TIG) welding (Gas Tungsten Arc Welding or GTAW) and laser welding techniques is to assess the post-welding strength, elongation and

ductility of the material. Tensile testing is a method used to evaluate the strength of material after welding. This process involves measuring the yield strength and ultimate tensile strength properties of the material; measuring ductility involves evaluating its deformation capacity. The utilisation of welding technologies and the performance of tensile testing can lead to a thorough comprehension of the mechanical properties of the material post-welding, specifically in terms of strength, elasticity, and ductility.



Table 6 Tensile test specimens for the HR TIG DC welding

The experimental setup enabled a comprehensive analysis of the impact of different welding processes and the strengthening effect of  $\kappa$ -carbides on the mechanical properties of the tested specimens. The findings of these tests can provide useful insights that can be used for the selection of materials and the optimisation of processes in a variety of different industries where such materials are utilised. Each class of welding samples has 6 specimens (3 each for hot rolled and solubilized). Table 7 shows the average value taken out from the samples.

Properties	TIG_DC_HR	TIG_DC_SOL	TIG_AC_HR	TIG_AC_SOL	LW_HR	LW_SOL
YS (MPa)	679	498	664	500	558	458
UTS (MPa)	993	842	816	869	760	782
Stress at Fracture (MPa)	877	479	549	664	708	760
Strain at Fracture (%)	38.2	53.8	11.1	46.2	9.4	33.4

Table 7 Tensile properties of Fe-Mn-Al-C steel samples after welding

The hot-rolled TIG welded specimens indeed exhibit higher strength (YS= 679 MPa, UTS=993 MPa), stress at fracture, and ultimate tensile strength (UTS) compared to the solubilized specimens. The process of hot rolling the material leads to the development of a refined and aligned grain structure. The enhancement of a material's strength and mechanical properties, such as its resistance to deformation and fracture, is achieved through microstructural refinement. Tungsten Inert Gas (TIG) welding is a process that can impact the microstructure of the material being welded. This can lead to grain refinements and strengthening mechanisms, such as precipitation hardening. Irrespective of welding technologies, it has been noted that solubilized specimens exhibit greater elongation at fracture but lower tensile strength when compared to as-hot-rolled specimens. The observed difference can be explained by the changes in microstructure resulting from the solubilisation process. The ductility and elongation properties of solubilized specimens are improved by the existence of larger grains. Increased elongation at fracture is achieved due to greater plastic deformation before fracture, which is facilitated by larger grain size. The enhanced ductility is advantageous in scenarios where materials undergo considerable deformation or require excellent formability. In contrast, the solubilized specimens' tensile strength is adversely impacted by the development of larger grains. The presence of larger grain sizes has been associated with decreased strength due to the possibility of dislocation movement. This can result in localised plastic deformation and a decrease in the overall tensile strength.

Overall, the hot-rolled TIG welded specimens contribute to their higher mechanical properties, including hardness and resistance to deformation and fracture. Laser welded specimens may exhibit a reduction in yield strength and ultimate tensile strength compared to other specimens, but the stress at fracture can still be comparable. This suggests that the laser weld joint can exhibit good resistance to fracture, despite the decrease in overall strength.

## 4. Discussion of the results:

In order to obtain a thorough comprehension of the microstructure of heat-treated samples prior to welding, it is necessary to partition them into solubilized and hot-rolled samples. The division facilitates the examination of microstructural evolution in both scenarios to provide valuable observations into the samples' initial state and their performance during the welding procedure. The Fe-30Mn-9Al-1C alloy, as shown in **(figure 20, figure 21, and figure 34)** indicates equiaxial and randomly oriented austenitic grains in both hot-rolled and solubilized samples. The two conditions exhibit variations in grain size and the occurrence of twin boundaries. The hot-rolled samples exhibit a higher degree of grain refinement in contrast to the solubilized specimens. The reason for this can be attributed to the hot rolling process, which involves the application of plastic deformation at temperatures that are elevated. Dynamic recrystallization occurs during the process of hot rolling, resulting in the development of smaller and more equiaxed grains in the material. Dynamic recrystallization is a phenomenon that takes place when fresh grains form and expand within the distorted matrix. This process is made possible by the increased mobility of grain boundaries and recrystallization that occurs at high temperatures. In contrast, the samples that have been solubilized through a heat treatment process exhibit larger grain sizes. Lack of dynamic recrystallization results in the growth and merging of grains, leading to an increase in grain size. Twin boundaries were observed in both hot-rolled and solubilized samples. These boundaries can arise from plastic deformation or particular crystallographic orientations. Twin boundaries are formed due to the application of shear stresses that result in the formation of regions within the crystal lattice having a mirror-image orientation across the boundary. Twin boundaries are indicative of the impact of two distinct plastic deformation mechanisms, namely, Twinning Induced Plasticity (TWIP) and Microband Induced Plasticity (MBIP). The TWIP and MBIP mechanisms are responsible for enhancing the material's plastic deformation capability while preventing fracture. The TWIP process relates to the development and displacement of twin structures, which are capable of withstanding significant levels of plastic deformation. This results in enhanced ductility and mechanical characteristics. MBIP is a phenomenon that occurs when localised deformation takes place within narrow shear bands known as microbands. This process allows to distribute deformation and prevent strain localization, ultimately enhancing the material's overall plasticity.

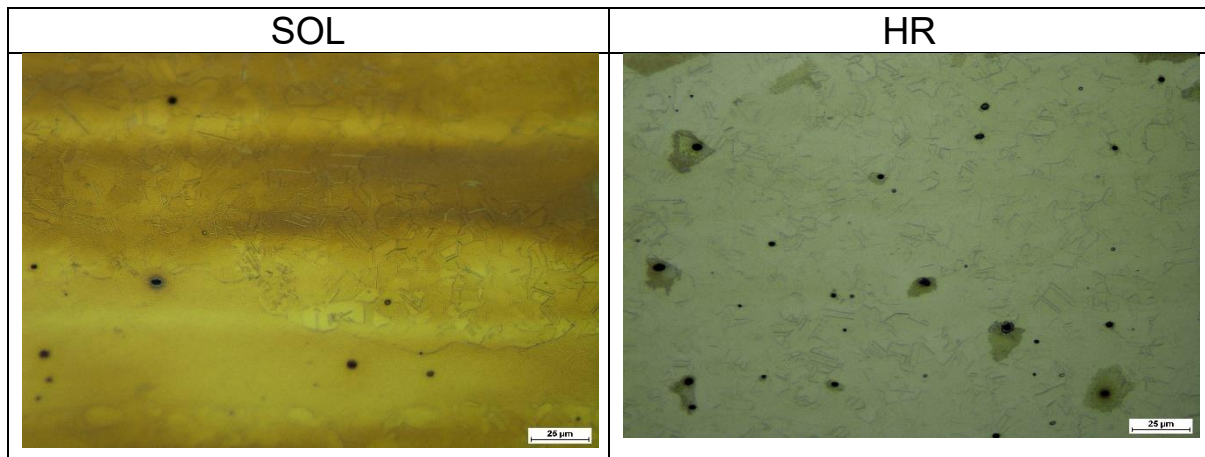


Figure 34 Optical micrograph of Solubilized and Hot-rolled state (500x)

GTAW clad material comprises three distinct zones: the fusion zone, heat-affected zone (HAZ), and base zone. Comprehending the microstructural alterations and features of these regions is essential in evaluating the mechanical characteristics and integrity of the clad joint. Under an optical microscope, the welded zone displays long dendritic structures that indicate the solidification front during the solidification of molten material. The Heat Affected Zone (HAZ) indicates certain modifications in contrast to the fusion area and the parent material. The Heat Affected Zone (HAZ) may undergo various microstructural changes such as grain growth, precipitation of secondary phases, and alterations in hardness. The mechanical properties of the clad joint, including strength, toughness, and corrosion resistance, are affected by the microstructural characteristics.

Table 5 demonstrates the measurements of the fusion and heat-affected zones (HAZ) regions in samples that were clad using GTAW. The measurements were obtained through the utilisation of imageJ software. AC cladding typically results in a shallower weld pool when compared to DC cladding. The even distribution of heat input between the electrode and the workpiece is a result of the alternating current polarity. DC welding results in greater weld penetration and a larger heat-affected zone (HAZ) than AC welding due to the concentrated heat input. The occurrence of twinning, a crystallographic phenomenon, is observable in both the heat-affected zone (HAZ) and the base material zone. The phenomenon of twinning arises due to the stress and strain encountered during the cladding procedure. The base material region exhibits equiaxed grains, which are uniform in size in all directions, and random grain orientation. The base material generally exhibits a finer grain size in comparison to the Heat Affected Zone (HAZ). The utilisation of SEM analysis, which is shown in **figure 35**, enabled a thorough comprehension of the microstructural features present within the fusion zone. The size distribution, spatial arrangement, and potential presence of twinning features of the identified dendrites and coarse grains were analysed.



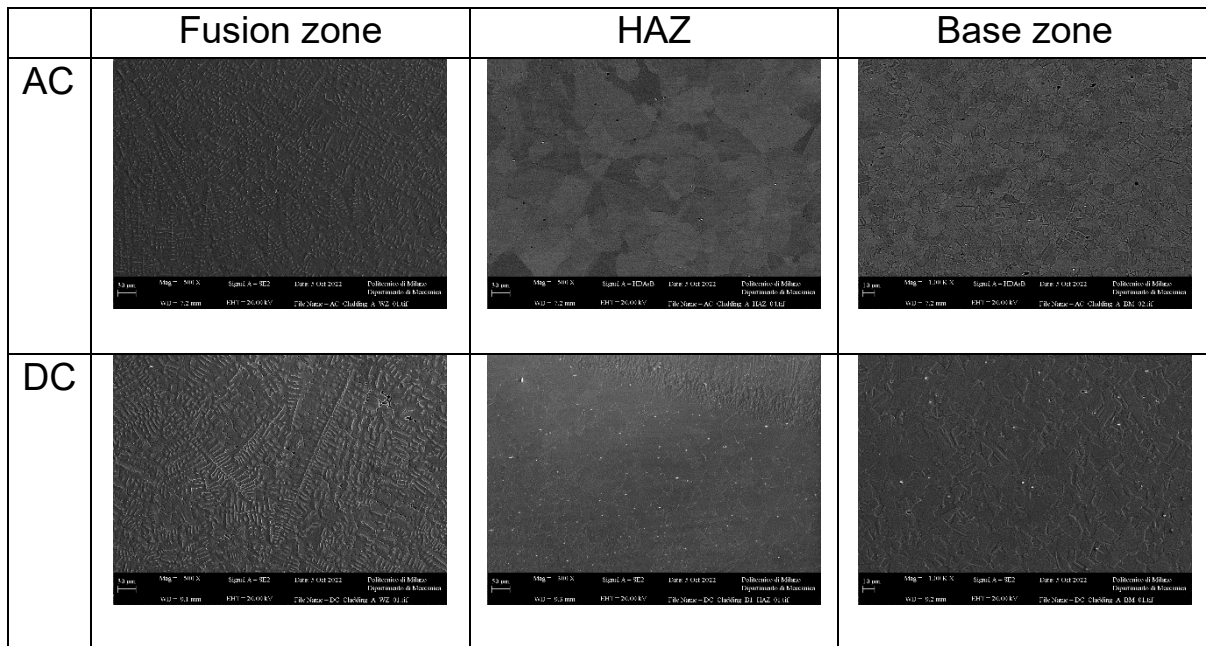


Figure 35 SEM analysis of TIG cladded samples

The compositional maps generated by Energy-Dispersive X-ray Spectroscopy (EDS) offer significant insights into the element distribution within a microstructure. The maps are highly beneficial in the examination of the distribution and composition of cladding layers in TIG-DC (Tungsten Inert Gas - Direct Current) cladded microstructures.

The microstructure of the TIG-DC cladding displays localised variations in the manganese (Mn) content, as evidenced by the dark spots observed in multiple small regions, as shown in Figure 36. The distribution of other elements, such as aluminium and iron, exhibits comparable trends. Variations in elemental composition can be attributed to factors such as differences in welding parameters, cooling rates, or the existence of impurities. Long dendritic structures are readily observable within the fusion zone, in addition to the compositional variations. The dendritic structures observed are a distinctive feature of solidification processes and can offer valuable information regarding the solidification behaviour of the cladding material. The solidification process affects the growth of dendrites, which is influenced by various factors, including temperature gradients and cooling rates. Valuable information related to the elemental distribution, local variations, and solidification behaviour within the TIG-DC cladded microstructure can be obtained by analysing the EDS compositional maps and observing the microstructural features. Understanding the properties of the material, assessing the cladding's quality, and optimising welding parameters are all dependent on this essential knowledge.

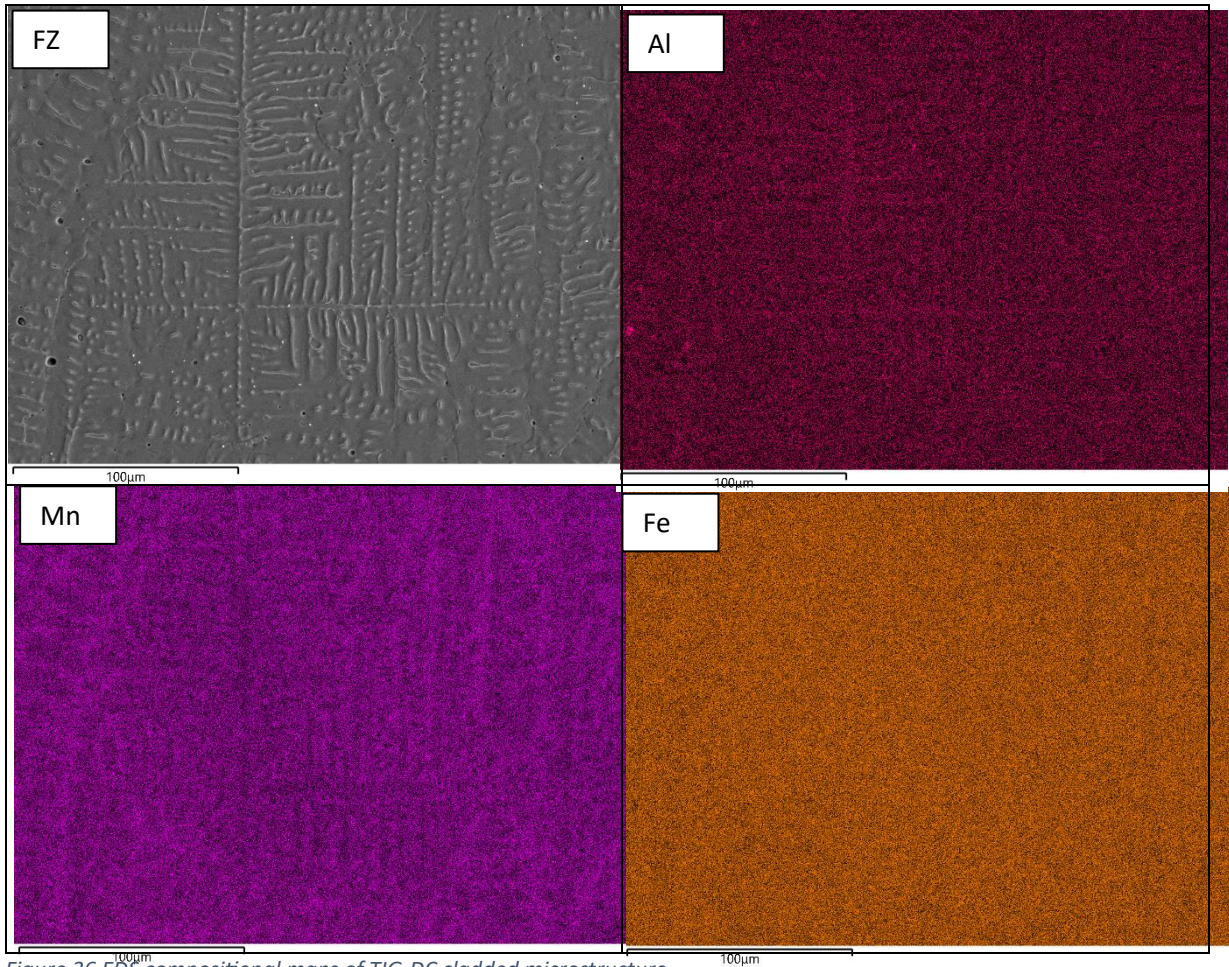


Figure 36 EDS compositional maps of TIG-DC cladded microstructure

Tables 8 and 9 provide the results of the compositional analysis conducted on the precipitates in relation to the matrix. The analysis indicates that the Tungsten Inert Gas (TIG) Direct Current (DC) cladding method yields higher levels of Aluminium (Al) and Iron (Fe) compared to the TIG Alternating Current (AC) cladding process. The present finding suggests that the DC cladding technique introduces a higher concentration of Al and Fe into the precipitates that are produced while cladding.

Differences in welding parameters, such as heat input and electrode choice, are responsible for the observed variations in elemental concentrations between the DC and AC cladding methods. The DC cladding technique employs a direct current flow, which can result in elevated temperatures and localised heat input. This may cause greater inclusion of Al and Fe into the cladded material. The AC cladding method is characterised by a more uniform distribution of heat input, which leads to the formation of precipitates with comparatively reduced levels of Al and Fe.

The analysis of elemental concentrations in the precipitates yields significant information regarding the composition and properties of the cladded material. The material's mechanical strength, corrosion resistance, and other relevant attributes can be significantly influenced by the presence and distribution of alloying elements such as Al and Fe. During the process of welding, the strong attraction between carbon and oxygen can result in the formation of carbon monoxide gas. Additionally, this attraction

can cause the gas to diffuse out of the weld pool. In contrast, the TIG DC clad, and TIG AC clad processes do not exhibit a significant alteration in the manganese (Mn) concentration. The findings indicate that the manganese distribution in the material is minimally affected by the welding process, whether it is TIG DC clad or TIG AC clad. The analysis of composition offers significant information regarding changes in the concentrations of elements during Tungsten Inert Gas (TIG) cladding procedures. This analysis emphasises the impact of welding conditions on the dispersion of alloying elements. Comprehending the aforementioned alterations is imperative in evaluating the quality and characteristics of the clad material.

Sample	Fe	Mn	Al	C
DC-A	55.2	28.5	8.7	7.6
DC-B1	55.5	29	7.7	7.8
DC-B2	55.6	28.9	7.3	8.5
DC-C	55	28.6	7.7	8.7

Table 8 The SEM-EDS outputs of the investigated sites of TIG DC clad

Sample	Fe	Mn	Al	C
AC-A	54.8	28.5	7.6	9.1
AC-B1	54.7	28.3	7.6	9.4
AC-B2	54.9	28.7	7.7	8.7
AC-C	55.1	28.8	7.5	8.6

Table 9 The SEM-EDS outputs of the investigated sites of TIG AC clad

In the process of the laser beam on the plate, which is similar to Tungsten Inert Gas (TIG) cladding, the region can be divided into separate zones. Each zone demonstrates distinct microstructural features and properties, as shown in **figure 25**, **figure 37**. Localised melting and subsequent solidification occur in the fusion zone, which is the area where the laser beam interacts with the base material. The microstructural features observed in this zone are a result of the high rates of heating and cooling. During the solidification process of the molten material, epitaxial growth occurs where the grains align with the crystallographic structure of the base material. Upon transitioning to the heat-affected zone (HAZ), there is a visible variance in microstructural features as compared to those present in the fusion zone. During the process of laser cladding, the Heat Affected Zone (HAZ) undergoes an increase in temperature, but it does not undergo full melting. The Heat Affected Zone (HAZ) shows an increase in grain sizes that are larger and coarser in comparison to both the base material and the fusion zone. The laser beam's heat input induces grain growth and coarsening within the heat-affected zone (HAZ). Under high temperatures, the pre-existing grains undergo growth and recrystallization, resulting in increased grain size in comparison to the original material. The base region usually exhibits a finer grain size in comparison to the heat-affected zone (HAZ) and the fusion zone. The material's strength and toughness are attributed to its fine-grain structure. Furthermore, the underlying substance may demonstrate twinning, a crystallographic

occurrence in which atoms are arranged in a mirrored fashion. The phenomenon of twinning has the potential to impact the mechanical properties and deformation behaviour of a given material. The mechanical properties and compatibility of the laser beam on the plate have significantly influenced by the microstructure of the base material.

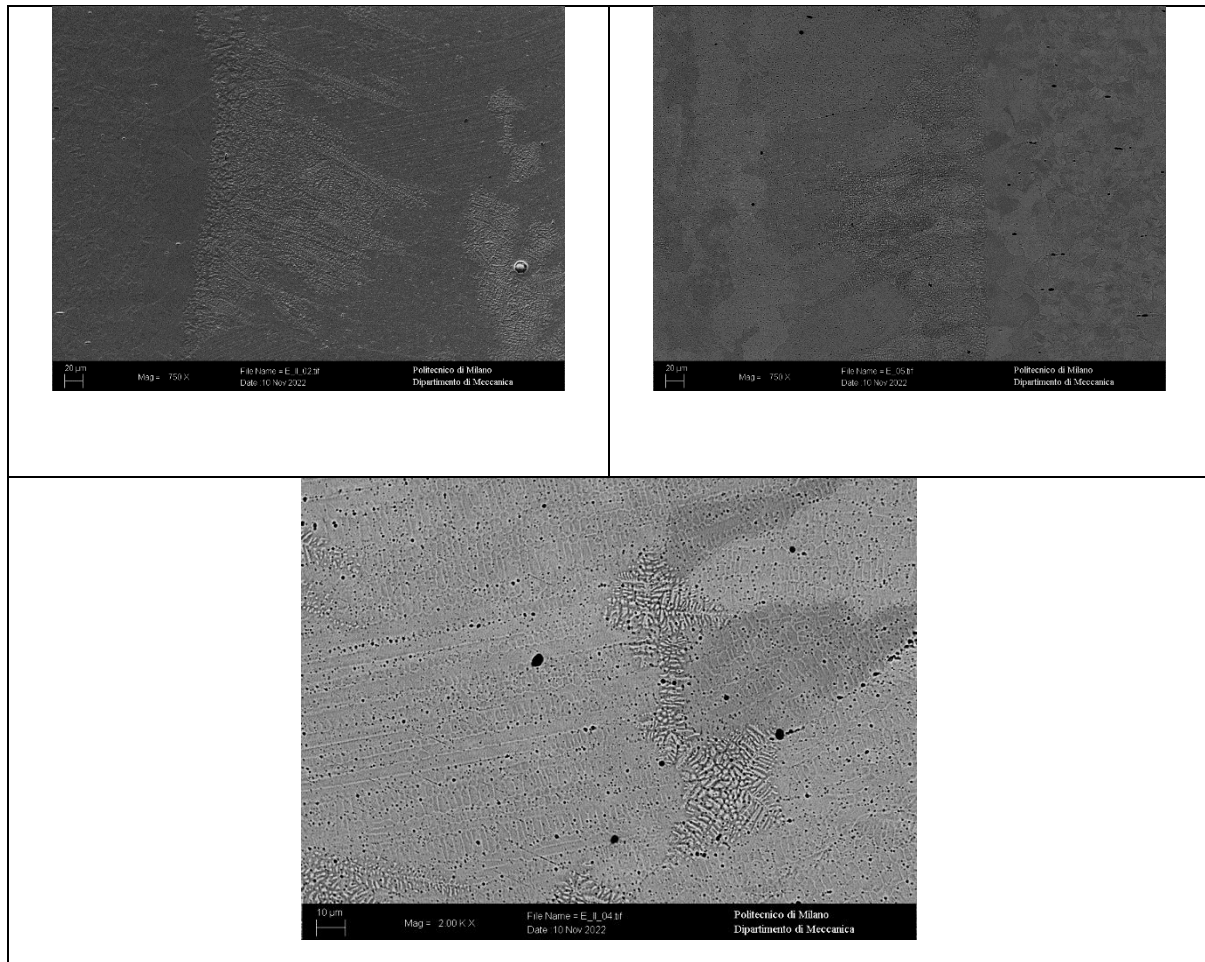


Figure 37 Micrographs of fusion zone with different magnification

For the purpose of improving comprehension, the welded joint has been segmented into three distinct sections, namely the fusion zone (FZ), heat-affected zone (HAZ), and base material (BM), as illustrated in **Figure 26**.

The microstructure in the fusion zone exhibits a fine grain structure due to the rapid solidification that occurs during the welding process. The smaller grain size observed in this area is a result of the rapid cooling rate it went through. Moreover, a rise in the density of grain boundaries can be noted, which suggests the development of fresh grain boundaries while the solidification process is underway. The optical microscope can detect the existence of dendritic structures within the fusion zone. The etching behaviours of the material within the fusion zone may differ, which could be attributed

to chemical inhomogeneity or microstructural variations, such as thin constituents. It is important to take note of this. To verify these assumptions, an examination utilising SEM (Scanning Electron Microscopy) has been carried out. The formation of coarse grains in the heat-affected zone (HAZ) is attributed to the fact that the region did not reach its melting point during the welding process. As a result, the Heat Affected Zone (HAZ) shows a greater grain size in contrast to the fusion zone. Microsegregation can occur in the base material region, resulting in an uneven distribution of certain elements within the solidified structure.

Laser welding involves the categorization of the microstructure into three distinct zones, namely the fusion region, the heat-affected zone (HAZ), and the base material. The fusion zone is the area where the two materials being joined are merged during the welding process, as shown in **figure 27**. The fusion region indicates visible long dendrites, which are solidified structures that arise during the cooling phase of the molten metal. The formation of dendrites is attributed to the greater thermal gradient and solidification process that takes place during laser welding. The rapid cooling process resulted in a fine-grained microstructure in the fusion region. The material exhibits a columnar morphology of grains that are aligned with the direction of heat flow. The area neighbouring the fusion region is commonly referred to as the heat-affected zone (HAZ). During the welding process, the Heat Affected Zone (HAZ) undergoes insufficient heating to reach its melting point. This leads to the formation of a grain structure that is coarser in comparison to the fusion region. Thermal cycling, which occurs during welding, can result in alterations in the material properties within the Heat Affected Zone (HAZ) due to fluctuations in temperature profiles. The region of the base material that is situated at a greater distance from the welding zone displays a smaller grain size in comparison to both the heat-affected zone (HAZ) and the fusion region. The material's strength and toughness are attributed to its fine-grained structure. The welding process has minimal impact on the microstructure and material properties in this particular region. Comprehending the microstructural characteristics present in every zone of the laser-welded joint is crucial for the evaluation of mechanical properties, assessment of weld integrity, and optimisation of welding parameters. The process offers valuable information on the solidification process, grain morphology, and possible alterations in material properties caused by thermal cycling. This data can be utilised to determine the most suitable welding parameters for achieving desired results.

The investigation comprised the carrying out of microhardness tests on diverse samples prior to welding or cladding. The results of the samples indicate that the hot-rolled samples demonstrated greater hardness compared to the solubilized samples. This is illustrated in **Figure 28**. Comparable outcomes were achieved by means of microhardness examination of the welded or cladded specimens. The specimens had categorized into three distinct regions, namely the fusion region, the heat-affected zone (HAZ), and the base region. The base region consistently demonstrated the

highest levels of hardness in various welding and cladding scenarios. The increased hardness of the base material can be attributed to various factors, including its composition, prior heat treatments, and distinct microstructural characteristics. The results consistently indicated that the fusion region exhibited average greater hardness when compared to the heat-affected zone (HAZ). The aforementioned trend was noted in every instance of welding and cladding. The Increased hardness observed in the fusion area can be attributed to the higher thermal gradient which leads to dendrites that occurs during cladding. The enhanced hardness in the cladded area is attributed to the incorporation of a separate cladding material and the reduction of the substrate material. In contrast, the heat-affected zone (HAZ) consistently demonstrated reduced hardness in comparison to the cladded area. The observed phenomenon is a result of decreased cooling rates and the thermal cycling effect that occurs in the Heat Affected Zone (HAZ) during the process of welding or cladding. The formation of larger grains and changes in microstructure are influenced by certain factors, resulting in a reduction in hardness. Upon comparing the hardness outcomes of Tungsten Inert Gas (TIG) cladding with the reference graphs depicted in **Figure 28**, it is apparent that the hardness values acquired for both Alternating Current (AC) and Direct Current (DC) cladding exhibit analogous patterns throughout all material sections. The data suggests that the current cladding modes exert negligible influence on the material's hardness. The reference graphs in Figure 30 serve as a baseline or expected range of hardness values for the material under evaluation. The comparison of actual hardness values obtained from TIG cladding, as presented in Figure 31, with the reference graphs enables the identification of any deviations or discrepancies. This process facilitates a more comprehensive comprehension of the material's hardness characteristics. Upon comparing the HV profiles of the laser beam on plate samples (as depicted in **Figure 30**) with the reference graphs (as shown in **Figure 28**), it can be observed that the overall outcomes exhibit resemblances. The base material's HV values exhibit some deviations that may be attributed to defects. Defects in the base material can occur due to several factors, including impurities, inclusions, or process parameters. Additional research is required to identify the precise elements that are responsible for these discrepancies. A comparison can be made between the outcomes of Tungsten Inert Gas (TIG) welding, as depicted in **Figures 31 and 32**, for both Alternating Current (AC) and Direct Current (DC) modes, with the cladding outcomes shown in **Figure 29** and the reference graphs illustrated in **Figure 28**. The Tungsten Inert Gas (TIG) welding process has yielded higher hardness values as compared to the cladding results. However, the hardness trends observed in TIG welding are consistent with the reference results. The observed rise in hardness during Tungsten Inert Gas (TIG) welding can be attributed to the welding process. The Tungsten Inert Gas (TIG) welding method utilises elevated temperatures and greater heat input in comparison to the cladding process. An increase in heat input may cause alterations in the microstructure of the material, leading to fluctuations in its hardness. The Tungsten Inert Gas (TIG) welding process has demonstrated conformity with the reference graphs, despite the observed increase in hardness values. This indicates that the welding process has successfully attained the desired hardness properties

within an acceptable range. After comparing the HV results obtained from laser welding (**Figure 33**) with the reference results (**Figure 28**) and laser beam results (**Figure 30**), it can be concluded that the welding process exhibits superior hardness outcomes. The enhancement in hardness attained via laser welding can be ascribed to multiple factors. The process of laser welding involves the use of a highly concentrated heat source that enables accurate regulation of heat input, which is directed towards the melting of the material. The aforementioned process results in a more precise microstructure, which has the potential to enhance the levels of hardness.

In summary, the hardness characteristics of welding processes, such as TIG or laser, differ significantly from those of cladding and reference results. The process of Tungsten Inert Gas (TIG) welding exhibits a rise in the values of hardness as compared to cladding. On the other hand, laser welding displays even greater levels of hardness in comparison to both laser beam and reference outcomes. The observed differences can be attributed to various factors, including the amount of heat input, alterations in microstructure, and the limited application of the welding procedures.

The results indicate that the hot-rolled Tungsten Inert Gas (TIG) welded specimens exhibit greater strength, stress at fracture, and Ultimate Tensile Strength (UTS) in comparison to the solubilized specimens. The hot rolling procedure facilitates the formation of a refined and well-arranged grain structure, thereby enhancing the mechanical characteristics of the material and its ability to withstand deformation and fracture. The process of hot rolling results in a refinement of the microstructure, which in turn leads to a corresponding increase in strength. The Tungsten Inert Gas (TIG) welding process has the ability to affect the microstructure of the welded material. This can lead to the refinement of grains and the activation of strengthening mechanisms, such as precipitation hardening. The hot-rolled TIG welded specimens can be strengthened and improved in their mechanical properties through this process. Irrespective of the welding techniques employed, it has been noted that solubilized samples demonstrate higher fracture elongation but lower tensile strength in comparison to the as-hot-rolled samples. The process of solubilisation results in alterations to the microstructure of the substance, which includes the formation of enlarged grains. The ductility and elongation properties of the solubilized specimens are enhanced by the existence of larger grains, which enables greater plastic deformation prior to fracture. The improved ductility of the material might prove advantageous in situations where there is substantial deformation or a need for exceptional formability. The tensile strength of solubilized specimens is negatively impacted by the presence of larger grain sizes. An increase in grain size is linked to a reduction in strength as it enhances the likelihood of dislocation movement. This, in turn, results in localised plastic deformation and a decline in the overall tensile strength. The mechanical properties of the hot-rolled TIG welded specimens are generally superior, that includes hardness, deformation resistance, and fracture. This

is attributed to the formation of a refined and aligned grain structure through hot rolling. However, it is noteworthy that laser-welded specimens may undergo a decrease in both yield strength and ultimate tensile strength in comparison to other types of specimens due to the fact that it caused a lot of porosity. Despite the reduction in overall strength, the laser weld joint can still demonstrate commendable fracture resistance, as demonstrated by the comparable stress at fracture. The mechanical properties of the tested specimens were thoroughly investigated using Tungsten Inert Gas (TIG) welding and laser welding techniques. The experimental setup included hot-rolled and solubilized specimens. **Table 7 and figure 38** displays the obtained results, which present average values that represent the performance of the samples.

In comparison to the solubilized specimens, the hot-rolled TIG welded specimens have greater yield strength, stress at fracture, and ultimate tensile strength values (yield strength = 679 MPa, ultimate tensile strength = 993 MPa). The refined and aligned grain structure is a result of the hot rolling process. The process of microstructural refinement is essential in improving the strength and mechanical properties of a material, which includes its ability to resist deformation and fracture.

Tungsten Inert Gas (TIG) welding can affect the microstructure of the welded material, resulting in grain refinement and strengthening mechanisms such as precipitation hardening. This holds true for all welding technologies employed. The enhanced mechanical properties observed in the hot-rolled Tungsten Inert Gas (TIG) welded specimens are attributed to these factors.

In contrast, the solubilized specimens exhibit increased elongation at fracture but decreased tensile strength in comparison to the as-hot-rolled specimens. The observed variation can be attributed to alterations in the microstructure caused by the solubilisation procedure. The presence of bigger grains in solubilized samples improves their ductility and elongation characteristics. Increased elongation at fracture is achieved due to greater plastic deformation before fracture, which is facilitated by increased grain size. The enhanced ductility offers benefits in situations that entail substantial deformation or necessitate exceptional formability. The tensile strength of solubilized specimens is negatively impacted by the existence of bigger grains. Increased grain size may increase the movement of dislocations, resulting in localised plastic deformation and a reduction in the overall tensile strength.

The mechanical properties of the hot-rolled TIG welded specimens are generally higher, which include hardness, resistance to deformation, and fracture. This is attributed to the development of a refined and aligned grain structure through hot rolling. Laser-welded specimens may exhibit a decrease in both yield strength and ultimate tensile strength when compared to other specimens. Despite the reduction in overall strength, the laser weld joint can still demonstrate commendable fracture resistance, as evidenced by the comparable stress at fracture.



Welding Type	Stress vs Strain curves
TIG-AC	<p>Stress (MPa)</p> <p>Strain</p> <p>HR_1 HR_2 HR_3 SOL_1 SOL_2 SOL_3</p>
TIG-DC	<p>Stress (MPa)</p> <p>Strain</p> <p>SOL_1 SOL_2 SOL_3 HR_1 HR_2 HR_3</p>
Laser	

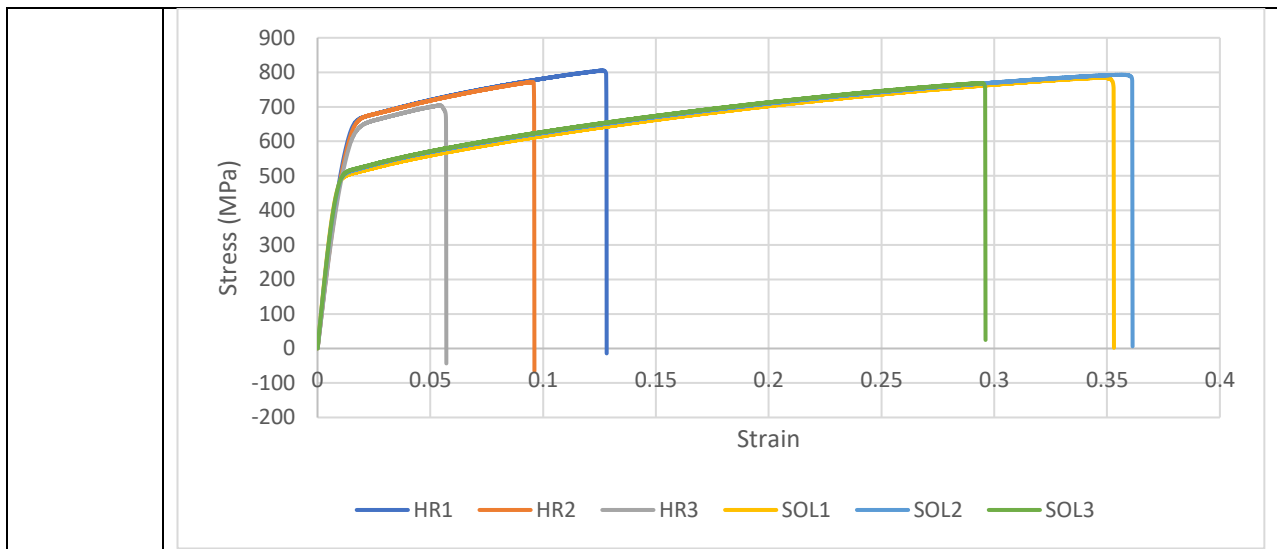


Figure 38 Stress-strain curve for different welding technologies

The occurrence of ductile fractures is commonly linked with the development of small, concave-shaped grooves known as dimples. The formation of these dimples is attributed to the localised necking and stretching of the material during the process of deformation. The observation of dimples indicates that the fracture underwent a gradual process and involved plastic deformation before reaching its ultimate failure point. Shear lips or shear ridges may be observed on the fracture surface, in addition to dimples. Shear lips are characterised by their rough and jagged appearance, which is perpendicular to the direction of the applied stress. The fractures exhibit indications of plastic deformation and material flow, which imply that shear deformation played a role in the process. Ductile fractures typically result from the merging of microvoids present within the material. Microvoids are minute cavities or voids that arise as a result of localised deformation. As the material is subjected to additional stress, the microvoids within it will expand and eventually combine, resulting in the creation of larger voids and eventual fracture. **Figure 39 and figure 40** shows that microvoids occur due to localized deformation.

The characteristics observed on the fracture surface may vary based on several factors, including the welding process, material properties, and testing conditions. It is crucial to consider these factors when analysing the fracture surface. The analysis of scanning electron microscopy (SEM) offers significant insights into the fracture behaviour of welded joints. This aids in comprehending the mechanisms that contribute to the failure of such joints.

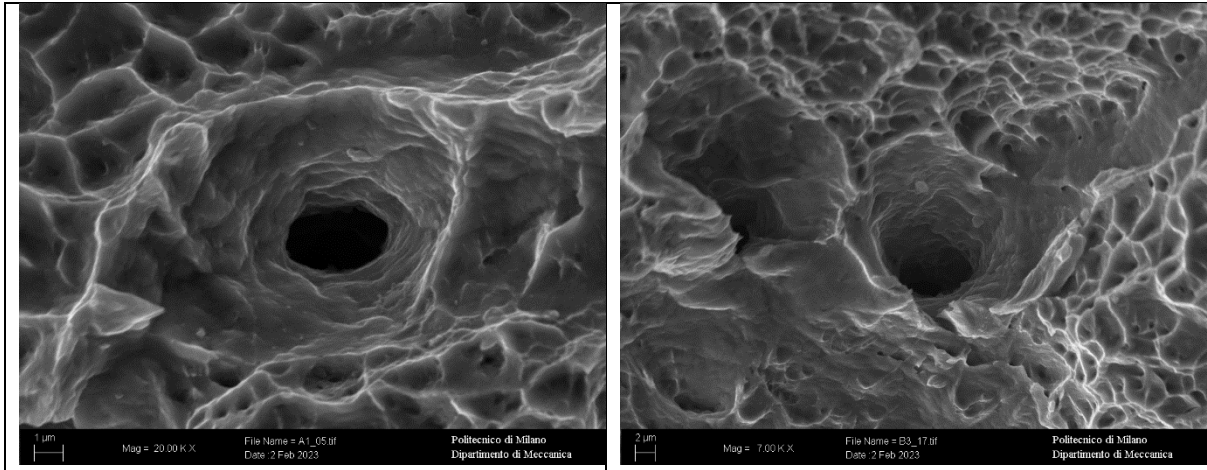


Figure 39 Fracture surface of TIG AC welded specimen.

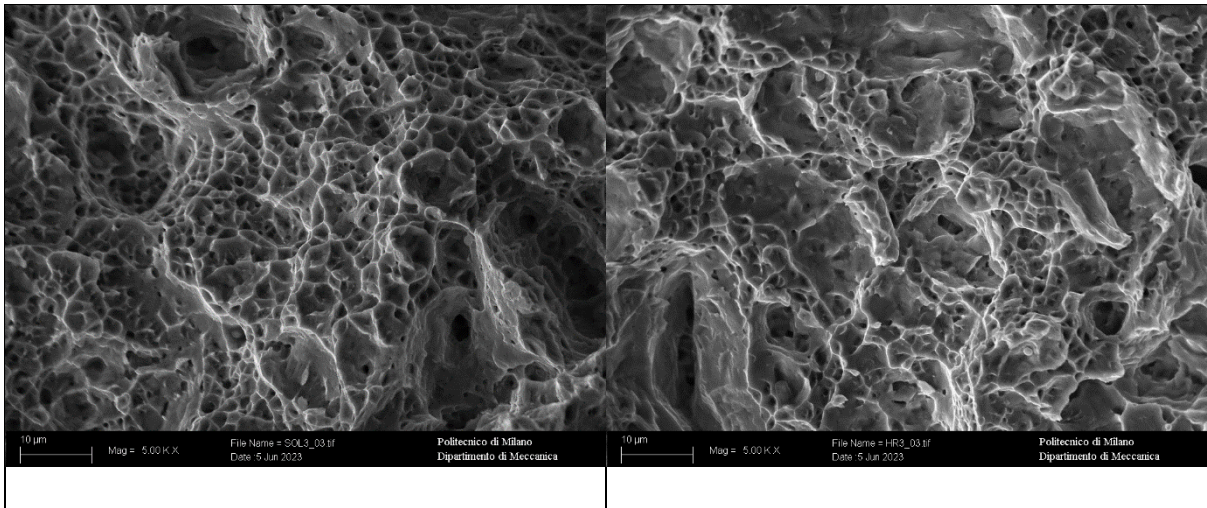


Figure 40 Fracture surface with dimples-like shape in laser welded specimen

## 5. Conclusions:

The results of this investigation allow for a number of inferences to be drawn. There have been reports that:

Regarding the effects of Hot-rolled and solubilized conditions.

- The microstructure of the material in its hot-rolled state exhibits small austenitic grains that are equiaxial and randomly oriented. The formation of such grains is attributed to the refinement of the grain structure through dynamic recrystallization during the hot rolling process.
- The microstructure of the material in its solubilized state exhibits coarse grain, equiaxial and randomly oriented as compared to the hot-rolled case.
- The hardness of the material under a hot rolled state is always higher than the material under solubilized state because of finer grains and an increase in grain boundaries, which act as an obstacle for dislocation.

Effect of welding technologies on the fusion zone.

- The fusion zone exhibited elongated dendrites along the high gradient direction.
- Due to the following characteristics, it is found fusion zone has a higher average hardness value as compared to the adjacent zone of the material (HAZ).
- The following characteristics are found in all welding technologies.

Effect of welding technologies on the Heat affected zone.

- The Heat-Affected Zone (HAZ) is a region in welding where the temperature is raised but does not reach its melting point. Atomic diffusion and rearrangement occur due to the slower cooling rate in comparison to the fusion zone. This phenomenon promotes the growth of larger grain structures within the Heat Affected Zone (HAZ).
- Compared to the clad region, the heat-affected zone (HAZ) consistently had lower hardness. The phenomenon under observation is a result of decreased cooling rates and thermal cycling effects experienced by the Heat Affected Zone (HAZ) during the operation.

Effect of welding technologies on the base material zone.

- The weld's base material exhibits a microstructural complexity due to the presence of a fine grain structure, and a combination of equiaxed and randomly oriented grains.
- The base material of the weld generally reveals the highest value for hardness in comparison to the remaining material.

### Effect of Welding Technologies on the tensile test

- The tensile strength and strain to fracture of the TIG-welded specimens are higher than those of the laser-welded specimens, irrespective of their initial state, i.e., hot rolled or solubilized.
- The fracture mode in all cases are ductile in nature
- In all welding technologies, the solubilized specimens exhibit a greater elongation at fracture, but a lower tensile strength compared to the hot-rolled specimen.

## Future Development:

Further research will be needed to gain a thorough comprehension of the microstructural and mechanical characteristics of the Fe-Mn-Al-C austenitic steel in upcoming studies. The research involves investigating the impact of thermo-mechanical treatments and chemical composition on steel. Additionally, it involves evaluating significant application properties such as fatigue behaviour, wear resistance, and corrosion behaviour. Conducting thorough research in these specific areas can provide significant insights that might help in the industrialization of lightweight steels. This can also enable the development of optimised processing-structure-property relationships. There are some key points that might help the industrialization of Fe-Mn-Al-C austenitic steel.

- Explore additional alloying elements, their concentrations, and their synergistic effects on steel microstructure and mechanical properties. Examine how trace elements refine grain structure, improve mechanical strength, and maintain austenitic phase stability.
- To customise steel's microstructure and mechanical properties, try extreme plastic deformation, additive manufacturing, and advanced heat treatments. To achieve the required mechanical qualities, study processing parameters on grain refinement, precipitation behaviour, and phase transitions.
- To assess steel's mechanical qualities, perform tensile, compression, hardness, and impact tests. Examine how microstructure, alloy composition, and processing affect steel strength, ductility, toughness, and fatigue.
- Develop and evaluate computational models and simulations to forecast Fe-Mn-Al-C austenitic steel microstructural evolution and mechanical properties under varied processing circumstances. These models can optimise alloy design and processing characteristics, reducing experimental trials.
- Study Fe-Mn-Al-C austenitic steel's corrosion resistance and oxidation in high-temperature and aggressive corrosive environments. To assure practical application, test alloying elements, surface treatments, and protective coatings on corrosion resistance.
- Explore Fe-Mn-Al-C austenitic steel's shape memory, magnetostriction, and magnetic characteristics. Study how composition and microstructure affect these functional behaviours and their applications.

## Bibliography

- [1] H. Chen, L. Zhao, S. Lu, Z. Lin, T. Wen, and Z. Chen, "Progress and Perspective of Ultra-High-Strength Martensitic Steels for Automobile," *Metals*, vol. 12, no. 12. MDPI, Dec. 01, 2022. doi: 10.3390/met12122184.
- [2] D. Haber, "Lightweight Materials for Automotive Applications: A Review," 2018.
- [3] T. B. Hilditch, T. de Souza, and P. D. Hodgson, "Properties and automotive applications of advanced high-strength steels (AHSS)," in *Welding and Joining of Advanced High Strength Steels (AHSS)*, Elsevier Inc., 2015, pp. 9–28. doi: 10.1016/B978-0-85709-436-0.00002-3.
- [4] S. Chen and R. Rana, "Low-density steels," in *High-Performance Ferrous Alloys*, Springer International Publishing, 2020, pp. 211–289. doi: 10.1007/978-3-030-53825-5\_6.
- [5] Y. F. Shen, X. X. Dong, X. T. Song, and N. Jia, "Carbon content-tuned martensite transformation in low-alloy TRIP steels," *Sci Rep*, vol. 9, no. 1, Dec. 2019, doi: 10.1038/s41598-019-44105-6.
- [6] H. Ding, D. Han, Z. Cai, and Z. Wu, "Microstructures and Mechanical Behavior of Fe-18Mn-10Al-(0.8-1.2)C Steels," *JOM*, vol. 66, no. 9, pp. 1821–1827, Sep. 2014, doi: 10.1007/s11837-014-1063-3.
- [7] H. Kim, D. W. Suh, and N. J. Kim, "Fe-Al-Mn-C lightweight structural alloys: A review on the microstructures and mechanical properties," *Science and Technology of Advanced Materials*, vol. 14, no. 1. Feb. 2013. doi: 10.1088/1468-6996/14/1/014205.
- [8] S. Chen, R. Rana, A. Haldar, and R. K. Ray, "Current state of Fe-Mn-Al-C low density steels," *Progress in Materials Science*, vol. 89. Elsevier Ltd, pp. 345–391, Aug. 01, 2017. doi: 10.1016/j.pmatsci.2017.05.002.
- [9] R. A. Howell and D. C. Van Aken, "A Literature Review of Age Hardening Fe-Mn-Al-C Alloys."
- [10] I. Gutierrez-Urrutia, "Low density Fe-Mn-Al-C Steels: Phase structures, mechanisms and properties," *ISIJ International*, vol. 61, no. 1. Iron and Steel Institute of Japan, pp. 16–25, 2021. doi: 10.2355/isijinternational.ISIJINT-2020-467.
- [11] S. Bai *et al.*, "Research status and development prospect of Fe–Mn–C–Al system low-density steels," *Journal of Materials Research and Technology*, vol. 25, pp. 1537–1559, Jul. 2023, doi: 10.1016/j.jmrt.2023.06.037.
- [12] S. Ren-ho, X. Jian-ying, and H. Dong-po, "Characteristics of Mechanical Properties and Microstructure for 316L Austenitic Stainless Steel," 2011. [Online]. Available: [www.sciencedirect.com](http://www.sciencedirect.com)
- [13] A. Rahnama, H. Kotadia, S. Clark, V. Janik, and S. Sridhar, "Nano-mechanical properties of Fe-Mn-Al-C lightweight steels," *Sci Rep*, vol. 8, no. 1, Dec. 2018, doi: 10.1038/s41598-018-27345-w.

- [14] M. T. Chen, A. Cai, M. Pandey, C. Shen, Y. Zhang, and L. Hu, "Mechanical properties of high strength steels and weld metals at arctic low temperatures," *Thin-Walled Structures*, vol. 185, Apr. 2023, doi: 10.1016/j.tws.2023.110543.
- [15] S. C. Chang, Y. H. Hsiau, and M. T. Jahn, "Tensile and fatigue properties of Fe-Mn-Al-C alloys," 1989.
- [16] T. Wegener, C. Haase, A. Liehr, and T. Niendorf, "On the influence of  $\kappa$ -carbides on the low-cycle fatigue behavior of high-Mn light-weight steels," *Int J Fatigue*, vol. 150, Sep. 2021, doi: 10.1016/j.ijfatigue.2021.106327.
- [17] D. Frómata *et al.*, "Microstructural effects on fracture toughness of ultra-high strength dual phase sheet steels," *Materials Science and Engineering A*, vol. 802, Jan. 2021, doi: 10.1016/j.msea.2020.140631.
- [18] C. Hu, C. P. Huang, Y. X. Liu, A. Perlade, K. Y. Zhu, and M. X. Huang, "The dual role of TRIP effect on ductility and toughness of a medium Mn steel," *Acta Mater*, vol. 245, Feb. 2023, doi: 10.1016/j.actamat.2022.118629.
- [19] D. Li, L. Qian, C. Wei, S. Liu, F. Zhang, and J. Meng, "The tensile properties and microstructure evolution of cold-rolled Fe–Mn–C TWIP steels with different carbon contents," *Materials Science and Engineering A*, vol. 839, Apr. 2022, doi: 10.1016/j.msea.2022.142862.
- [20] R. Kuziak, R. Kawalla, and S. Waengler, "Advanced high strength steels for automotive industry: A review," *Archives of Civil and Mechanical Engineering*, vol. 8, no. 2. Oficyna Wydawnicza Politechniki Wroclawskiej, pp. 103–117, 2008. doi: 10.1016/s1644-9665(12)60197-6.
- [21] J. H. Schmitt and T. Lung, "New developments of advanced high-strength steels for automotive applications," *Comptes Rendus Physique*, vol. 19, no. 8. Elsevier Masson SAS, pp. 641–656, Dec. 01, 2018. doi: 10.1016/j.crhy.2018.11.004.
- [22] K. Choi *et al.*, "Effect of aging on the microstructure and deformation behavior of austenite base lightweight Fe-28Mn-9Al-0.8C steel," *Scr Mater*, vol. 63, no. 10, pp. 1028–1031, Nov. 2010, doi: 10.1016/j.scriptamat.2010.07.036.
- [23] C. I. Garcia, "High strength low alloyed (HSLA) steels," in *Automotive Steels: Design, Metallurgy, Processing and Applications*, Elsevier Inc., 2016, pp. 145–167. doi: 10.1016/B978-0-08-100638-2.00006-7.
- [24] O. A. Zambrano, "A general perspective of Fe–Mn–Al–C steels," *Journal of Materials Science*, vol. 53, no. 20. Springer New York LLC, pp. 14003–14062, Oct. 01, 2018. doi: 10.1007/s10853-018-2551-6.
- [25] "135741a0".
- [26] G. Frommeyer and U. Brück, "Microstructures and mechanical properties of high-strength Fe-Mn-Al-C light-weight TRIPLEX steels," *Steel Res Int*, vol. 77, no. 9–10, pp. 627–633, 2006, doi: 10.1002/srin.200606440.
- [27] Z. Q. Wu, H. Ding, X. H. An, D. Han, and X. Z. Liao, "Influence of Al content on the strain-hardening behavior of aged low density Fe-Mn-Al-C steels with high Al content,"



*Materials Science and Engineering A*, vol. 639, pp. 187–191, Jul. 2015, doi: 10.1016/j.msea.2015.05.002.

- [28] G. Frommeyer and U. Brück, “Microstructures and mechanical properties of high-strength Fe-Mn-Al-C light-weight TRIPLEX steels,” *Steel Res Int*, vol. 77, no. 9–10, pp. 627–633, 2006, doi: 10.1002/srin.200606440.
- [29] “Stainless Steels: Martensitic.”
- [30] C. Dulucheanu, T. L. Severin, D. A. Cerlinca, and L. Irimescu, “Structures and Mechanical Properties of Some Dual-Phase Steels with Low Manganese Content,” *Metals (Basel)*, vol. 12, no. 2, Feb. 2022, doi: 10.3390/met12020189.
- [31] P. Fu, Z. Bing Zheng, W. Ping Yang, and H. Kun Yang, “Influence of carbon addition on mechanical properties of Fe–Mn–C twinning-induced plasticity steels,” *Journal of Iron and Steel Research International*, vol. 29, no. 9, pp. 1446–1454, Sep. 2022, doi: 10.1007/s42243-021-00688-x.
- [32] I. Kalashnikov, O. Acselrad, A. Shalkevich, and L. C. Pereira, “Chemical Composition Optimization for Austenitic Steels of the Fe-Mn-Al-C System.”
- [33] L. Kučerová, M. Bystrianský, and Š. Jeníček, “The Effect of Annealing Temperature on Microstructure and Mechanical Properties of Lightweight Steel with Increased Aluminium Content,” 2017.
- [34] H. Huang, D. Gan, and P. W. Kao, “EFFECT OF ALLOYING ADDITIONS ON THE I<sub>c</sub> PHASE PRECIPITATION IN AUSTENITIC Fe-Mn-Al-C ALLOYS,” 1994.
- [35] S. H. Mousavi Anijdan *et al.*, “The influence of aluminum on microstructure, mechanical properties and wear performance of Fe–14%Mn–1.05%C manganese steel,” *Journal of Materials Research and Technology*, vol. 15, pp. 4768–4780, Nov. 2021, doi: 10.1016/j.jmrt.2021.10.054.
- [36] M. K. Yadav, D. Kumar, N. Kumar, and T. K. Bandyopadhyay, “Hot-rolled Al-added medium Mn steel (Fe-8Mn-2.85Al-1Si-0.2C): Microstructural evolution and tensile behavior,” *Materialia (Oxf)*, vol. 29, p. 101790, Jun. 2023, doi: 10.1016/j.mtla.2023.101790.
- [37] N. Rasooli, H. Shirazi, and M. Nili-Ahmadabadi, “Significance of Mn concentration on aging behavior, microstructure evolution and mechanical properties of Fe–Ni–Mn alloys,” *Journal of Materials Research and Technology*, vol. 24, pp. 1–15, May 2023, doi: 10.1016/j.jmrt.2023.02.207.
- [38] H. Wang *et al.*, “High temperature deformation behavior and microstructure evolution of low-density steel Fe30Mn11Al1C micro-alloyed with Nb and V,” *Materials*, vol. 14, no. 21, Nov. 2021, doi: 10.3390/ma14216555.
- [39] J. Zhang *et al.*, “Revisiting the formation mechanism of intragranular  $\kappa$ -carbide in austenite of a Fe-Mn-Al-Cr low-density steel,” *Scr Mater*, vol. 199, Jul. 2021, doi: 10.1016/j.scriptamat.2021.113836.
- [40] P. Chen, X. Li, and H. Yi, “The  $\kappa$ -carbides in low-density Fe-Mn-Al-C steels: A review on their structure, precipitation and deformation mechanism,” *Metals*, vol. 10, no. 8. MDPI AG, pp. 1–14, Aug. 01, 2020. doi: 10.3390/met10081021.

- [41] Z. Q. Wu, H. Ding, X. H. An, D. Han, and X. Z. Liao, "Influence of Al content on the strain-hardening behavior of aged low density Fe-Mn-Al-C steels with high Al content," *Materials Science and Engineering A*, vol. 639, pp. 187–191, Jul. 2015, doi: 10.1016/j.msea.2015.05.002.
- [42] A. N. de Moura *et al.*, "Microstructure, crystallographic aspects and mechanical properties of AISI 420 martensitic stainless steel after different thermomechanical process routes," *Mater Chem Phys*, p. 127723, Apr. 2023, doi: 10.1016/j.matchemphys.2023.127723.
- [43] V. Shterner, I. B. Timokhina, and H. Beladi, "On the work-hardening behaviour of a high manganese TWIP steel at different deformation temperatures," *Materials Science and Engineering A*, vol. 669, pp. 437–446, Jul. 2016, doi: 10.1016/j.msea.2016.05.104.
- [44] H. Springer and D. Raabe, "Rapid alloy prototyping: Compositional and thermo-mechanical high throughput bulk combinatorial design of structural materials based on the example of 30Mn-1.2C-xAl triplex steels," *Acta Mater*, vol. 60, no. 12, pp. 4950–4959, Jul. 2012, doi: 10.1016/j.actamat.2012.05.017.
- [45] D. Varshney and K. Kumar, "Application and use of different aluminium alloys with respect to workability, strength and welding parameter optimization," *Ain Shams Engineering Journal*, vol. 12, no. 1. Ain Shams University, pp. 1143–1152, Mar. 01, 2021. doi: 10.1016/j.asej.2020.05.013.
- [46] Y. C. Yoon, S. I. Lee, D. K. Oh, and B. Hwang, "Microstructure and low-temperature toughness of intercritically annealed Fe–9Mn–0.2C Medium-Mn steels containing Al, Cu, and Ni," *Materials Science and Engineering A*, vol. 854, Sep. 2022, doi: 10.1016/j.msea.2022.143804.
- [47] O. Acselrad, J. Dille, L. C. Pereira, and J.-L. Delplancke, "Communications Room-Temperature Cleavage Fracture of FeMnAlC Steels."
- [48] J. Li, D. Zhan, Z. Jiang, H. Zhang, Y. Yang, and Y. Zhang, "Progress on improving strength-toughness of ultra-high strength martensitic steels for aerospace applications: a review," *Journal of Materials Research and Technology*, vol. 23. Elsevier Editora Ltda, pp. 172–190, Mar. 01, 2023. doi: 10.1016/j.jmrt.2022.12.177.
- [49] Y. Chen, G.-M. Liu, H.-Y. Li, X.-M. Zhang, and H. Ding, "Microstructure, strain hardening behavior, segregation and corrosion resistance of an electron beam welded thick high-Mn TWIP steel plate," *Journal of Materials Research and Technology*, vol. 25, pp. 1105–1114, Jul. 2023, doi: 10.1016/j.jmrt.2023.06.010.
- [50] R. Seede *et al.*, "A lightweight Fe–Mn–Al–C austenitic steel with ultra-high strength and ductility fabricated via laser powder bed fusion," *Materials Science and Engineering A*, vol. 874, May 2023, doi: 10.1016/j.msea.2023.145007.
- [51] A. Grajcar, M. Opiela, and G. Fojt-Dymara, "The influence of hot-working conditions on a structure of high-manganese steel," 2009.
- [52] X. Li, L. Hu, and D. Deng, "Influence of contact behavior on welding distortion and residual stress in a thin-plate butt-welded joint performed by partial-length welding," *Thin-Walled Structures*, vol. 176, Jul. 2022, doi: 10.1016/j.tws.2022.109302.

- [53] R. H. Gonçalves e Silva, K. Correa Riffel, M. Pompermaier Okuyama, and G. Dalpiaz, "Effect of dynamic wire in the GTAW process," *J Mater Process Technol*, vol. 269, pp. 91–101, Jul. 2019, doi: 10.1016/j.jmatprotec.2019.01.033.
- [54] J. H. Chen, P. N. Chen, C. M. Lin, C. M. Chang, Y. Y. Chang, and W. Wu, "Microstructure and wear properties of multicomponent alloy cladding formed by gas tungsten arc welding (GTAW)," *Surf Coat Technol*, vol. 203, no. 20–21, pp. 3231–3234, Jul. 2009, doi: 10.1016/j.surfcoat.2009.03.058.
- [55] R. S. Gonzaga, F. W. C. Farias, and J. da C. Payão Filho, "Microstructural characterization of the transition zone between a C–Mn steel pipe and a 70%Ni30%Cu alloy cladding welded by HW-GTAW," *International Journal of Pressure Vessels and Piping*, vol. 192, Aug. 2021, doi: 10.1016/j.ijpvp.2021.104433.
- [56] C. R. C. Lima, M. J. X. Belém, H. D. C. Fals, and C. A. D. Rovere, "Wear and corrosion performance of Stellite 6<sup>®</sup> coatings applied by HVOF spraying and GTAW hotwire cladding," *J Mater Process Technol*, vol. 284, Oct. 2020, doi: 10.1016/j.jmatprotec.2020.116734.
- [57] Z. Q. Wang *et al.*, "In situ synthesis of carbide reinforced Fe-Cu-Ni-Mo-Ti high entropy alloy coatings using GTAW cladding with cable-type welding wire," *Mater Lett*, vol. 324, Oct. 2022, doi: 10.1016/j.matlet.2022.132706.
- [58] J. H. Park, Y. H. Kim, H. J. Baek, and S. M. Cho, "A study on process development of super-TIG welding for 9% nickel steel with Alloy 625," *J Manuf Process*, vol. 40, pp. 140–148, Apr. 2019, doi: 10.1016/j.jmapro.2019.03.017.
- [59] V. F. Viebranz, T. Hassel, T. Niendorf, and H. J. Maier, "Welding characteristics and microstructure of an industrially processed Fe-Mn-Al-Ni shape memory alloy joined by tungsten inert gas welding," *Welding in the World*, vol. 66, no. 11, pp. 2207–2216, Nov. 2022, doi: 10.1007/s40194-022-01364-8.
- [60] T. A. Tejedor, R. Singh, and P. Pilidis, "Maintenance and repair of gas turbine components," in *Modern Gas Turbine Systems: High Efficiency, Low Emission, Fuel Flexible Power Generation*, Elsevier Ltd., 2013, pp. 565–634. doi: 10.1533/9780857096067.3.565.
- [61] M. Pouranvari and S. P. H. Marashi, "On failure mode of resistance spot welded DP980 advanced high strength steel," *Canadian Metallurgical Quarterly*, vol. 51, no. 4, pp. 447–455, Oct. 2012, doi: 10.1179/1879139512Y.0000000034.
- [62] R. Manti, D. K. Dwivedi, and A. Agarwal, "Pulse TIG welding of two Al-Mg-Si alloys," *J Mater Eng Perform*, vol. 17, no. 5, pp. 667–673, Oct. 2008, doi: 10.1007/s11665-008-9210-z.
- [63] M. Haghshenas and A. P. Gerlich, "Joining of automotive sheet materials by friction-based welding methods: A review," *Engineering Science and Technology, an International Journal*, vol. 21, no. 1. Elsevier B.V., pp. 130–148, Feb. 01, 2018. doi: 10.1016/j.jestch.2018.02.008.
- [64] A. R. Pavan, B. Arivazhagan, M. Vasudevan, T. N. Prasanthi, and C. Sudha, "Study on the microstructure and mechanical properties of hybrid laser + MIG welded joints of

316LN stainless steel," *Opt Laser Technol*, vol. 163, Aug. 2023, doi: 10.1016/j.optlastec.2023.109410.

- [65] J. Yang *et al.*, "The influence of laser power on microstructure and properties of laser welding-brazing of Al alloys to Al-Si coated 22MnB5 steel," *Opt Laser Technol*, vol. 162, Jul. 2023, doi: 10.1016/j.optlastec.2023.109318.
- [66] L. Kang, H. Yuan, H. Li, Y. Ji, H. liu, and G. Liu, "Enhanced Mechanical Properties of Fe-Mn-Al-C Low Density Steel via Aging Treatment," *Front Mater*, vol. 8, Jun. 2021, doi: 10.3389/fmats.2021.680776.
- [67] J. kuan Ren *et al.*, "Fe-Mn-Al-C high-entropy steels with superior mechanical properties at 4.2 K," *Mater Des*, vol. 228, Apr. 2023, doi: 10.1016/j.matdes.2023.111840.

## Appendix

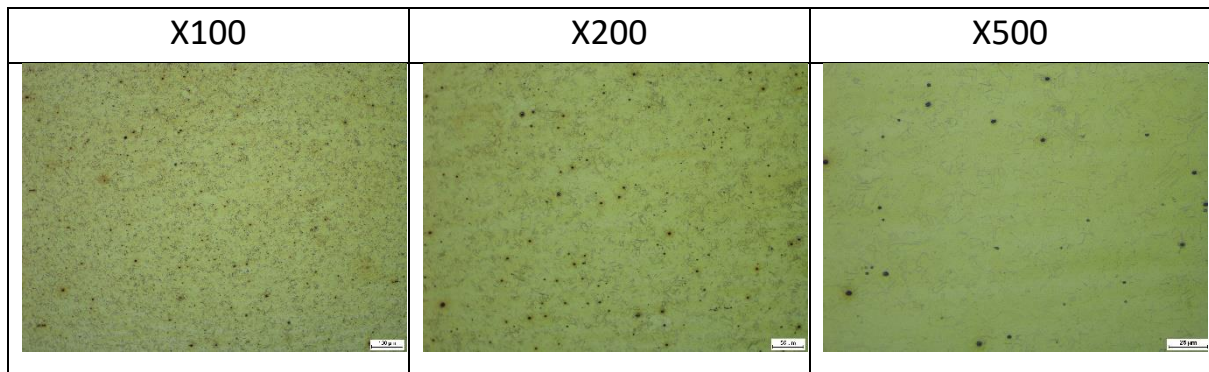


*Figure 41 A hot-rolled microstructure with different magnification*

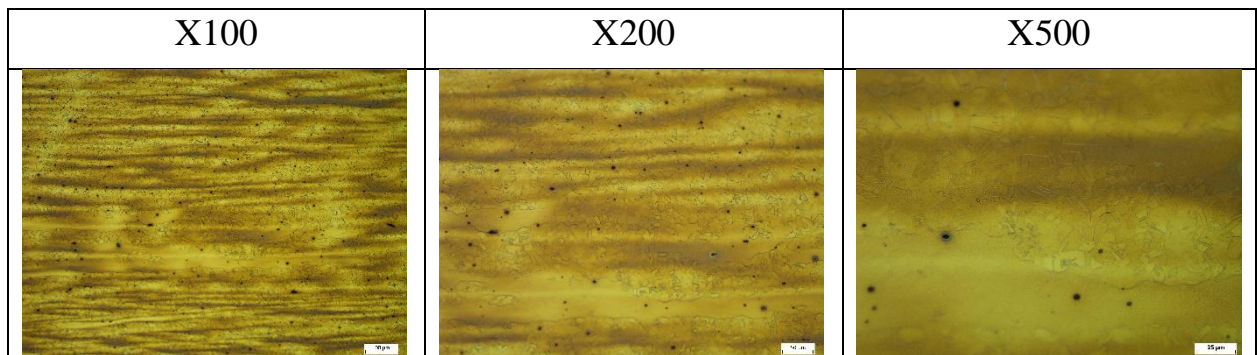


*Figure 42 A solubilized microstructure with different magnification*

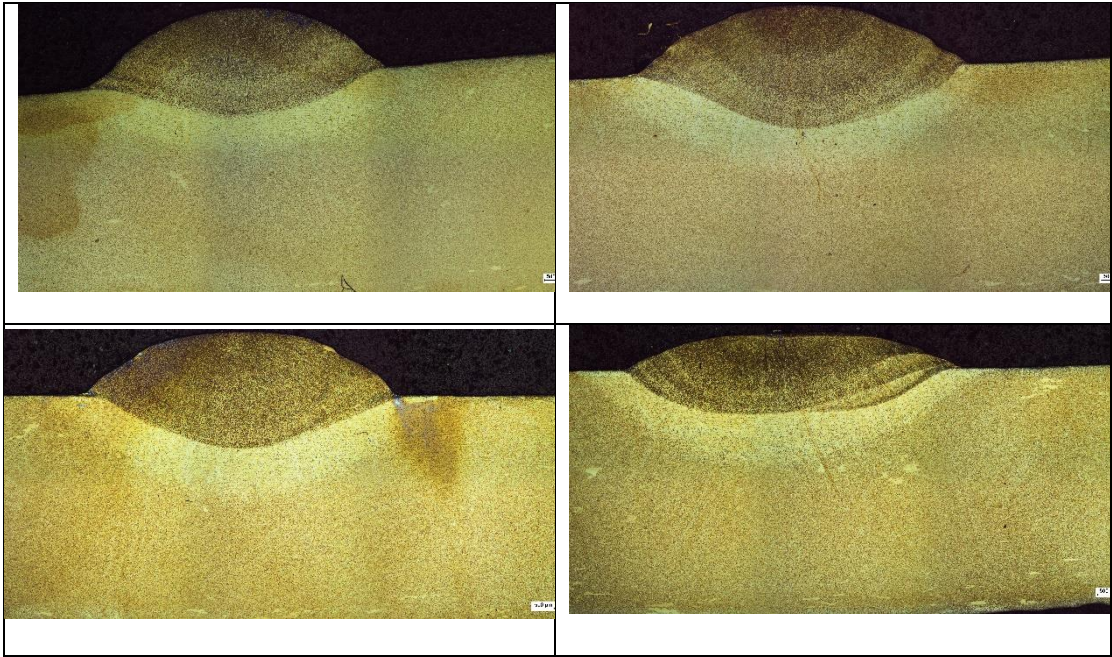


Figure 43 TIG AC clad optical Micrographs

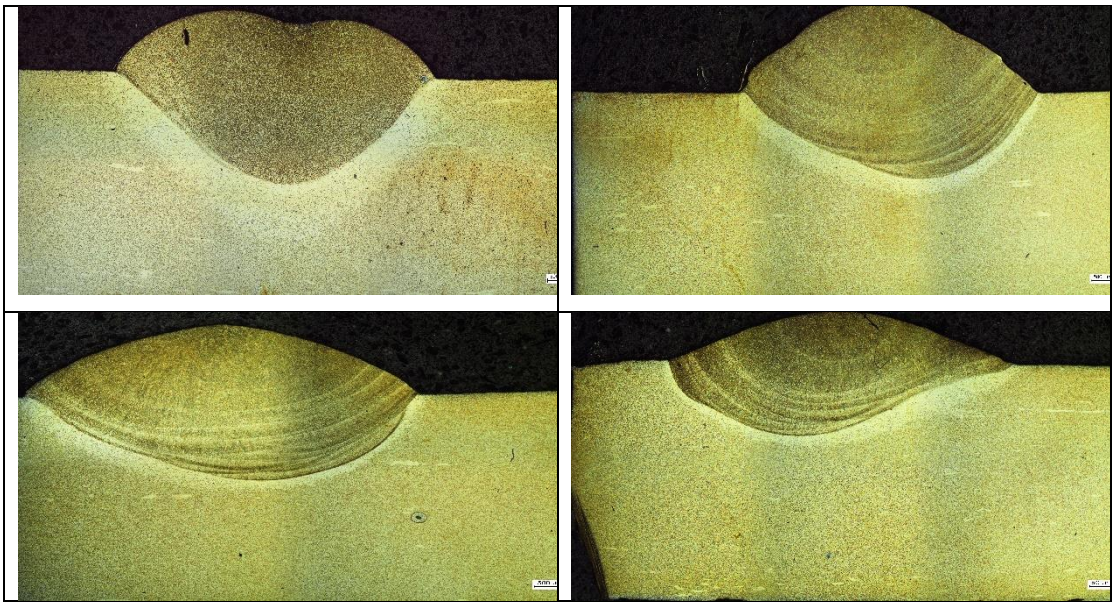


Figure 44 TIG DC clad optical Micrographs

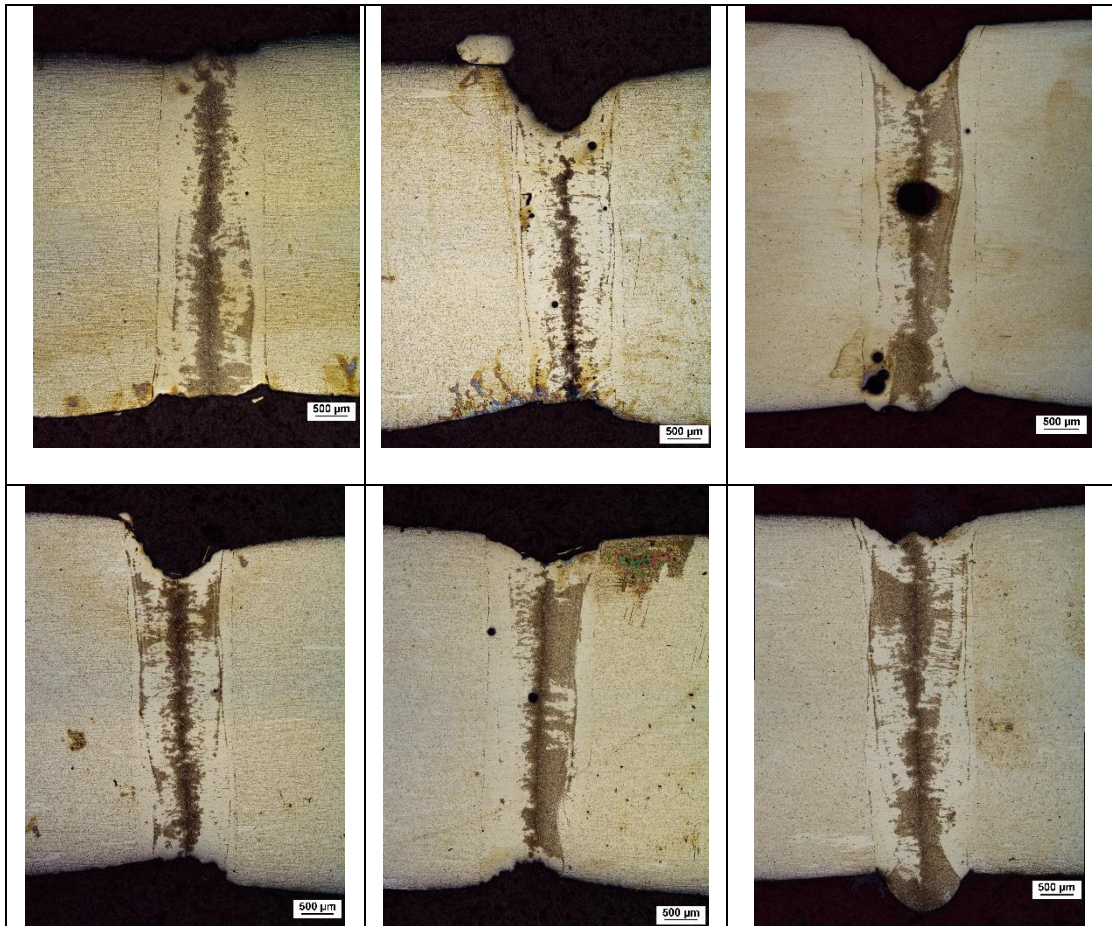
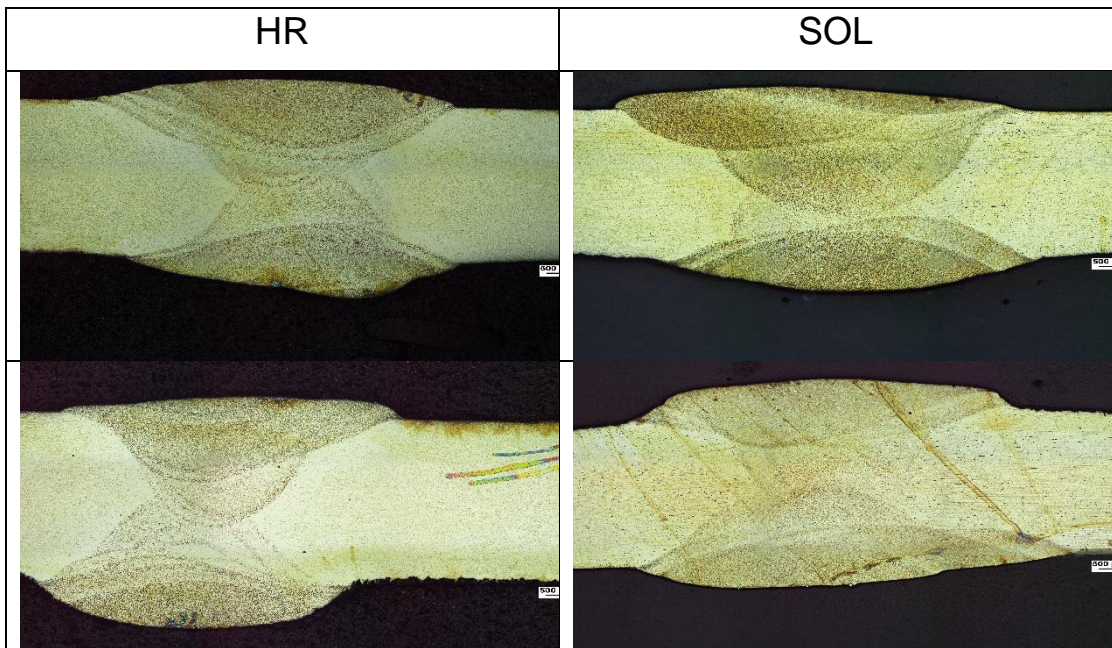


Figure 45 Optical Micrograph of laser cladded samples



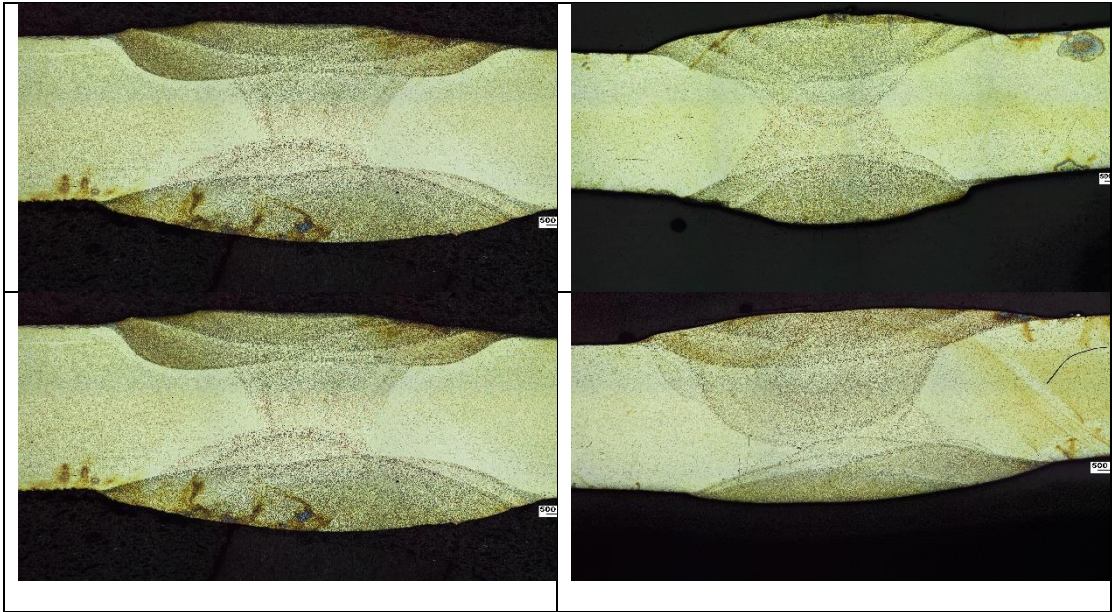
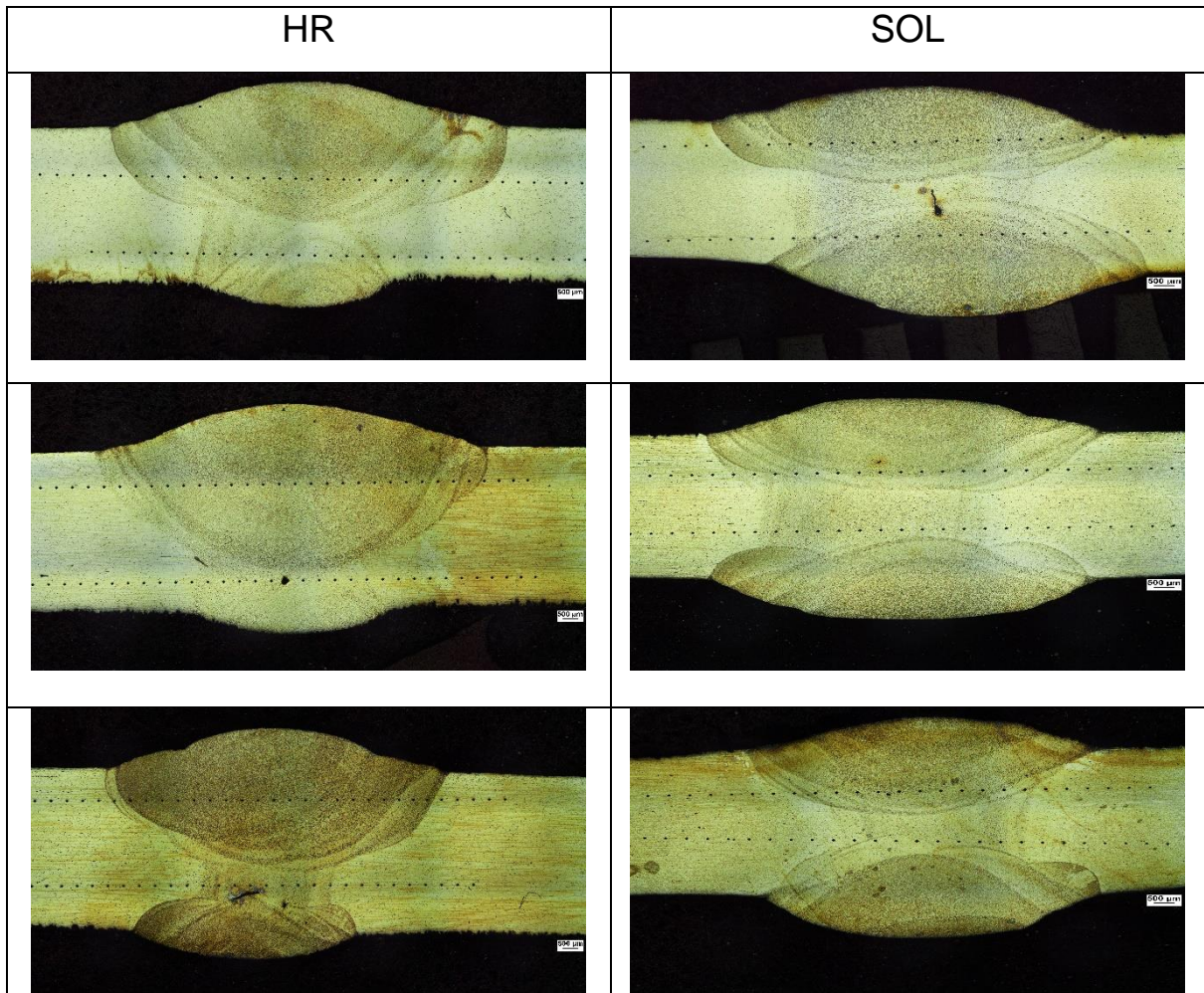


Figure 46 optical micrograph of both HR and SOL TIG AC welded samples





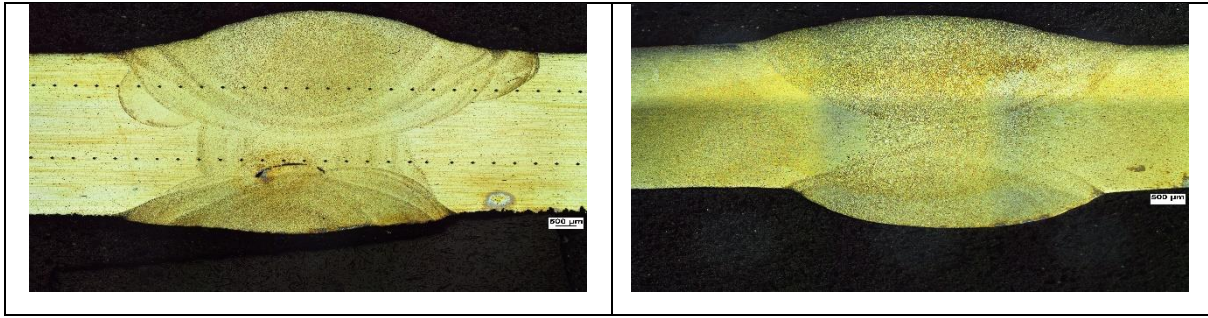


Figure 47 optical micrograph of both HR and SOL TIG DC welded samples

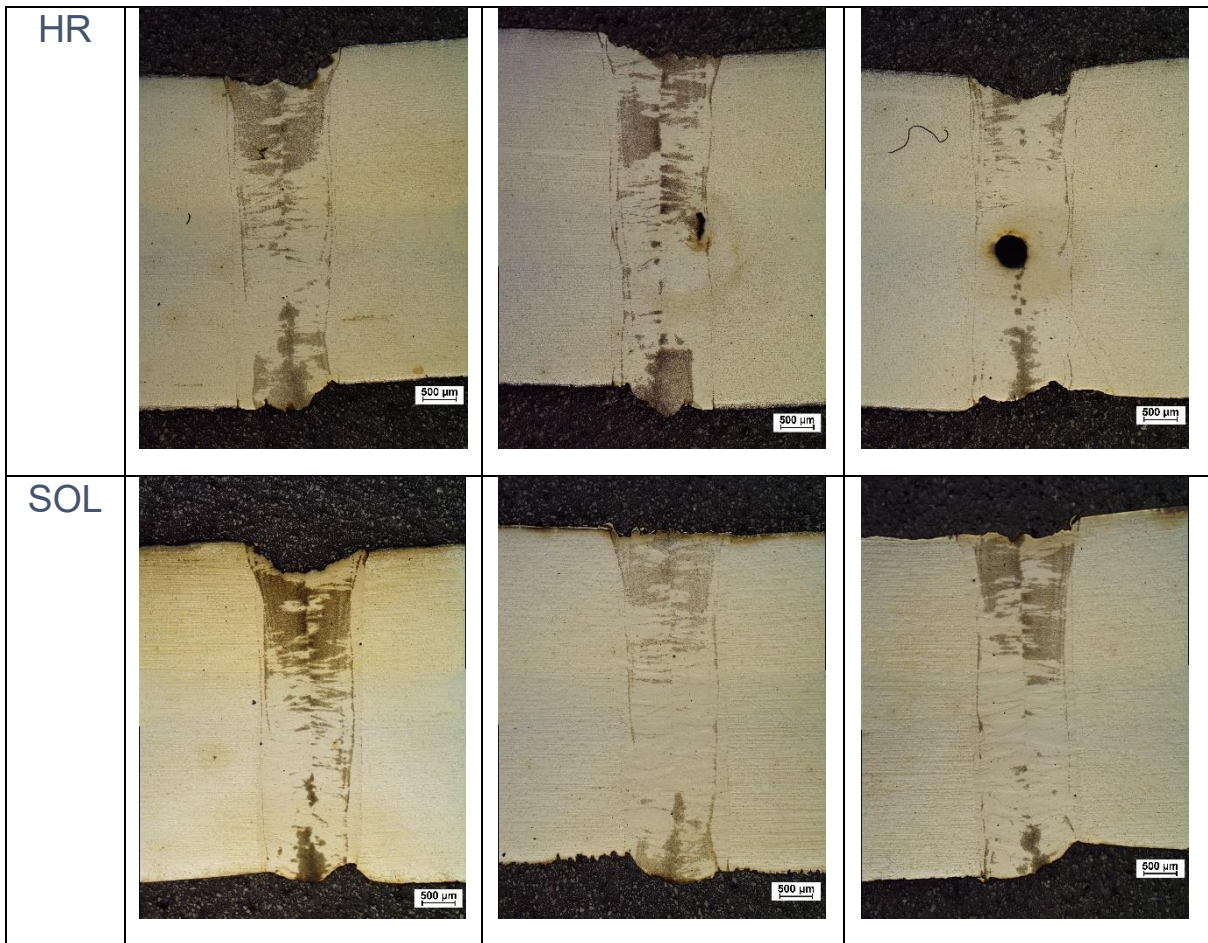


Figure 48 Optical micrograph of HR and SOL laser welded samples

## List of table

Table 1 Classification of lightweight steels based on their microstructures prior to hot rolling. ....	6
Table 2 Deformation mechanisms in austenitic Fe–Mn–Al–C steels as a function of SFE .....	14
Table 3 Chemical composition of Fe-Mn-Al-C lightweight steel .....	31
Table 4 ASTM standard, which is utilized for microhardness test.....	36
Table 5 Dimensions of fusion and HAZ regions of GTAW cladded samples .....	41
Table 6 Tensile test specimens for the HR TIG DC welding .....	54
Table 7 Tensile properties of Fe-Mn-Al-C steel samples after welding .....	54
Table 8 The SEM-EDS outputs of the investigated sites of TIG DC cladded .....	61
Table 9 The SEM-EDS outputs of the investigated sites of TIG AC cladded .....	61

## List of figures:

Figure 1 An increasing trend of research in Fe–Mn–Al–C in Scopus alloys during the last half-decade.	2
Figure 2 Yield strength-total elongation relationship of automotive steel classes. ....	3
Figure 3 Carbon's effect on mechanical properties. Al 9%, Mn 30%. ....	7
Figure 4 Effect of manganese on mechanical properties .....	8
Figure 5 Phase diagrams at the equilibrium of four Fe-Mn-Al-C systems with respectively 20 wt.% (a), 25 wt.% (b), 30 wt.% (c) and 35 wt.% (d) Mn content, as a function of the C content.....	11
Figure 6 The $\kappa$ -carbide unit cell, from left: (a) as initially conceived; (b) with ideal stoichiometry; (c) and $Mn_2FeAlC$ transitions observed experimentally; (d) and (e) with the partial carbon vacancy]. ...	12
Figure 7 Schematic representation of the stacking sequence of perfect structure .....	13
Figure 8 A schematic representation of the deformation mechanisms of Fe-Mn-Al-C steel.....	15
Figure 9 fcc materials with different stacking fault energies .....	16
Figure 10 Overview of the mechanical properties with respect to alloy composition .....	17
Figure 11 Effect of alloy elements on the density of austenite.....	19
Figure 12 CVN impact energy as a function of test temperature for two austenitic steels .....	21
Figure 13 Effect of Mn content on Young's modulus .....	23
Figure 14 Effect of Austenitic grain size with respect to temperature.....	25
Figure 15 Schematic diagram of TIG welding.....	26
Figure 16 Schematic representation of TIG welding .....	28
Figure 17 Design of Experiments .....	32
Figure 18 Hot rolled samples after embedding. ....	33
Figure 19 Draft of the specimen adopted for tensile tests. ....	37
Figure 20 Optical micrograph of Hot-rolled case (500x) .....	39
Figure 21 Optical micrograph of Solubilized sample (500x).....	39
Figure 22 Optical micrograph of TIG clad plate .....	41
Figure 23 Magnified optical micrograph of DC clad sample. ....	42
Figure 24 Optical micrograph of the laser beam on plate .....	43
Figure 25 Magnified micrograph of the laser beam on the plate. ....	44
Figure 26 Optical micrograph of TIG welded plate .....	45
Figure 27 Optical micrograph of laser welded plate .....	46
Figure 28 HV profile for HR and SOL condition for different sheet grades .....	48
Figure 29 shows the variation of hardness value with the distance in TIG cladding. ....	49
Figure 30 shows the variation of hardness value with the distance on the laser beam.....	50
Figure 31 shows hardness variation with distance in TIG AC welding.....	51
Figure 32 shows hardness variation with distance in TIG DC welding.....	52
Figure 33 Hardness variation with distance in laser welding.....	53
Figure 34 Optical micrograph of Solubilized and Hot-rolled state (500x) .....	58
Figure 35 SEM analysis of TIG clad samples .....	59
Figure 36 EDS compositional maps of TIG-DC clad microstructure .....	60
Figure 37 Micrographs of fusion zone with different magnification.....	62
Figure 38 Stress-strain curve for different welding technologies .....	68
Figure 39 Fracture surface of TIG AC welded specimen. ....	69
Figure 40 Fracture surface with dimples-like shape in laser welded specimen.....	69

Figure 41 A hot-rolled microstructure with different magnification.....	81
Figure 42 A solubilized microstructure with different magnification.....	81
Figure 43 TIG AC cladded optical Micrographs .....	82
Figure 44 TIG DC cladded optical Micrographs .....	82
Figure 45 Optical Micrograph of laser cladded samples.....	83
Figure 46 optical micrograph of both HR and SOI TIG AC welded samples .....	84
Figure 47 optical micrograph of both HR and SOI TIG DC welded samples .....	85
Figure 48 Optical micrograph of HR and SOL laser welded samples .....	85

List of Equations:

Equation 1 demonstrates the austenitic alloy with linear combination of alloy elements ..... 18  
Equation 2 demonstrates the ferritic alloy with linear combination of alloy elements..... 18